

Christian Helledal Trandem  
Colin Ringdalen MacDonald

# Impact of Cooling Methods on Ageing in Lithium-Ion Battery Cells

Master's thesis in MIPROD, MTING

Supervisor: Odne Stokke Burheim

Co-supervisor: Markus Solberg Wahl, Lena Spitthoff, Bjørn Austbø,  
Jacob Joseph Lamb

June 2021



Christian Helledal Trandem  
Colin Ringdalen MacDonald

# **Impact of Cooling Methods on Ageing in Lithium-Ion Battery Cells**

Master's thesis in MIPROD, MTING  
Supervisor: Odne Stokke Burheim  
Co-supervisor: Markus Solberg Wahl, Lena Spitthoff, Bjørn Austbø,  
Jacob Joseph Lamb  
June 2021

Norwegian University of Science and Technology  
Faculty of Engineering  
Department of Energy and Process Engineering





---

# Abstract

That temperature has a considerable effect on the lifespan of Lithium-ion batteries (LIBs) is well documented in the literature. The temperature of LIBs under cycling is dependent on the properties of the cells the usage and the Thermal management system (TMS) used. To increase the lifespan of the cells, managing them at optimal temperature is essential. To contribute the understanding of the LIBs lifetime, this study looked into the properties of the cells and quantified their cooling capabilities. These properties were studied during degeneration of the cells under cycle ageing to identify how the cells change through their lifespan.

In the first part of the thesis, the workings of Li-ion batteries is described from the very fundamentals to assembly, thermal behaviour, ageing mechanisms, and methods to characterize the cells. The theory part is written with that in mind that others could read it to learn about Li-ion battery basics.

The main goal of the thesis is to contribute to the understanding of ageing mechanisms and how these affect and are affected by the cells thermal properties and behaviour. Cells were cycled in different cooling setups, and characterization tests were done before, during and after the ageing cycles. The difference in degradation mechanisms between the different cooling setups was then studied. A novel approach using the recently developed Cell Cooling Coefficient (CCC) was performed, where the cycled cells CCC were characterized during the ageing process, and the changes in how the cells were cooled were monitored. The CCC together with other characterization techniques were used to study the changes happening in the cell thru their lifetime.

The results gathered to show that as the cells degrade, the heat production increase, this is studied through internal resistance, over-potentials, and entropy changes. Another aspect not so well documented is the cells thermal behaviour during degradation. The CCC for pouch cooled cells is seen to more than half during the lifespan of the studied cells. The thermal conductivity change measured on the anode from a dismantled cells shows some of the reason for this drop in CCC. Mechanical inspections of the physical changes in the cell underline the importance of the degradation of the anode on the cells performance.

The goal of the thesis was to contribute to the total understanding of the behaviour of battery cells. The data gathered from the ageing study used in this thesis has been uploaded to Mendeley Data and is accessible from: DOI: [10.17632/p98wcs3g4b.1](https://doi.org/10.17632/p98wcs3g4b.1)

---

# Sammendrag

At temperatur har en betydelig effekt på levetiden til Litium-ione batterier er godt dokumentert i litteraturen. Temperaturen til battericellene under bruk avhenger av egenskapene til cellene, bruken og kjølesystemet som brukes. For å øke cellens levetid er det viktig å kunne kontrollere temperaturen. For å bidra til forståelsen av Litium-ione batterienes levetid, har vi i denne studien sett på egenskapene til cellene og kvantifisert hvor enkle de er å kjøle. Disse egenskapene ble studert gjennom degenerering av cellene under aldring gjennom bruk, dette for å identifisere hvordan cellene endres gjennom levetiden.

I den første delen av oppgaven er Lithium-ion batterier beskrevet fra det helt grunnleggende til montering, termisk oppførsel, aldringsmekanismer samt metoder for å karakterisere cellene. Teoridelen er skrevet med tanke på at andre kunne lese den for å lære det grunnleggende om Lithium-ione batterier.

Hovedmålet med oppgaven er å bidra til forståelsen av aldringsmekanismer og hvordan disse påvirker og påvirkes av cellens termiske egenskaper og oppførsel. Celler ble syklet i forskjellige kjøleoppsett, og karakteriseringstester ble gjort før, under og etter aldringssyklusene. Forskjellen i nedbrytningsmekanismer mellom de forskjellige kjøleoppsettene ble deretter studert. Den nylig utviklede Celle Kjølings Koeffisienten (CCC) ble brukt til å karakterisere kjøleegenskapene til cellene gjennom aldringsprosessen. CCC sammen med andre karakteriseringsteknikker ble brukt til å studere endringene i cellen gjennom levetiden.

Resultatene viser at når cellene brytes ned, øker varmeproduksjonen, dette ble observert i endring i intern motstand, overpotensialer og entropi. Et annet aspekt som ikke er så godt dokumentert er cellens termiske oppførsel under aldring. CCC for de cellene kjølt gjennom celleposen ble mer enn halvert gjennom cellens levetid. Den endrede termiske ledningsevnen målt på anoden fra åpne celler viser noe av årsaken til dette fallet i CCC. De fysiske endringene i cellen som ble observert understreker viktigheten av nedbrytningen til anoden på cellenes ytelse.

---

# Preface

When starting the work on the project thesis this autumn neither of us knew much about batteries or that batteries would be the topic for our master thesis. Both of us came from Revolve NTNU seeking a topic for the master thesis as a side project beside building race-cars for our third consecutive year. We had not imagine that the side project would be this exiting and lead jobs in the until know unknown battery industry.

Thru the year we have learned more than we could imagine about a completely new subject. As can be seen thru the thesis, curiosity has led us to investigate as many aspects as possible with batteries, not all of them as relevant to the main subject of the thesis, but the goal about learning as much as possible about all aspects of the topics we work with has triumphed having a clean and narrow thesis.

We would like to give a huge thanks to Odne Burheim for saying yes to supervise two students coming from completely irrelevant backgrounds most eager to build racecars. Lena Spitthoff and Markus Solberg Wahl for taking the main responsibility for us and always helping, without your constant reminders about us starting to write things down and not just start new experiments, the thesis would probably never have been finished.

Thanks to Bjørn Austbø, Jacob Lamb and Preben Vie for participating in the guidance meetings with valuable feedback and lessons. And thanks to Bjørn Volseth and Silje Brynteson for helping out in the lab.

Lastly we would like to say a huge thanks to Revolve NTNU and all the members we have worked with there for the last three years. We would never have learned close to this much without Revolve, and would certainly never have come into working with batteries. We hope that at least the theory part of this thesis could serve as a useful introduction for future students in Revolve working with batteries.

Christian Helledal Trandem and Colin Ringdalen MacDonald  
Trondheim 28.06.2021

---



# Table of Contents

<b>Abstract</b>	<b>i</b>
<b>Sammendrag</b>	<b>ii</b>
<b>Preface</b>	<b>iii</b>
<b>Table of Contents</b>	<b>vii</b>
<b>List of Tables</b>	<b>ix</b>
<b>List of Figures</b>	<b>xiii</b>
<b>Abbreviations</b>	<b>xiv</b>
<b>1 Introduction</b>	<b>1</b>
1.1 Cooling systems effect on cost and environmental impact . . . . .	1
1.2 Objective . . . . .	2
<b>2 Theory</b>	<b>3</b>
2.1 Lithium-ion battery basics . . . . .	3
2.2 Construction of a LiB . . . . .	3
2.2.1 Electrodes . . . . .	4
2.2.2 Separator . . . . .	8
2.2.3 Electrolyte . . . . .	8
2.2.4 Current collectors . . . . .	9
2.2.5 Tabs . . . . .	10
2.2.6 Assembly of a cell . . . . .	10
2.2.7 Packaging . . . . .	11
2.2.8 Physical properties of electrodes . . . . .	12
2.3 General terminology . . . . .	15
2.3.1 Open circuit voltage (OCV) . . . . .	15
2.3.2 Terminal voltage . . . . .	15

---

2.3.3	C-rate . . . . .	16
2.3.4	State of health (SOH) . . . . .	16
2.3.5	State of Charge (SOC) . . . . .	16
2.3.6	Constant current - constant voltage (CC-CV) . . . . .	18
2.4	Degradation . . . . .	19
2.4.1	External triggering conditions and their effects on operational function . . . . .	19
2.4.2	Cracking of electrode particles . . . . .	23
2.4.3	Solid Electrolyte Interphase (SEI) growth . . . . .	24
2.4.4	Lithium plating . . . . .	26
2.4.5	Decomposition and structural change of the cathode . . . . .	27
2.5	Thermal properties of a Lithium-ion batteries . . . . .	29
2.5.1	Heat generation in a Lithium-ion batteries . . . . .	29
2.5.2	Thermal conductivity in LIB's . . . . .	35
2.5.3	Thermal gradients in a LiB and their impact on performance . . . . .	37
2.5.4	Heat rejection from Lithium-ion batteries . . . . .	39
2.6	Melasta SLPBB042126 . . . . .	41
<b>3</b>	<b>Characterization and ageing cycles</b>	<b>43</b>
3.1	Degradation cycles . . . . .	43
3.2	Degradation setup . . . . .	45
3.3	Specific heat capacity (Cp) . . . . .	46
3.4	Cell Cooling Coefficient (CCC) . . . . .	47
3.4.1	$CCC_{Pouch}$ . . . . .	48
3.4.2	$CCC_{Tabs}$ . . . . .	51
3.5	Visual and mechanical inspection . . . . .	53
3.5.1	Opening of cell . . . . .	53
3.5.2	Thickness . . . . .	53
3.5.3	SEM . . . . .	53
3.5.4	Density . . . . .	54
3.5.5	Thermal conductivity . . . . .	55
3.6	Incremental Capacity Analysis (ICA) . . . . .	56
3.7	Overpotentials . . . . .	58
3.8	Capacity analysis . . . . .	60
3.9	Entropy . . . . .	62
<b>4</b>	<b>Results &amp; Discussion</b>	<b>65</b>
4.1	Results labeling . . . . .	65
4.2	Ageing . . . . .	66
4.2.1	Ageing by different cooling methods . . . . .	66
4.2.2	Capacity during cycling . . . . .	69
4.2.3	Isolated tests . . . . .	71
4.2.4	Temperature effects on cycle life . . . . .	74
4.2.5	Calibration error in battery cycler . . . . .	75
4.3	CCC characterization . . . . .	76
4.3.1	$CCC_{pouch}$ . . . . .	76

---

---

4.3.2	CCC <sub>tabs</sub> . . . . .	79
4.3.3	Change in CCC as function of SOH . . . . .	81
4.3.4	Independence of C-rate . . . . .	82
4.3.5	Error estimates . . . . .	82
4.4	ICA . . . . .	84
4.5	Heat generation . . . . .	87
4.5.1	Specific heat capacity (Cp) test results . . . . .	87
4.5.2	Overpotentials . . . . .	88
4.5.3	Entropy . . . . .	89
4.5.4	Validation . . . . .	90
4.6	Visual, mechanical and thermal inspection . . . . .	94
4.6.1	Thickness . . . . .	94
4.6.2	Density . . . . .	96
4.6.3	Thermal conductivity . . . . .	96
4.6.4	Visual inspection of electrodes . . . . .	99
4.6.5	Scanning electron microscope (SEM) Images . . . . .	102
4.6.6	Summary of visual, mechanical and thermal properties . . . . .	105
4.7	Degradation mode and mechanisms . . . . .	105
4.7.1	Capacity fade . . . . .	105
4.7.2	Decrease of CCC . . . . .	106
<b>5</b>	<b>Conclusion &amp; Further Work</b>	<b>109</b>
5.1	Conclusion . . . . .	109
5.2	Further Work . . . . .	111
	<b>Bibliography</b>	<b>113</b>
	<b>Appendix</b>	<b>125</b>
<b>A</b>	<b>Melasta SLPBB042126HN Product specification</b>	<b>127</b>

---

---

# List of Tables

2.1	Thermal conductivity measurments done on components in the Melasta cell by Trandem [29]. The thermal conductivity for the electrode materials is for the active material only. . . . .	36
2.2	Values from the Melasta SLPBB042126 Datasheet, the complete datasheet could be found in Appendix A, [98] . . . . .	41
3.1	Values used for calculating the heat thru the CCC jig . . . . .	48
4.1	For identification of each cell, all plots for a cell keep the same colour . . .	65
4.2	Measured and calculated variables for specific heat from test. $C_{p_{cell}}$ calculated from equation 3.1 and $C_{p_{water}}$ tabulated the rest measured . . . .	87
4.3	Measurements done on the battery cell and electrodes (current collector with active material) on pristine and aged cell. All number reported with double standard deviation 2s . . . . .	95
4.4	Measurements done on the electrodes (current collector with active material) on pristine and aged cell. All number reported with double standard deviation 2s . . . . .	96
4.5	Thermal conductivity. The thermal conductivity for the electrode materials is for the active material only, the current collector thickness is removed. All measurements were done on dry electrodes. Values for fresh electrodes for comparison is from Trandem [29] and is done in the same rig under the same conditions . . . . .	97

---

# List of Figures

2.1	Main components of a LiB . . . . .	4
2.2	Characteristics of the most common Lithium-ion batteries (LiB) chemestries. . . . .	6
2.3	Intercalation illustration . . . . .	7
2.4	SoC-OCV curve . . . . .	8
2.5	SEM of separator with electrode particle . . . . .	9
2.6	Electrode stacking . . . . .	10
2.7	Casing types . . . . .	11
2.8	Separator configurations . . . . .	12
2.9	SEM of anode . . . . .	12
2.10	Electrode illustration with addetives . . . . .	13
2.11	Heat generation dependency on electrode function . . . . .	13
2.12	Resistivity versus electrode compression . . . . .	14
2.13	Halfcell voltage profiles . . . . .	15
2.14	Typical SoH dependency on cyclces . . . . .	17
2.15	CC-CV . . . . .	18
2.16	Degradation rate dependency on temperature. . . . .	20
2.17	Degradation rate dependency on C-rate. . . . .	21
2.18	Impedance as a function of temperature of an cobalt-oxide electrode. . . . .	22
2.19	Degradation dependency on production quality . . . . .	23
2.20	Degradation mechanisms . . . . .	24
2.21	SEM of cracked particle. . . . .	25
2.22	Lithium dendrites . . . . .	27
2.23	LCO electrode structure . . . . .	28
2.24	Heat generation sources . . . . .	29
2.25	Ohmic resistance dependency on temperature . . . . .	32
2.26	Charge transfer resistance dependency on temperature and SoC . . . . .	33
2.27	Total impedance dependency on temperature and SoC. . . . .	34
2.28	Cell coordinate system . . . . .	34
2.29	Cell coordinate system . . . . .	35
2.30	Parallel cells with different impedance . . . . .	38

---

2.31	Thermal gradient impact on performance . . . . .	39
3.1	Simulated maximum temp during ageing cycles . . . . .	44
3.2	Specific heat measurement . . . . .	47
3.3	CCC <sub>Pouch</sub> setup . . . . .	48
3.4	Sideview with thermocouple placements of CCC <sub>Pouch</sub> Jig . . . . .	49
3.5	Render of the setup used to measure the CCC <sub>Pouch</sub> . . . . .	50
3.6	Current profile used for the CCC test . . . . .	51
3.7	CCC <sub>Tab</sub> placements . . . . .	51
3.8	Render of CCC <sub>Tab</sub> setup without isolation. . . . .	52
3.9	CCC <sub>Tab</sub> setup with. (a) in thermal camber, (b) without top isolation. . . . .	52
3.10	The thermal conductivity meter used. Reprinted from Richter et al. [61] . . . . .	55
3.11	IC of the Melasta cell at 100 SOH. . . . .	56
3.12	IC of graphite half cell . . . . .	57
3.13	IC of a LCO half cell. Reprinted from Xia et al. [107] . . . . .	58
3.14	Current step test . . . . .	59
3.15	Capacity fade dependency on cycles in different cooling setups. . . . .	61
3.16	Entropy calculation through interpolation . . . . .	63
4.1	Ageing cycles with SOH and temperature for all cells . . . . .	67
4.2	SoH as a function of cycles for all tested cells . . . . .	68
4.3	Ageing cycles with capacity and temperature for all cells . . . . .	70
4.4	SoH during isolated tests versus SoH at cycles in cooling jigs. . . . .	72
4.5	Capacity as a function of cycles. Both cooled and isolated test. . . . .	73
4.6	SOH against ATU and Cycles . . . . .	74
4.7	The columbic efficiency measured by the Arbin battery cycler . . . . .	75
4.8	CCC measurements done on cell 27-10 . . . . .	77
4.9	CCC measurments done on cell 16-8 and 24-8 . . . . .	78
4.10	CCC measurments done on cell 27-4 . . . . .	80
4.11	CCC as a function of SOH . . . . .	81
4.12	CCC testing at different C-rates . . . . .	82
4.13	Heat transfer in fin 2 of the CCC <sub>Pouch</sub> Jig . . . . .	83
4.14	IC for 27-4. . . . .	85
4.15	IC for 27-10. . . . .	85
4.16	IC for cells in setup 1. . . . .	86
4.17	Specific heat capacity test results . . . . .	87
4.18	Internal resistance as a function of temperature at different SoC. . . . .	88
4.19	Charge transfer resiistance as a function of temperature at different SoC. . . . .	89
4.20	27-10 at 30°C. . . . .	89
4.21	$\frac{dV}{dT}$ of the aged (50% SOH) and fresh cells. . . . .	90
4.22	Temperature profile of model and point mass model 27-10. . . . .	92
4.23	Temperature profile of model and point mass model for 27-4. . . . .	93
4.24	Side-view picture of aged and new cell . . . . .	94
4.25	Thickness measurement of cells as a function of SOH. . . . .	95
4.26	Thermal conductivity as function of compaction pressure . . . . .	98
4.27	Picture of anode of a aged cell . . . . .	99

---



---

4.28	Signs of mechanical damage on anode. . . . .	100
4.29	Pictures of aged and fresh electrodes . . . . .	101
4.30	SEM of Anode . . . . .	103
4.31	SEM of Cathode . . . . .	104

---

# Abbreviations and definitions

<b>ATU</b>	Accumulated thermal unit
<b>BOL</b>	Beginning of life
<b>C-rate</b>	Normalized Current-rate
<b>CC-CV</b>	Constant Current-Constant Voltage
<b>CC</b>	Constant Current
<b>CCC</b>	Cell Cooling Coefficient
<b>C<sub>p</sub></b>	Specific heat capacity
<b>DC</b>	Direct current
<b>EIS</b>	Electrochemical Impedance Spectroscopy
<b>EV</b>	Electrical vehicles
<b>EOL</b>	End of life
<b>HF</b>	hydrofluoric acid
<b>HPPC</b>	Hybrid pulse power characterization
<b>ICA</b>	Incremental Capacity Analysis
<b>ICEV</b>	Internal Combustion Engine vehicles
<b>IC</b>	ICA curve
<b>LAM</b>	Loss of active material
<b>LCO</b>	Lithium Cobalt Oxide
<b>LFP</b>	Lithium iron phosphate
<b>LIB</b>	Lithium-ion battery
<b>LLI</b>	Loss of Lithium Inventory
<b>LMNO</b>	Lithium Manganese Nickel Oxide
<b>LiB</b>	Lithium-ion batteries

---

<b>NMC</b>	Lithium Nickel Manganese Cobalt Oxide
<b>NTNU</b>	Norwegian University of Science and Technology
<b>OCV</b>	Open circuit voltage
<b>PCM</b>	Phase Change Material
<b>RMS</b>	Root-mean-square
<b>SEI</b>	Solid Electrolyte Interphase
<b>SEM</b>	Scanning electron microscope
<b>SOH</b>	State of Health
<b>eSOH</b>	Energy State of Health
<b>SOC</b>	State of Charge
<b>SOF</b>	State of Function
<b>SOH</b>	State of health
<b>TMS</b>	Thermal management system
<b>TM</b>	Transition Metals
<b>pSEI</b>	Positive solid electrolyte interphase

---

# Introduction

To reach the emission target for  $CO_2$  set by the Paris agreement of 2015, decarbonisation of the transport section is necessary [1]. The leading technology in decarbonisation of the transport section are Electrical vehicles (EV) powered by LiB. Several papers indicate that  $CO_2$  per km can be cut to half of the EV is produced in Europa and used there [1–3]. If the car is charged with a decarbonised grid, such as France or Sweden, the emission can be cut by over three quarters. [2, 3]

The  $CO_2$  emissions throughout the life cycle is in a much higher fraction tied up in the production of the vehicle for EV than Internal Combustion Engine vehicles (ICEV). For a EV used with a decarbonised grid, up towards 90% of the emissions are tied to the production of the car, 40% of this in the battery production [3]. Therefore, two methods can cut the majority of  $CO_2$  emissions; decrease emissions during production or increase life span.

## 1.1 Cooling systems effect on cost and environmental impact

It is well documented that there is a strong correlation between temperature and lifespan of LiB. [1, 4–7] It follows, therefore, that the choice and dimensioning of TMS is crucial for the cost and carbon footprint for an EV.

Lander et al. [1] shows how the lifetime of a battery pack is affected by different types of cooling systems and strategies. It is found that the lifetime of the cell is one of the factors that have the highest dependency on the life cycle cost and the carbon footprint. A doubling of the battery pack's lifetime reduces the carbon footprint by 23 % and the life cycle cost by 33 %. It is revealed that as of now, cooling the pouch surface with water cooling blocks or immersion cooling is the most effective and air cooling is the least effective cooling method. But if the tabs of the cell are designed better for cooling, the tab

cooled cells can be cooled more effectively, giving a longer lifetime. [8]

The cooling strategies' impact on the cell lifetime can be predicted by the use of the Cell Cooling Coefficient (CCC) [8]. When the cell has a known heat generation, and the CCC is known, the expected operating temperature of the cell can be calculated, giving the possibility to predict the degeneration. In this thesis cell, degeneration and the use of CCC will be looked into in-depth for a Lithium Cobalt Oxide (LCO) cell.

## 1.2 Objective

The objective of the thesis is to determine how different cooling systems impact the dimensioning of both capacity, the cooling system demands through the battery life cycle, as well as the underlying mechanisms which induce the change of capacity and thermal properties of a cell through cycling.

Existing research has documented the SOH degradation rate of cells in different cooling systems. However, less research exists on the difference in underlying mechanisms which differentiate the cells operational degradation rate. This thesis will aim to identify any difference in underlying degradation mechanisms between pouch and tab cooling. Identification is made through a mixture of electrical tests, such as ICA as well as dissecting the cell and physically inspecting the cell's components.

No research to the knowledge of the authors has been conducted regarding the difference in change of thermal properties through cycling in the different cooling system. The thesis aims at documenting how cells thermal properties change through ageing in different cooling systems and how this impacts dimensioning of the TMS. Hales et al. [8] introduced a novel approach of measuring a cell's ability to remove heat through the pouch or tab by the introduction of the Cell Cooling Coefficient (CCC). In contrast to most thermal conductivity measurements of LiB, the CCC is a non-destructive test. This allows monitoring cells thermal conductivity throughout their life. In addition, measuring entropy and overpotentials are conducted. By monitoring thermal conductivity and heat generation through its life cycle, the needed dimensioning of TMS can be determined.

# Theory

## 2.1 Lithium-ion battery basics

LiBs are electrochemical storage devices that can store and deliver power to a circuit. Every cell has two electrodes store which can store Lithium ions. These electrodes can have a difference in potential depending on how many Lithium ions they store. This potential can drive a Lithium-ion and electron current between the electrodes. Intercalation is the insertion of ions into the electrode, while deintercalation is the removal of ions.

## 2.2 Construction of a LiB

This section introduces the most critical components of a LiB:

- Electrode - stores the Lithium ions and electrons - i.e. stores the energy
- Separator - separates the electrode to prevent short circuit
- Electrolyte - pathway for ions
- Current collectors - pathway for electrons
- Tabs - external connection to the electrodes
- Casing - will be discussed in as it varies widely from cell to cell

Figure 2.1 shows a schematic sketch of the main components of a LiB as well as the direction of electrons and ions during charge and discharge. Note that the electrodes are not one single mass but rather particles. The light blue substance surrounding the particles is the electrolyte.

This thesis uses three terminologies to describe three different levels of electrochemical storage:

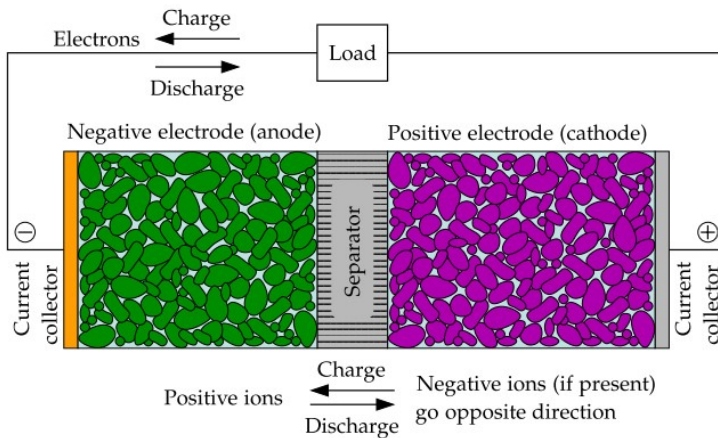


**Figure 2.1:** Schematic sketch of the main components of a LiB. Reprinted from Gregory L. Plett [9]

- Unit cell - the smallest functional unit, with one electrode pair as well as all the needed auxiliary parts
- Cell - the assembly of several unit cells in parallel in one container.
- Battery - the assembly of several cells, casing, cooling system, battery management system

Note that eventhough a LiB is called a battery, it usually refers to a cell. For this thesis unless stated otherwise a LiB is a reference to a cell. For the following sections the components descriptions are applicbale for a pouch cell. A pouch cell is where the electrodes with auxiliary parts are encapsulated in an aluminum foil casing and will be explained further in 2.2.7

## 2.2.1 Electrodes

The electrode is the part of the cell which stores the electrochemical energy. A unit cell consists of two electrodes, which can intercalate ions. The electrodes have a potential depending on their lithiation state (how many Lithium ions they store). [10] The potential of the cell is the potential deviation of the two electrodes. This potential can induce a current if an external circuit is applied.

The two electrodes are called the anode and cathode. Technically the anode is where oxidation occurs (lithium ions deintercalated) and the cathode is where reduction occurs (lithium ions intercalated). However, this could easily be confusing, as the electrodes change names regarding if the cell is charging or discharging. Therefore most literature



(including this thesis) refers to them as if the unit cell is discharging.

The electrode consists of two main types of components; active mass and additives. Active mass is material which lithium ions can intercalate, while the additives give the electrode other favorable properties. Some of the most common additives in a LiBs are [11]:

- Carbon black - added to electrodes to enhance its electron conductivity
- Binder - Bonding additive which bonds electrode particles together as well as to the current collector
- Pore-forming additives
- Wetting additives added for safety

### **Chemistries**

LiB is a term for batteries that intercalate Lithium ions in their electrodes. The rest of the chemistry varies. Note that in this thesis, unless specified, the term "chemistry" refers to the active mass in the cathode in a LiB, not other battery chemistries such as alkaline batteries.

### **Anode**

The vast majority of LiB have a carbon-based anode, either structured as hard carbon or graphite  $C_6$ . [12, 13] Cell chemistries are therefore usually referred to as the cathode chemistry of the battery. In addition to the carbon anode structure, the most crucial difference between anodes is their content of silicon. Modern anodes often have a small percentage of silicon in their anode. Silicon increases the energy density but introduces challenges regarding the stability of the cell, limiting the amount of silicon. [14, 15]

### **Cathode**

Cathode materials vary from cell to cell, and the characteristics of a cell are highly dependent on the cathode material. Some of the main characteristics are; power and energy density, resilience to degradation, safety, and cost.

Two of the most common chemistries found today are; Lithium iron phosphate (LFP), and nickel cobalt manganese (NMC), but also nickel cobalt aluminum (NCA), Lithium Manganese Oxide (LMO) and Lithium Cobalt Oxide (LCO) are also widely used [16]. Nitta et al. [17] grouped cathode materials in two: transition metal oxides and polyanion compounds. Of the chemistries mentioned above, LFP is of the latter, while the rest is transition metal oxides. A significant limitation of many of the transition metal oxides is that they contain cobalt. It is costly, somewhat rare, toxic, has low thermal stability, and

high degradation at high current. [13, 18] A general trend is, therefore, that newly developed chemistries usually reduce or altogether removes the use of cobalt.

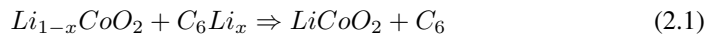


**Figure 2.2:** Characteristics of the most common LiB chemistries. Reprinted from Zubi et al. [16]

The cell studied in this thesis is of type Lithium Cobalt Oxide (LCO), which only has cobalt as a transition metal. LCO is one of the first developed commercial cathodes. It has high specific energy but a relatively low life span compared to newer chemistries. Due to its high % of cobalt, both cost and safety are an issue due to low thermal stability [16].

## Reactions

In this section, the chemical reactions during charge and discharge is discussed. The chemical reaction for a LCO battery is:



$$0.5 < x < 1 \quad (2.2)$$

Note that the cobalt oxide can only be partly be delithiated. In a low lithiation state, the cobalt oxide structure collapses, rendering the cathode unable of intercalation. [9].

When lithium is intercalated and deintercalated into the structure, the structures are not changed chemically, but are changed structurally. This is a much less harsh process than changing chemically, and is one of the reasons intercalation cells have longer life spans than most traditional redox batteries such as alkaline batteries.

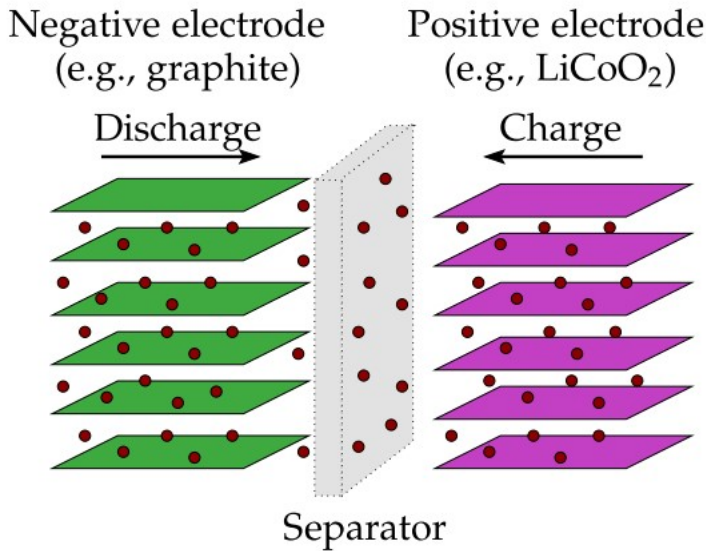


**Figure 2.3:** Illustration of intercalation. Green and purple plates are electrode material, while red dots are lithium ions. Note that the lithium is stored in the structure of the electrode, rather than a part of the material itself. Reprinted from Gregory L. Plett [9]

However, as lithium is added, the volume of a structure will change significantly. As graphite has a higher volume expansion than LCO electrode, an LCO cell will expand during charge.

Each electrode with a certain amount of lithium has a particular potential. As the lithium is moved from the anode to the cathode, the potential difference between the two electrodes decreases. The cell is usually only stable in a specific voltage window, and transition metal oxide chemistries LiB have a voltage window around 4.2-3V.

## SEI

In addition to all the initial components, one crucial component is also created during the first cycles of the LiB; the SEI. SEI is a passivation layer on the anode, which is created

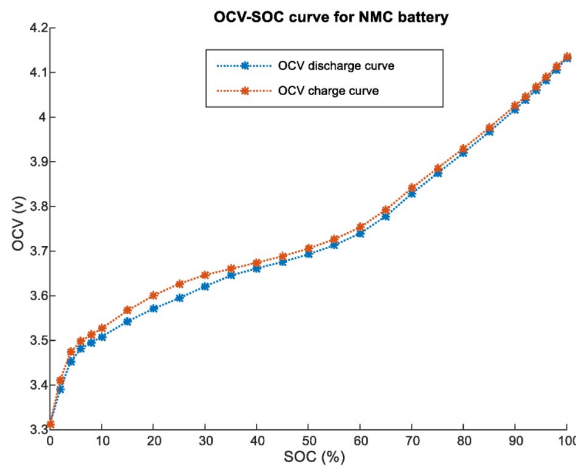


**Figure 2.4:** Figure of how Voltage (OCV) changes through discharged and charged. 100% SOC is fully charged and 0 % SOC is fully discharged. Reprinted from Baccouche et al. [19]

due to the instability of the electrolyte at the anodes operational voltage [5, 20] A further explanation of the SEI will is given in 2.4

## 2.2.2 Separator

To prevent an internal short circuit, the two electrodes need to be separated by a material that does not conduct electrons. This component is called the separator. Additionally, as the Lithium ions need to move between the two electrodes, the separator must allow Lithium-ions to pass. Note that the separator does not conduct the Lithium-ions; the electrolyte does. The separator is usually a membrane with holes big enough for Lithium ions to pass while small enough to prevent electrode particles from passing through. Figure 2.5 shows a picture of a separator with an electrode particle on top of it. Note the contours of the opening, which allows ions to pass.

## 2.2.3 Electrolyte

The electrolyte gives the ions a conductive path between the electrodes. It has two main parts; a solvent and a salt with some additives to improve the cell's performance. The salt gives the electrolyte its ionic conductive properties, while the solvent does not participate in the chemical processes it dissolves the salt and facilitates the ionic migration[21]. The most common salts in use is lithium hexafluorophosphate ( $LiPF_6$ ), while other common salts among others are  $LiBF_4$  and  $LiClO_4$ . The solvent is usually a mixture of several solvents. Some of the common ones are ethylene carbonate (EC), propylene carbonate (PC), dimethyl carbonate (DMC), ethyl methyl carbonate (EMC), and diethyl carbonate (DEC). [9]

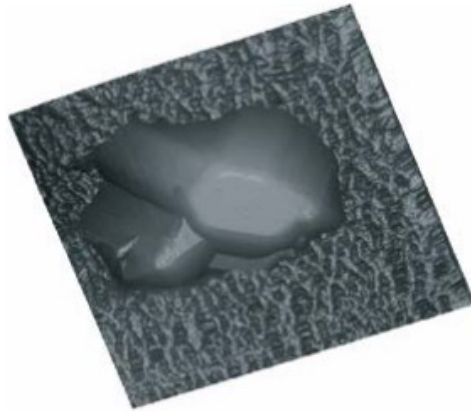


**Figure 2.5:** SEM of separator with electrode particle. Reprinted from Gregory L. Plett [9]

The electrolyte is present in nearly the whole cell as it impregnates the porous electrodes and separators. As the electrolyte is in contact with many different chemicals, one of the main challenges for an electrolyte is stability. The stability of the electrolyte is a common theme in the aging mechanisms in a LiB, which will be discussed in 2.4.

## 2.2.4 Current collectors

The current collectors are thin metal foils that give electrons a low resistance path to the electrodes. In the majority of modern LiB both electrodes have one current collector each. The current collectors also function as a material to which can be welded to the external terminals.

The current collector material for the anode and cathode are in the majority of LiB copper and aluminum, respectively. These are chosen due to their electrical conductivity as well as stability. The current collectors must be electrochemically stable in their working conditions. For a cell to have high potential, it is required that the cathode has a high potential ( $4V$  vs.  $Li/Li^+$ ) for  $LiCoO_2$  cathode and ( $0.01V - 0.25V$  vs.  $Li/Li^+$ ) for graphite anode. Contact with electrolyte under these potentials can make unfavorable reactions occur. After the aluminum has gotten a  $AlF_3$  passivating film from the reaction between  $Al_2O_3$  and  $HF$ , which comes from the decomposition of  $LiPF_6$ , it becomes electrochemically stable at high potentials, making aluminum suitable for use at the cathode. The aluminum current collector is not stable for the low anode potential. Copper is stable for potentials under ( $3V$  vs.  $Li/Li^+$ ) making copper suitable for anode current collectors. However, over-discharging the cell may lead to copper dissolution. [22]

### 2.2.5 Tabs

Tabs are connected to the electrodes through the current collectors to give an external terminal connection. An external circuit can be powered if the circuit is connected to the terminals.

The tabs consists of a conductive material, usually plated with a stable metal to prevent any corrosion. Tabs come in a wide array of widths, thicknesses, aswell as placements. Tabs can be on both same side or opposite side.

### 2.2.6 Assembly of a cell

This section will describe how the previously mentioned parts are assembled into one unit.

A majority of commercial pouch cells consist of several electrode pairs connected in parallel, i.e., all anodes and cathodes are connected, as illustrated in 2.6. The cell studied in this thesis has 41 and 40 anodes and cathodes, respectively. The uneven amount of electrodes is due to the current collectors having electrode material on both sides. It follows that both sides of the cell have an "unpaired" electrode. As the anode electrode is lighter than the cathode, an extra anode is used.

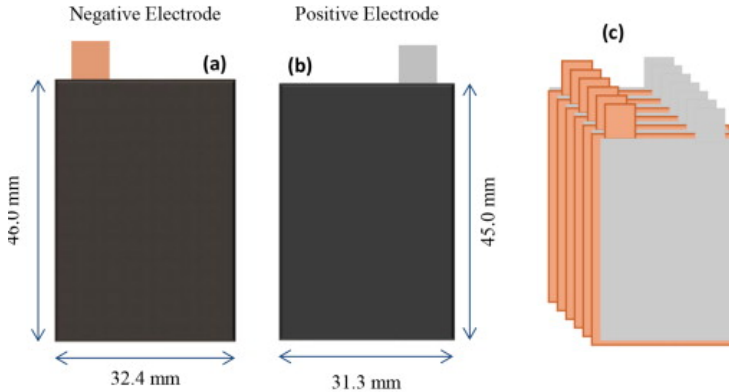


**Figure 2.6:** Illustration of electrode stack consisting of several unit cells making up a cell Reprinted from Trask et al. [23]

Separators and current collectors are usually as thin as manufacturing, and safety allows, both in the order of  $20 \mu\text{m}$  thick. [9]. Increasing their thickness will not significantly increase performance, while a decrease in thickness will give less weight, leading to higher specific and volumetric energy density. In addition, thinner separators have more prone to being penetrated. Electrode thickness varies but is usually in the range of  $50 - 60 \mu\text{m}$  for high energy cells and thinner for higher power cells [24]. A more in-depth explanation of

electrode thickness is given in-depth in section 2.2.8

Internally the electrodes are connected in parallel by letting one part of the current collector stick up from the square electrode and welding the current connectors, which are to be connected in parallel together. In addition, the current collectors are welded to the tab. This is illustrated in Figure 2.6.

A casing encapsulates the unit cells. For a pouch cell, the casing is an aluminum foil coated with a non-conductive material.

## 2.2.7 Packaging

LiBs come in different casings. The most common ones are cylindrical-, prismatic-, button- and pouch-cells. The types are seen in figure 2.7. The different casings have their advantages, where the coin cell is usually used in smaller electronics, the cylindrical and prismatic cells have sturdy casings and can endure handling. The pouch cells have the highest specific and volumetric energy density and are used where packing density or weight is crucial.

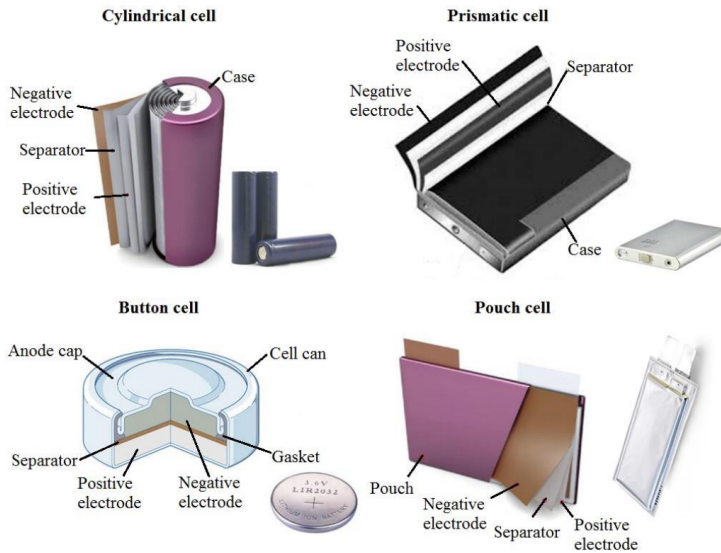


**Figure 2.7:** Different casing types for LiBs Reprinted from Murashko [25]

In this thesis, the focus is on the pouch cells. The pouch cells can have a separator that is either discrete between each electrode, or it can be a continuous Z-folded separator [26]. The Melasta cell used in this thesis has a Z-fold configuration, as can be seen in figure 2.8

where the entire separator is one continuous sheet wrapped between all electrode layers.

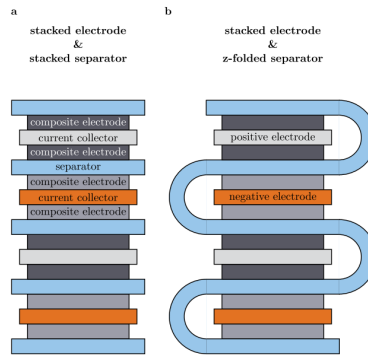


**Figure 2.8:** Separator configurations for pouch cells. Reprinted from Rheinfeld et al. [26]

## 2.2.8 Physical properties of electrodes

In addition to the electrode chemistry and additives, the physical structure of the electrode effects the cells characteristics. In this section the following will be discussed; particles, porosity of electrode, loading and compression.

### Particles

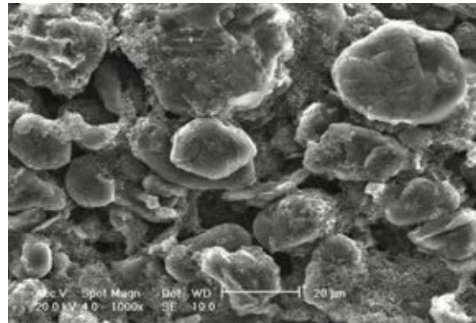


**Figure 2.9:** Scanning electron microscope (SEM) picture of a graphite electrode. The width of the picture is approximately 100 micro meters. [9]

The active mass is not one mass, but rather millions of electrode particles. This is to increase the surface area of the electrode to the carbon black and electrolyte, which are much better conductors of electrons and ions respectively than electrodes. This decreases the resistance of the cell. 2.9 shows a SEM of an graphite electrode. The width of the picture is approximately 100 μm. Note that the electrolyte is not visible in the picture. 2.10



shows an illustration of how the carbon black (black) and binder (orange) connects with the active mass particles.

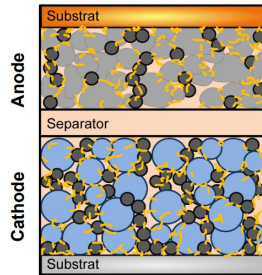


**Figure 2.10:** Illustration of the electrode particles with additives. Reprinted from Haserieder et al. [11]

### Loading, compression and pores

Tuning of different mechanical parameters can achieve different characteristics. This section discussed the loading (active mass per area), compression (active mass per volume), and pore structure and their impact on cell characteristics.

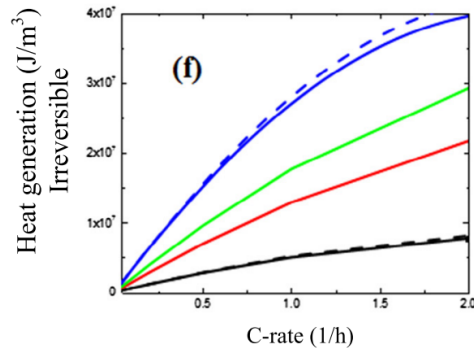


**Figure 2.11:** Heat generation per volume of an electrode as a function of C-rate. Charge cycles are shown as solid lines, while discharge cycles as dotted lines. The plotted lines have following capacities in  $\frac{Ah}{m^2}$ ; 18 (blue), 12 (green), 8 (red) and 2 (black). The lower capacities, the thinner electrode, and the lower heat generation. Reprinted from Nazari and Farhad [27].

The loading of an electrode defines the weight of active mass per area applied to the current collector. In general, a higher loaded electrode will give higher specific energy as more % of the cell is an electrode and non-energy-containing elements such as separator and current collectors. On the other hand, a higher loaded electrode will give a lower resistance, decreasing heat generation and increasing maximum power output. Cells with thick electrodes usually are called energy cells, while cells with thinner electrodes are called

power cells. [28]

The cells studied in this thesis have an anode with an active material thickness of  $43\mu\text{m}$  on each side of the current collector and a cathode with an active material thickness of  $34\mu\text{m}$  on each side [29], meaning the cell leans slightly towards being a high power cell. As discussed in 2.2.6 Singh et al. [24] states high energy cells are in the range of  $50\text{-}60\mu\text{m}$ .

In addition, loading and the compression/porosity of the electrode are crucial. A higher compression of the electrode will decrease the volume, but it also impacts the cell's resistance. A more compressed cell will give lower resistance to the electrons. This is due to the carbon black being packed at higher densities, giving a low resistance path for the electrons. However, a lower compressed cell will give lower ionic resistance due to more electrolyte allowed access to electrode surface through pores between the particles.

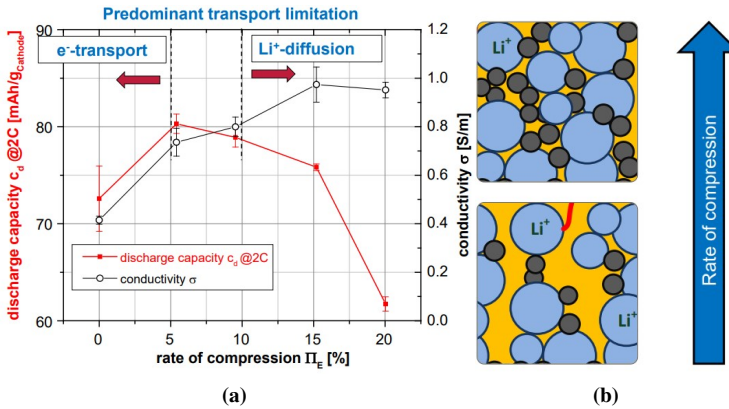


**Figure 2.12:** Electron and ionic resistivity dependency of compression. Reprinted from Haserieder et al. [11]

The "straightness" of the paths the pores create impacts the ionic conductivity, as it determines the length of the ionic pathways. This property is called tortuosity and is calculated by equation 2.3

$$\text{Tortuosity} = \frac{\text{Length of path}}{\text{Distance between ends}} \quad (2.3)$$

## 2.3 General terminology

This section explains general battery terminology and in what context they can be applied in.

### 2.3.1 Open circuit voltage (OCV)

Open circuit voltage (OCV) is the thermodynamical voltage of a cell or the "true potential" of the electrodes. OCV must not be confused with the terminal voltage, i.e., the voltage measured at the terminal of the cells. These differ during and after a load is applied. OCV occurs when no load is applied, and the cell is in electrochemical equilibrium [10]. A quasi-OCV can be obtained within an hour or even at low voltages. As obtaining the true OCV is usually not obtainable in most use-cases, most literature uses the term OCV for quasi-OCV [30].

When Lithium intercalates into the electrodes, the OCV changes. For a commercial cell, the measured OCV is the potential between the electrode. However, by creating half cells, i.e., a cell where one of the electrodes is pure lithium, the OCV for each electrode can be measured independently. OCV as a function of SOC indicates the different processes and phases which the electrodes experience during charge and discharge. [6, 31–33]

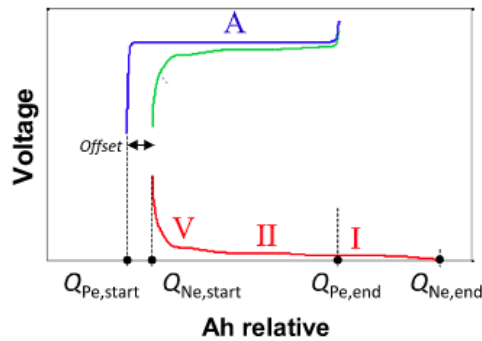


**Figure 2.13:** Figure of voltage during cycling of two half cells and a full cell (green). The red voltage profile is the anode, while the blue is the cathode. Reprinted from [32]

### 2.3.2 Terminal voltage

Terminal voltage is the voltage that can be measured externally at the LiB tabs, and it represents the available voltage for an external device. It is given by

$$U_{Terminalvoltage} = U_{OCV} - \eta(I) \quad (2.4)$$

Where  $U_{Terminalvoltage}$  is the terminal voltage,  $U_{OCV}$  is the OCV,  $\eta(I)$  is the overpotential as a function current. Overpotential are discussed in 2.5.1.

### 2.3.3 C-rate

Normalized Current-rate (C-rate) describes the current of a battery, normalized by its capacity. At a given current, the C-rate is defined as follows:

$$\text{C-rate} = \frac{\text{Current}[A]}{\text{Capacity}[Ah]} \quad (2.5)$$

If a current equal to a C-rate of 3 is drawn, it will be denoted by 3. Capacity in the context of c-rate is the manufacture stated capacity.

Research usually refers to C-rates instead of current due to increasing the comparability between cells. Comparing results when cycling two different cells, one with 1 Ah capacity and 10 Ah at 1 Amp, is usually not of interest. However, comparing the two cells both with a current of 1C is usually more of interest.

### 2.3.4 State of health (SOH)

State of health (SOH) for short, describes the condition of a cell, compared to its condition as new. SOH is defined as follows;

$$\text{SoH} [\%] = \frac{\text{Capacity at current state when fully charged [Ah]}}{\text{Capacity as new [Ah]}} \times 100 \quad (2.6)$$

Note that the capacity of the current state and capacity as new must be measured at the same temperature and C-rate, as capacity is dependent on both.

There are no standard for at what SOH End of life (EOL) occurs. EOL is usually defined at the occurrence of the so-called ageing knee or cell drop-off [5], where the SOH suddenly drops [20]. The aging knee occurs at different SOH depending on cell chemistry as well as production quality, but for most chemistries, it occurs in the range of 80-90 SOH. This is illustrated in 2.14 where the cell start to increase more reapidly at around 80 % SOH. Note that cell A-D are of the same model under same conditions, and the different curves are due to production differences.

The term Energy State of Health (eSOH) will be used when the energy (Wh) is used to calculate the SOH instead of capacity (Ah).

### 2.3.5 State of Charge (SOC)

State of Charge (SOC), is the % of usable charge left in the cell. It is defined as follows:

$$\text{SoC} [\%] = \frac{\text{Usable charge left [Ah]}}{\text{Capacity at 100\% SoC [Ah]}} \times 100 \quad (2.7)$$

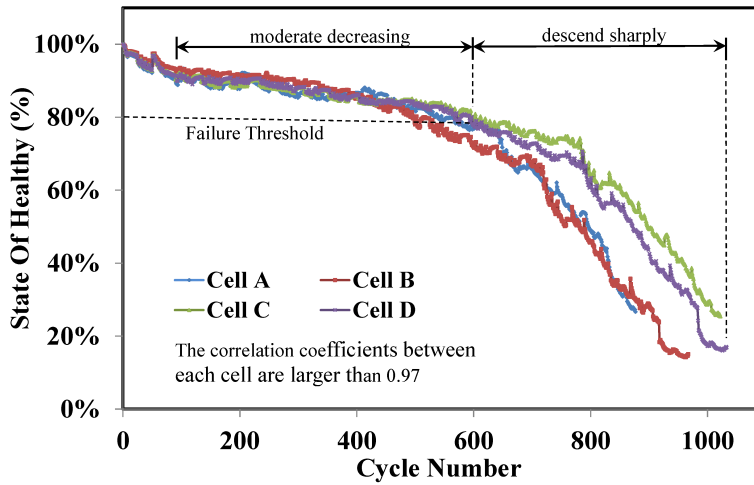


**Figure 2.14:** SOH as a function of cycle numbers. All cells are the same model, and the difference between them is due to manufacturing inaccuracies. Note that the SOH decreases more rapidly at approximately 80 % SoH. Reprinted from Tseng et al. [34]

Note that "Capacity at 100% SoC" is the current capacity of the cell and not the capacity at Beginning of life (BOL).

There is no direct way of measuring SOC. The two most common methods are coulomb counting and using the OCV-SOC relationship. In this thesis, Coulomb counting is used as the SOC estimator. Coulomb counting is the method of counting the net charge transfer (coulombs) in and out of a cell and by that calculating the cells SOC. This requires a known reference SOC and the capacity of the cell. Coulomb counting uses the following formula:

$$\text{SoC} [\%] = \text{SoC}_{ref} + \frac{\text{Net current since reference point [Ah]}}{\text{Capacity [Ah]}} \times 100 \quad (2.8)$$

Where  $\text{SoC}_{ref}$  is the reference point where the SOC has to be estimated by other methods, and where the net current is negative if discharged.

Coulomb counting is an accurate method for few cycles. However, it is prone to drifting, due to measurement inaccuracies as well as coulombic inefficiency. Therefore it periodically needs a new reference point.

### SoC Window

SOC window refers to the extremities of SOC which the cells are to be cycled at. A cell cycled from 30 % to 60 % and discharged from 60 % to 30 % has a SOC window of between 30 and 60% SOC.

### 2.3.6 Constant current - constant voltage (CC-CV)

CC-CV is the most common charging strategy for LiB. The charging protocol starts with a constant current step. The current is kept stable until the a certain voltage is reached. The protocol then moves into the constant voltage step where the terminal voltage is kept stable. As the OCV moves towards the terminal voltage the current will decrease. Charging concludes when the current reaches a certain cut-off current. This is illustrated in figure 2.15.

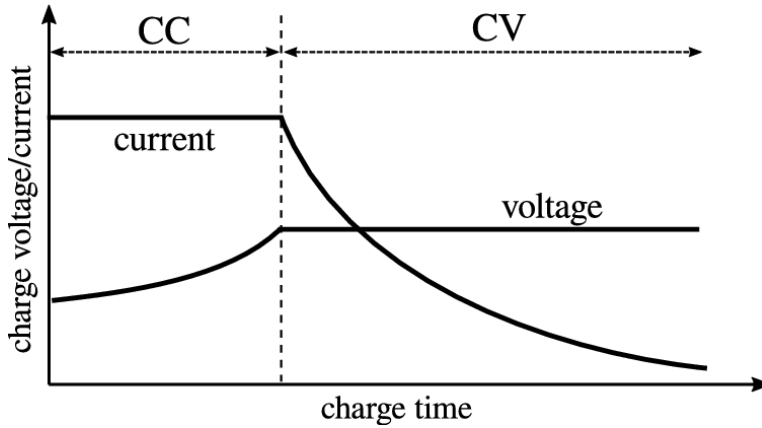


**Figure 2.15:** Current and voltage profile of a CC-CV charge. Reprinted from Maranda [35]

## 2.4 Degradation

This section will introduce the most common degradation mechanisms in a LiB. The degradation is split into three levels; operation effects, effects at the cell level, and the mechanisms that trigger these effects. In addition, the triggering condition will be discussed.

Degradation of cells is the physical change to cells induced by either a current profile or time. Degradation studies are generally split into cycle life and storage (calendar) life studies [12]. In this thesis, if a current profile induces the degradation, it will be referred to as cyclic degradation, while if it is introduced due to time, calendar degradation.

### 2.4.1 External triggering conditions and their effects on operational function

This section will show how the three most important conditions (temperature, SoC window, and current) affect the operational functions; SOH, State of Function (SOF) and impedance. The loss of SOH and SOF is known as capacity and power fade. Note that the correlations explained here are simplified and that the external conditions do not individually impact the degradation but rather the sum of them.

#### Temperature

The correlation between aging and temperature is well documented, where higher temperature increases the degradation rate. The degradation rate approximately grows exponentially with temperature, both for calendar and cyclic aging. [5, 12, 36]

Higher temperatures have an impact on all three operational functions of the battery. The increase of impedance will also harm both SOF and SOH, as well as increasing heat generation.

Lower temperatures will usually decrease the degradation rate. However, lower temperatures, usually from 10  $C^{\circ}$  and down, can temporarily reduce the charging capability of LiB. [5, 37].

Though not always true, degradation due to a temperature is usually connected to the fact that higher temperatures usually increase the reaction rate. [38]

#### C-rate

Degradation rate increases with C-rate [39–42], as illustrated in 2.17.

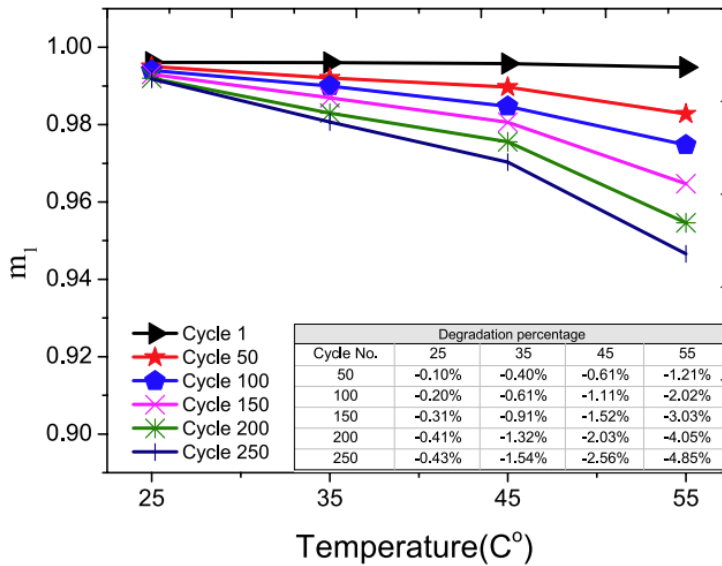


**Figure 2.16:** Cyclic SOH degradation as a function of temperature of an cobalt-oxide electrode.  $m_1$  is SOH given between 0 and 1. Reprinted from Leng et al. [36]

Through de- and intercalation of lithium ions, degradation occurs, mainly due to the mechanical stresses due to volume changes [39]. In addition, higher C-rates follow higher temperatures and, therefore, higher degradation. Research has shown that for cells cycled in poor cooling setups, a large part of the C-rate induced degradation can be explained by the increase in temperature [12, 43]. An increase in impedance is also observed at higher resistance. However, these operational functions are not as strongly correlated to c-rate as temperature.

## SOC

In regards to cyclic and calendar degradation SOC window and SOC impacts degradation, where storage or cycling at high or low SOC promotes degradation. [44, 45]

The degradation due to SOC comes from two main categories of degradation mechanisms. First, at higher SOC materials usually move away from the stable voltage window, which promotes certain reactions, specifically with the electrolyte. [5, 22, 37] Secondly, at these SOC the electrodes are either fully lithiated or delithiated, causing structural stresses. As mentioned in 2.2.1, LCO have to have approximately a lithium-ion for every two cobalt oxide to keep its functional structure. LCO is near this limit at high SOC. Wikner [44] showed that the combination of high C-rates at high SOC windows increase degradation rate in combination with each other.



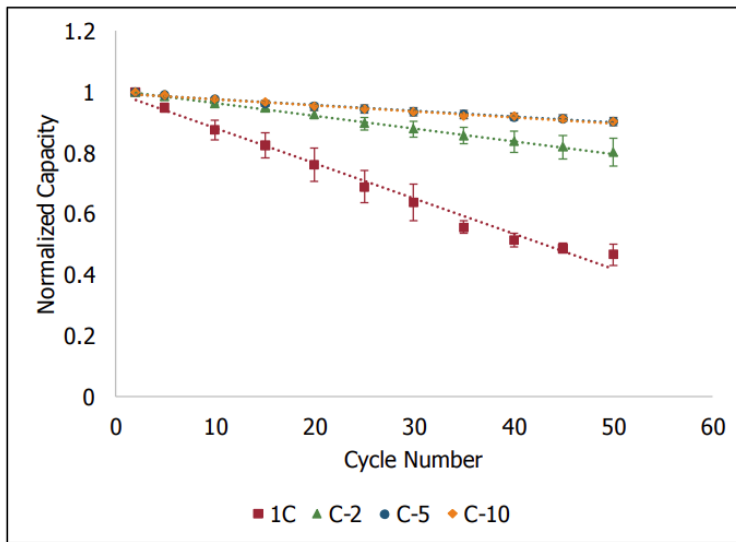


**Figure 2.17:** SOH as a function of cycles at different C-rates. C-10 is notation for 0.1C. Note that C-5 and C-10 lie on each other, making C-10 not very visible. Reprinted from Snyder [39]

### Materials, design and production

In addition to external factors, three other important factors can affect the degradation rates: chemistries, cell design, and cell production.

The most important is the chemistries in addition to all the additives and electrolytes. It is well documented that different chemistries show different degradation rates. [12].

Cell design parameters such as geometry, electrode thickness, porosity, tab placement, etc. affect the degradation effects. These parameters will affect temperature, current densities, inhomogeneous, the cell's resilience to volume change, etc. Cell design can therefore give two cells with the same electrode and electrolyte different degradation rates.

Cell production and deviations from cell to cell can have a meaningful impact on performance. Haserieder et al. [11] cycled three cells which only differed in electrode size and overlap, which can occur accidentally during production. 2.19 shows how this drastically impacted the degradation rate.

### Degradation mechanisms

The following section discusses the underlying mechanisms of degradation. In addition each mechanism is put into the associated category and the external triggering effects identified.

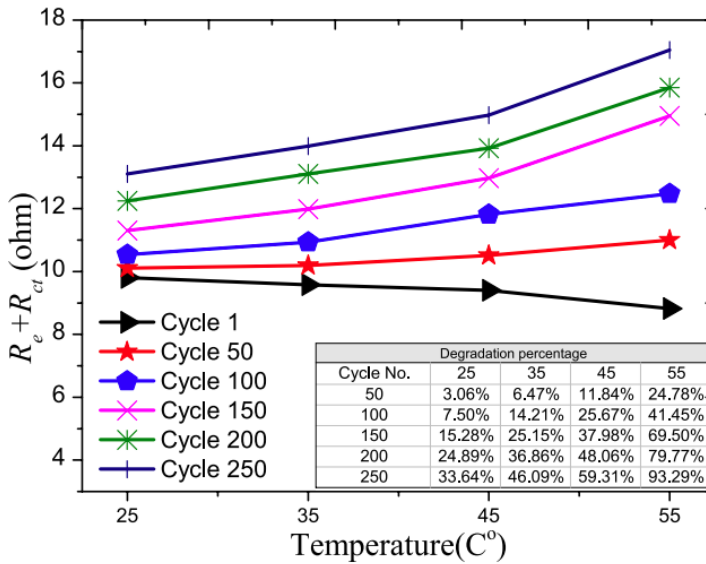


**Figure 2.18:** Impedance as a function of temperature of a cobalt-oxide electrode. Reprinted from Leng et al. [36]

At cell level the degradation can be split into three main modes [5, 6, 12]:

- Loss of active material (LAM) - loss of electrode material that is active in the intercalation processes during discharge or charge.
- Loss of Lithium Inventory (LLI) - loss of cyclable Lithium-ion
- Increase in impedance - causes the cut-off voltage to be reached earlier

Numerous mechanisms can cause these modes, some of the illustrated in 2.20. In this thesis, only the four most relevant mechanisms will be in focus:

- Cracking of electrode particles
- Solid Electrolyte Interphase (SEI) growth
- Lithium plating
- Changes in cathode structure and decomposition

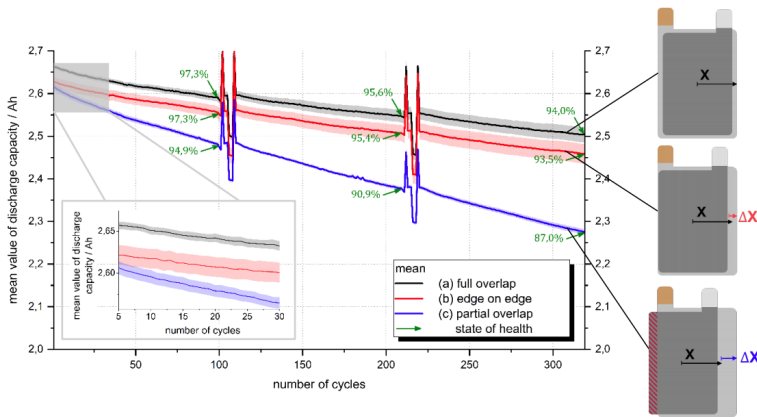


**Figure 2.19:** SOH as a function of number of cycles for three different cells. The cells differ in regards to their anode and cathode placement relatively to each other. Reprinted from Haserieder et al. [11]

## 2.4.2 Cracking of electrode particles

As discussed in 2.2.1 the electrode are made up of many small particles. Due to volume expansion during cycling the particles are prone to cracking [5]. This mechanism is usually triggered by large SOC windows and high currents.

Cracked particles can disrupt paths between electrode particles, carbon black and current collectors [5, 37]. This will lead to a ionic and electronic conductivity loss, i.e. impedance increase, which again leads to both power and capacity fade. If the cracking becomes too severe, particles can become "isolated", leaving no conductive paths for the electrons [48]. This will both give LAM as well as LLI, due to active material not being able to be lithiated anymore and due to the lithium not being "reachable", also known as dead lithium [5]. Lastly, cracking promotes to SEI growth, which will be discussed in 2.4.3.

As discussed in 2.2.1, modern anodes often contain silicon. However, due to its high volume expansion during intercalation, anodes that contain silicon is more prone to cracking.[5, 14, 37] The cell studied in this thesis has a graphite anode with no silicon and is, therefore, less prone to cracking than many other modern cells. However Nishi [49] reports that graphite anodes is experiencing a greather volume change during intercalation than hard carbon, due to the interlayer spacing ( $d_{002}$ ) for graphite is  $0.335nm$  and needs to expand to  $0.372nm$  when the lithium intercalets between the layers. For hard carbon anodes the  $d_{002}$  spacing are over  $0.372nm$  and no expansion can be observed.

Electrodes are more prone to cracking when exposed to use over a large SOC window, i.e., either used to very low or very high SOC or both. This is due to the volume change then being the largest. High currents will also amplify this as the volume change is rapid.

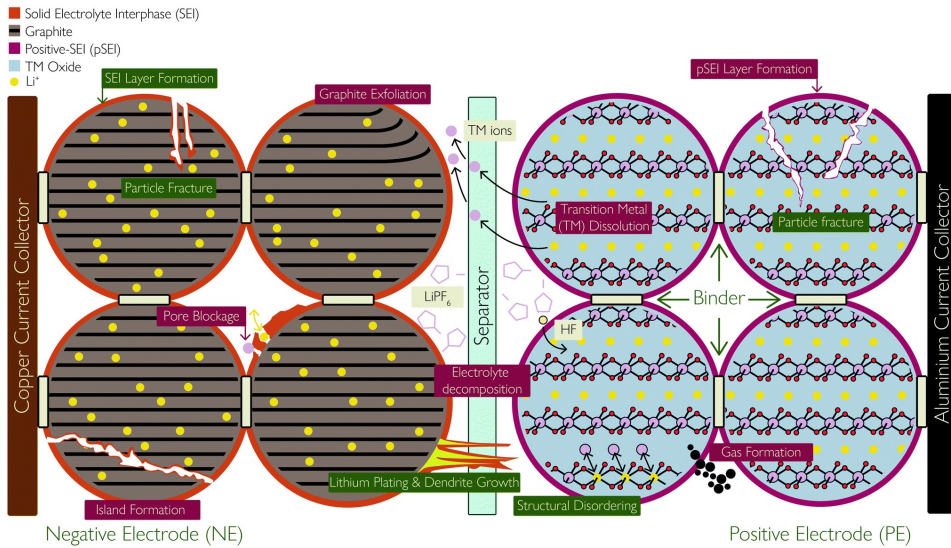


**Figure 2.20:** Degradation mechanisms in a Lithium ion cell. Reprinted from Edge et al. [5], Merla et al. [46]

In addition to intercalation-induced volume change, side reactions during the creation of SEI, discussed in 2.4.3, can create gas inside the electrode. This can lead to the build-up of pressure, which can cause cracking. [37]

Properties of the electrode and especially the binder properties are key factors in the occurrence of cracking. Binders containing fluorine, such as in PVDF, react with the carbon anode and form lithium fluoride. This contributes to degradation in the mechanical stability of the electrode [50–52]. The cell studied in this thesis uses PVDF.

Certain research has hypothesized that a thickness decrease can occur if an electrode has started cracking. This is due to smaller electrode particles being allowed to expand (during intercalation) into smaller and smaller voids between the particles. [53]

### 2.4.3 Solid Electrolyte Interphase (SEI) growth

SEI is a passivation film that forms around the anode particles. It consumes electrolyte and lithium, and the layer itself has relatively high resistance. SEI growth leads to increase resistance and LLI. Research indicates that this effect is the largest of all degradation effects on the anode [12, 37]

In the presence of lithium and the anode's operational voltage, the solvent will react with the lithium ions. They are both consumed, and the product deposits SEI on the anode. SEI works as a passivation film hindering further reactions of the solvent. [5, 22, 37]

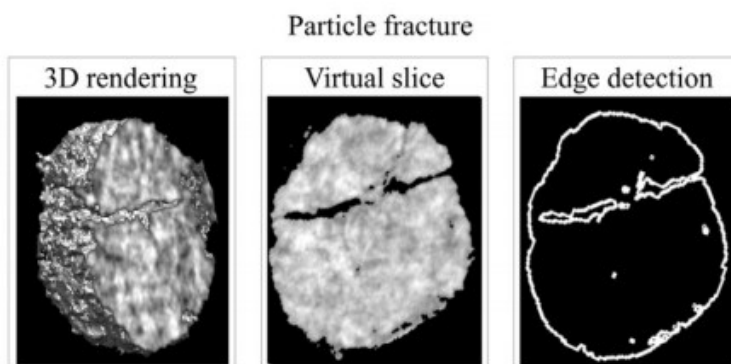


**Figure 2.21:** Multi scale imaging of NMC particle where fracture has occurred. Reprinted from Xu et al. [47]

Note that SEI is not one unique product, but a collective term of products.

Most of the SEI is created at the first cycles known as forming cycles [11, 37]. As the anode is fully delithiated at production, the solvents do not react until the first cycle, when the anode is lithiated and voltage increases. The first charge cycle of the cell results in an approximately ten % reduction in capacity, depending on the cell. [5, 54] The first cycles and the forming of the SEI is considered as a part of the production and not degradation. [11]

After the first cycle, the creation of the SEI the reactions slow down but do not come to a halt. There are three main causes for SEI growth after the initial formation, diffusion, cracking and transition metals diffusing to the anode.

As the SEI is not fully impermeable [20, 37], the electrolyte will continue to diffuse through the SEI and create more SEI. As the SEI thickens, the diffusion slows down. [5, 54] The diffusion rate increases with an increase in temperature. In addition to increasing diffusion rate, an increase of temperature will increase the rate at which the SEI degrades. [37, 55]. The higher voltage at high SOC further destabilises the electrolyte, increasing the SEI growth as well [5, 22, 54, 56]

Due to the same mechanisms as described in 2.4.2 the SEI is prone to cracking, exposing the solvents to the anode, leading to the growth of more SEI [57]. Manufacturers, therefore, design the solvent and add additives to increase the mechanical durability of the SEI [58].

Reactions throughout the cell can deposit products, such as Lithium metal and Transition Metals (TM), on the anode. These can react with electrolyte and create SEI. [5].

Imhof and Novák [59] found that during SEI forming reactions gas side products were created. If this occurs this can be seen as a thickness increase in the pouch.

In the creation of SEI there is the consumption of lithium, leading to LLI which again leads to capacity loss. Growth in SEI increases impedance in several ways; the SEI has low conductivity, it can block anode pores, increasing the tortuosity [5, 20] and in some cases, it is even reported that it can block separator pores. [37] This will lead to a loss of both capacity and power and an increase in heat generation.

The consumption of electrolyte could also decrease the thermal conductivity of a battery. Previous research shows that over half the thermal conductivity of separators and electrodes is due to the electrolyte. [60–62]

### **Materials on the cathode surface**

Though the term SEI is reserved for the layer which forms on the anode, the cathode is not reserved from materials creating an ecapolating film. Some research refers to the materials as positive-SEI, or Positive solid electrolyte interphase (pSEI) [5], though not technically a SEI in the same sense as on the anode.

Previous research [20] have reported that electrolyte oxidation formed could form on the cathode, probably caused by soluble organic materials formed at the anode which has migrated to the cathode [63]. Other side reactions are also documented, and a recurring theme is the reactions caused by hydrofluoric acid (HF), leading to the decomposition of electrolyte and a low conductive film surrounding the cathode. [20] Both lead to an increase in ohmic impedance.

### **2.4.4 Lithium plating**

Lithium plating is when the lithium ions are reduced to lithium metal instead of intercalated into the anode. This consumes lithium ions, leading to LLI, and in extreme cases, lithium metal dendrites grow and puncture the separator, causing an internal short circuit. Plating is prone to happen during high charge C-rate at low temperature.

Initially, lithium ions intercalate into the electrode particle surface. Due to lithium ion concentration gradients, the ions diffuse towards the center. [37] Lithium plating occurs when the charge rate is higher than the diffusion rate, leading to the particle surface is fully lithiated. This renders the particle not able to intercalate lithium ions. Instead of intercalating into the particle, the lithium-ions are reduced, resulting in lithium metal on the anode [5]. A voltage range close to that of pure lithium promotes lithium metal occurring; therefore, lithium plating predominantly occurs on the anode. [37]

The plated lithium can react with the electrolyte leading to SEI growth. This consumes lithium but can also electronically isolate the rest of the lithium. [5] This is known as "dead lithium." Both these processes lead to LLI. Plated lithium can also close pores, leading to higher tortuosity, leading to an increase in impedance.

If the Lithium metal is not yet covered in SEI the Lithium can be stripped. This is the inverse reaction, where the Lithium metal diffuse back into the electrolyte as Lithium ions. The Lithium ions are then still cyclable. [5]

In extreme cases, the plated lithium can create dendrites that grow through the separator and reaches the cathode. As shown in 2.22, this can create an internal short circuit, which will render the battery useless and can lead to thermal runaway, where the cell uncontrollably increases in temperature. [64]

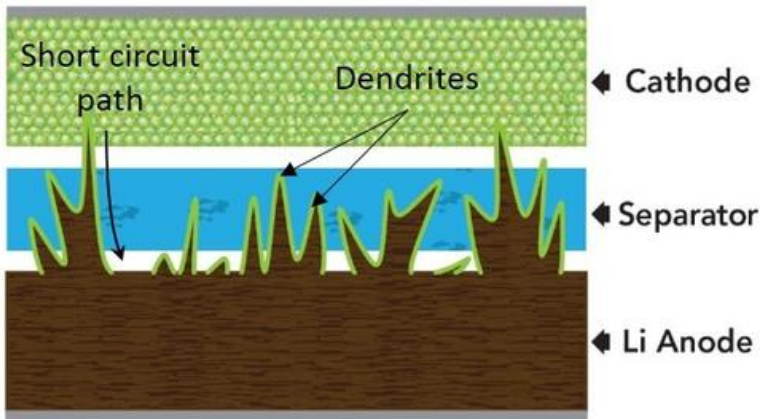


**Figure 2.22:** Illustration of Lithium metal forming dendrites which penetrates the separator. Reprinted from MSE Supplies [64]

The volume of plated Lithium is larger than the volume change due to lithium intercalation into the electrodes. Plated lithium, therefore, can show itself through a thickness increase. However, this is shown to be of less importance than cracking. [53]

Lithium plating comes due to a mix of circumstances; temperature, high SOC and high currents. At lower temperatures, intercalation reactions and diffusion rates slow down. This increases the chances of plating. High SOC implies a highly lithiated anode, which also lowers the diffusion rate. Lastly, the current is highly impactful due to if the reactions and diffusion rates can not facilitate the current densities, then plating will occur. [37]

LAM and areas of high resistivity will increase the chance of Lithium plating. This is due to less active material being available to intercalate, and therefore the threshold between diffusion rate and current will be reached at a lower current. [5, 20]

### 2.4.5 Decomposition and structural change of the cathode

The three sections above regarding SEI growth, cracking, and lithium plating is about mechanisms that have a higher impact on the anode than the cathode. These mechanisms have in common that they do not change the anode's structure but rather the interphases

and mechanical properties. However, the degradation mechanisms for the cathode are mainly through decomposition and structural changes.

Cobalt oxide has a what is referred to as a layered structure. [9, 12, 37] To maintain a structure which lithium ions can be intercalated into, the material has to keep in the range of [9, 65]:

$$Li_{1-x}CoO_2 \text{ where } 0.5 < x < 1 \quad (2.9)$$

Though there are structural changes in these ranges, these changes are reversible. A deviation from this, can cause the irreversible structure to change, and the cathode can not correctly function again.[9, 37] At higher voltages, some of the transition metals can decompose from the cathode and deposit on the anode. [66]

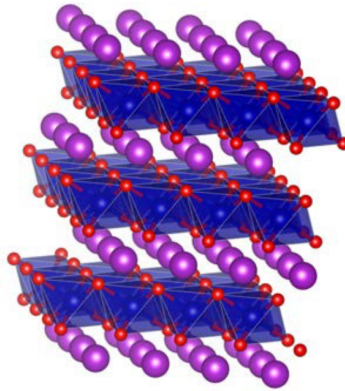


**Figure 2.23:** Illustration of the crystal structure of an LCO electrode. Blue spheres are cobalt, purple lithium and red oxygen. Reprinted from Gregory L. Plett [9]

The cell studied has a  $LiPF_6$  electrolyte solution and with the unavoidable presence of trace HF. These react and consume the electrolyte. [37, 54] This can also cause gas products [67, 68] and migration of transition metals from the cathode to the anode. The latter can cause higher thermal resistance and well as LAM. [54, 69]



## 2.5 Thermal properties of a Lithium-ion batteries

In this section, the thermal properties of LiB will be discussed. First, heat generation and thermal conductivity will be discussed, then how thermal gradients develop through the cell during use. Lastly, the consequences of thermal gradients will be discussed.

### 2.5.1 Heat generation in a Lithium-ion batteries

In this section, the different heat generation sources will be discussed. 2.24 shows the four primary sources of heat generation in a LiB; overpotentials/impedance, reversible entropic heating, the heat of mixing, the heat of phase change. However, only overpotentials and reversible entropic heating will be discussed in this work, as the three others are negligible in many use cases. [70–72]

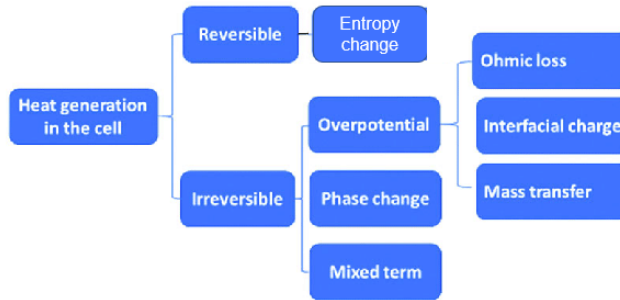


**Figure 2.24:** Illustration of all the heat generation sources in a LiB. Reprinted from Zhang et al. [72]

Heat generation in a LiB is described in equation 2.10 where  $\dot{Q}_{irr}$  is the irreversible contribution and  $\dot{Q}_{rev}$  its the reversible heating. The next paragraphs will describe the different contributions.

$$\dot{Q} = \dot{Q}_{irr} + \dot{Q}_{rev} \quad (2.10)$$

#### Irreversible heating

Irreversible heating is heating due to overpotentials. An overpotential is the potential difference between the theoretical voltage of the electrodes and the measured voltage during operation [73]:

$$\eta = OCV - U_{terminal} \quad (2.11)$$

where  $\eta$  is overpotential.

There are three main overpotential contributors, all related to kinetic polarization effects, which occurs when a load is applied. [74, 74, 75];

1.  $R_{ohmic}$  - Ohmic overpotential - related to the resistance in cell materials and contact between them. Occurs instantaneously with an applied current.
2.  $\eta_{ct}$  Charge transfer overpotential - related to the charge-transfer processes which occur at the interface of the electrodes. The majority occurs in the range of 50 to 5000 ms after a current is applied. Charge transfer overpotential is also known as interfacial charge or activation overpotentials.
3.  $\eta_{con}$  Concentration overpotential - related to concentration gradients in the materials, mainly in the active material. Highly dependent on load hysteresis. Also known as diffusion or mass transfer overpotential.

These overpotentials will impact the voltage measured at the cell's terminals, and instead of providing usable power, these voltage drops will instead cause heat generation. This implicitly means that the efficiency ( $\varepsilon$ ) and heat generation of a cell is highly correlated, as efficiency is defined as:

$$\varepsilon = \frac{OCV - \eta}{OCV} \quad (2.12)$$

Where  $\eta$  is the sum of all the overpotentials.  $\eta$  can be expanded and written more precisely as:

$$\eta = R_{ohmic} \times I + \eta_{ct}(I) + \eta_{con}(I) \quad (2.13)$$

$R$  is the ohmic resistance,  $I$  is the current, and  $\eta_{ct}(I)$  and  $\eta_{con}(I)$  are the charge transfer and concentration overpotentials as a function of  $I$ . Note that the ohmic overpotential acts as a regular resistance. The overpotential is therefore proportional to the current squared, while the other overpotentials are not as easily described in relation to the current.

Charge transfer overpotential is associated with the reactions at charge transfer processes at the electrode surface. The loss in potential is due to the barrier for the reaction to occur. The dynamics of the process can be described by the Butler-Volmer equation [54, 73]:

$$j = j_0 \left( \exp \left[ \frac{\alpha_a z F}{RT} (\eta) \right] - \exp \left[ \frac{\alpha_c z F}{RT} (\eta) \right] \right) \quad (2.14)$$

$j$  is the current density,  $j_0$  is the exchange current density,  $E$  the electrode potential,  $E_{eq}$  the equilibrium potential,  $T$  the absolute temperature,  $z$  the number of electrons,  $F$  the

Faradays constant,  $R$  the universal gas constant and  $a_c$  and  $a_a$  respectively the cathodic and anodic charge transfer coefficient.

Due to the complexity of acquiring the Butler-Volmer parameters inputs as well as being computationally heavy, the charge transfer overpotentials are often calculated through simplified equations. One equation is used for large overvoltages where the overvoltage is proportional to the log of current, and one for small overvoltages where the overvoltage is proportional to the current. [54, 73] The simplest method for describing the charge transfer overpotential is by describing it as a resistance. [76] This is in many applications accurate enough with the benefit of being simple in both measuring and modeling.

In this thesis, the overpotential caused by concentration polarisation will not be characterized. Due to its strong correlation to hysteresis and the smaller amount of contribution to heat generation, the neglect of this overpotential reduces complexity at a cost of accuracy.

The irreversible heat generation is given as following<sup>1</sup>:

$$\dot{Q}_{irrev} = -I(U_{OCV} - U) = I^2 \times R_{ohmic} + \eta_{ct}(I) \quad (2.15)$$

### Overpotential dependency with temperature and SOC

Overpotentials have a strong correlation to a long range of factors, most notably temperature and SOC [77]. These dependencies also change with aging, as described in 2.4

The internal resistance is a sum of several contributions; tabs, current collectors, contact between electrode particles, contact between electrodes and current collectors, and the electrolyte, [78, 79] where the majority lies in the electrolyte [80]. A decrease in temperature increases the viscosity of the electrolyte. This reduces the mobility of ion-carrying salts in the solvent, increasing the impedance. This increases the resistance [80].

Figure 2.25 shows that internal resistance increases with ageing. The correlation with SOC is also minimal and will be neglected in this thesis.

Figure 2.26 shows how the charge transfer overpotential changes with temperature and SOC. As with ohmic resistance, the charge transfer has an approximately logarithmic increase with temperature decrease. Charge transfer resistance has a complicated dependency to SOC but increases at very high and low SOC. This is related to the mechanisms that occur when one of the electrodes is fully lithiated or delithiated. This correlation is shown in figure 2.27. The y-axis is  $R_d$ , which is the "Direct current (DC) resistance." This is in this thesis defined as the sum of the ohmic resistance and charge transfer resistance. Note

<sup>1</sup>The sign for heat follows the convention of the IUPAC (International Union of Pure and Applied Chemistry), where heat adsorbed by the system is positive, and heat emitted negative.

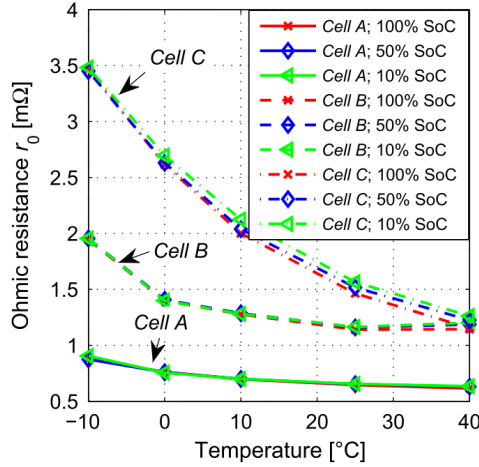


**Figure 2.25:** Ohmic resistance of a LiB as a function of temperature. Cell A is a new cell, Cell B a calendar aged cell, and C a cycled aged cell. Reprinted from Waag et al. [77]

that ohmic resistance has a negligible dependency on SOC and the change in  $R_d$  with SOC can be contributed to a change in the charge transfer resistance.

With the equation for irreversible heating 2.15 and 2.27, it can be deduced that the amount of irreversible heating is highly dependent on temperature and to some extent SOC.

### Entropic reversible heating

The de- and intercalation of lithium ions during cycles can cause endo- or exothermic reactions due to entropy changes. The change in the direction of de- and intercalation will change exothermic reactions to endothermic and also the other way around. The reversible heat is given by: [81]:

$$\dot{Q}_{rev} = I \times \frac{\Delta S \times T}{F} \times T = I \times \frac{\delta U}{\delta T} \times T \quad (2.16)$$

$I$  is current in ampere,  $\Delta S$  is change in entropy in Joules per Kelvin,  $T$  is absolute temperature in Kelvin,  $F$  is the Faraday constant and  $U$  the potential in volts. Note that a change in sign in current or  $\Delta S$  will change the sign of the heat generation.

The  $\Delta S$  coefficient is strongly dependant SOC and somewhat pressure and temperature [81]. The structure of the electrodes heavily impacts the profile of  $\Delta S$ , which can give distinct profiles for different chemestries. [82] The entropy coefficient for the Melasta cell in this thesis has been measured by MacDonald [83] and can be seen in figure 2.28. As the

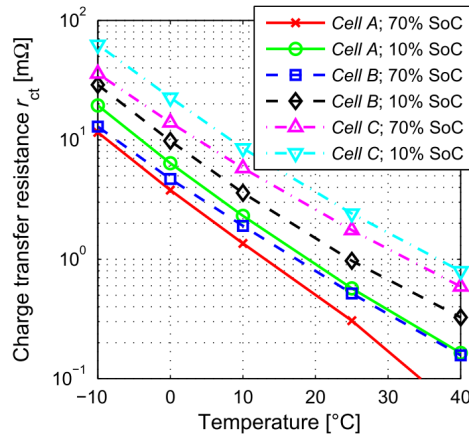


**Figure 2.26:** Charge transfer overpotential presented as resistance as a function of temperature. Cell A is a new cell, Cell B calendar aged and Cell C a cycled aged cell. Note that the y-axis is logarithmic. Reprinted from Waag et al. [77]

cell in question has LCO electrode which have high  $\Delta S$  compared to the other common cathodes [84], the reversible heating can actually be seen clearly during constant current cycles 4.22c.

Note that even though the entropic heat is proportional to the temperature, as it is the absolute temperature, even a substantial temperature change in the operational temperature window will not change the  $\dot{Q}_{rev}$  substantially.

The reversible heat is proportional to the current, opposed to the Joule heating, which is proportional to the current squared, meaning that for lower currents, the entropic heating term will have a higher relative impact on the heating of the battery than under higher currents. [84]

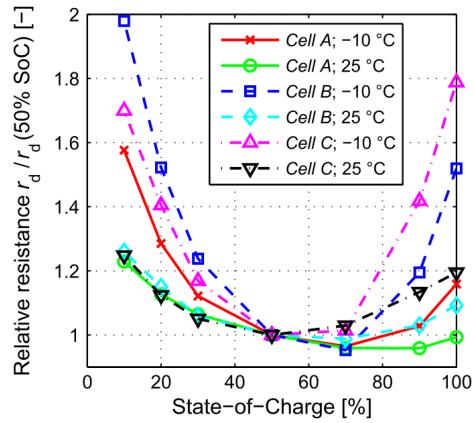


**Figure 2.27:** The sum of ohmic resistance and charge transfer resistance as a function of SOC. The resistance is normalized by the resistance at 50% SOC. Cell A is a new cell, Cell B calendar aged and Cell C a cycled aged cell. Reprinted from Waag et al. [77]

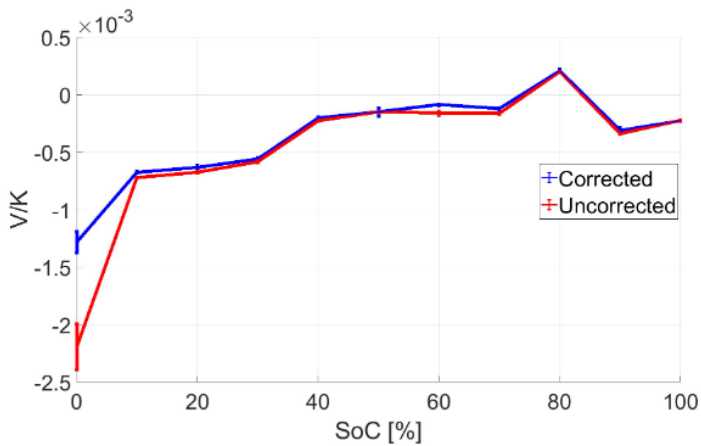


**Figure 2.28:** Entropy curve for the same cell used in this thesis. Uncorrected shows the entropy without correction for the non-equilibrium state of the cell during the measurement. Reprinted from MacDonald [83]

### 2.5.2 Thermal conductivity in LIB's

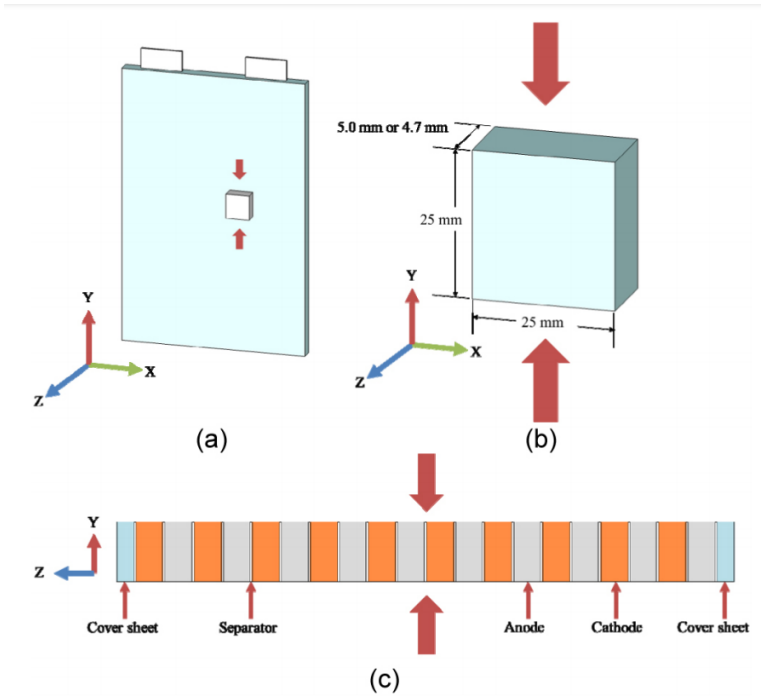


**Figure 2.29:** Figure of the coordinate system used to describe Pouch Cells in this thesis. Reprinted from Sung et al. [85]

The thermal conductivity of a battery cell is not homogeneous or isotropic, which makes it hard to characterize. Because of the layered structure of the cell, the thermal conductivity varies in the directions of the cell. The coordinate system referred to in the cell is shown in figure 2.29. The thermal conductivity of a LIB pouch cell is usually at least an order of magnitude higher in the X-Y plane (in-plane) than thru the cell in the Z direction (thru-plane) [60]. The high conductivity in the X-Y plane is due to the current collectors working as heat sinks through the planes. The separator and active components with lower thermal conductivity work like insulation in the Z-direction, drastically lowering the thermal conductivity. To calculate the thermal conductivities, it is usually necessary to measure the conductivity for each component and to sum the conductivity in equation 2.17 and 2.18 [86] where  $k_i$  is thermal conductivity and  $d_i$  is the thickness of the respective component, and  $d_{cell}$  is the total thickness of the cell.

$$k_{eff\ through-plane} = \frac{d_{cell}}{\sum \frac{d_i}{k_i}} \quad (2.17)$$

$$k_{eff\ in-plane} = \frac{\sum(k_i \cdot d_i)}{d_{cell}} \quad (2.18)$$

The thermal conductivity of the Melasta SLPBB042126HN cell used for the characterization tests in this thesis was done by Trandem [29], the thermal conductivity of each component were tested, and the total conductivity was calculated. With the conductivity values from table 2.1 from the wet measurements at 2.7 bar compaction pressure, the total thermal conductivity of the cell is in the two directions were measured to be  $k_{eff\ in-plane} = 50.45 \frac{W}{m \cdot K}$  and  $k_{eff\ through-plane} = 0.69 \frac{W}{m \cdot K}$ . The conductivity in the in-plane direction is two orders of magnitude greater than in the thru plane direction, which is a significant contributor to how thermal gradients spreads in a LiB. When calculating the effective thermal conductivity for a dry cell without electrolyte, which can be seen as a worst-case of degraded electrolyte the same in- and thru plane thermal conductivities becomes  $k_{eff\ in-plane} = 49.97 \frac{W}{m \cdot K}$  and  $k_{eff\ through-plane} = 0.32 \frac{W}{m \cdot K}$ . It can be seen that the in-plane conductivity is almost unaltered due to the current collectors maintaining their conductivity while the dry thru-plane conductivity is down to 46% of a wet cell. These results are similar to what Bazinski and Wang [75] reports on measurements thru plane on a whole pouch cell. The thermal conductivity of an equal wet and dry cell is measured to be  $0.42131 \frac{W}{mK}$  and  $0.21916 \frac{W}{mK}$  respectively, meaning the dry cell has only 52% of the wets conductivity.

**Table 2.1:** Thermal conductivity measurements done on components in the Melasta cell by Trandem [29]. The thermal conductivity for the electrode materials is for the active material only.

Material	dry 2.7bar	wet 2.7bar
Separator	$0.111 \pm 0.016$	$0.21 \pm 0.03$
LCO Cathode	$0.36 \pm 0.14$	$1.1 \pm 0.5$
Graphite Anode	$0.5 \pm 0.2$	$1.21 \pm 0.06$

It is thought that the thermal conductivity can change when a LiB changes when the cell degrades with ageing. Richter [87] measured the thermal conductivity of the electrodes on a Lithium Nickel Manganese Cobalt Oxide (NMC) cell with hard carbon Anodes in pristine condition and after 4400 normalized 1C cycles. He reports that the conductivity of the active material is close to unaltered after the ageing of the cell, he found an insignificant change in the anode conductivity and an increase in the conductivity for the cathode material.

### Changes in thermal conductivity in LiB

It is known that the thermal conductivity of a  $LiCoO_2$  cathode decrease when it delithiates. Cho et al. [88] made material with electrochemically tuneable thermal conductivity based on a  $LiCoO_2$  cathode materials lithium filling. Their results showed a reversible change from 5.4 to  $3.7 \frac{W}{mK}$  when the material delithiated from  $Li_{1.0}CoO_2$  to  $Li_{0.6}CoO_2$ . The results showed the SOC dependence on the thermal conductivity of a LiB could vary, so when looking at the SOH dependant properties, it is important to do the measurement at the same SOC to get the comparable results.



The degradation of thermal conductivity in a Lithium Manganese Nickel Oxide (LMNO) cell was investigated by Jagannadham [62]. In their findings, it is reported that there are four clear contributors to an increase in the thermal resistance thru the cell due to aging by charge-discharge cycling the cell. These are the volume change together with the crack formation in the cell, formation of interfacial phases such as  $Li_2O$  and  $LiOC$  with low ionic and thermal conductivity, and interface thermal conductance between the cathode and current collector due to the volume change and the formation of discontinuities in the cathode layer.

### 2.5.3 Thermal gradients in a LiB and their impact on performance

Several studies show that the geometry and chosen cooling method impacts the thermal gradients within a cell. These thermal gradients will result in current gradients, lower efficiency, and therefore loss in capacity. [4, 7, 89, 90]

Thermal gradients in cells occur because the thermal conductivity of the cell material is finite. The in-plane thermal conductivity in a LiB is usually one or two orders of magnitude greater than the thru plane conductivity[60]. This leads to the build-up of thermal gradients in the cross-plane direction, leading to the core or the un-cooled surface of the cell being hotter than the rest for a pouch cooled cell[90]. It is thought that tab-cooling limits the build-up of gradients because the heat is transported thru the current collectors up to the tabs.

With thermal gradients follows impedance gradients. As the impedance grows exponentially with a temperature decrease, the cell's total impedance will increase if the average temperature is steady while gradients increase.

Each unit cell within the cell can be looked at as separate cells connected in parallel. It is well documented that a different internal resistance results in different currents for each cell. [43, 89, 91] This follows due to Ohms law:

$$I = \frac{\Delta U}{R} \tag{2.19}$$

As cells that are connected in parallel have the same terminal voltage, a cell with lower resistance has to have a higher current to achieve the same terminal voltage. Note that this is given equal OCV. If the current drawn from the cell is the same, resistance gradients will result in a total higher Root-mean-square (RMS) for the current densities.

As the ohmic overpotential is proportional  $I^2$ , a higher RMS current will give for a lower efficiency as well as reaching the cut off voltage earlier. This effect is also self-inducing as a higher overpotential for the hotter unit-cells will give for more heat genera-

tion, further increasing the temperature gradients.

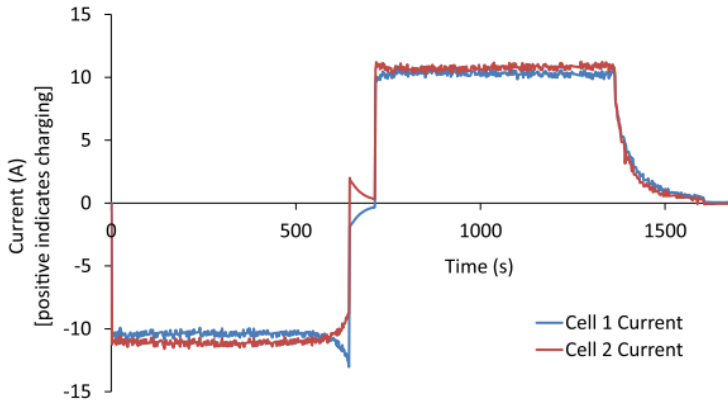


**Figure 2.30:** Current profile for two cells in parallel. Cell 2 has lower resistance than Cell 1. Note that between 650 and 750 seconds, no external loads are on the cells, and the current is due to a voltage difference in the two cells. Reprinted from Gachot et al. [92]

Inhomogenous current densities will make the cell internal balanced, i.e., that the SOC of each unit cell is different [90]. For LCO at lower SOC the voltage drastically decreases [10]. This will make the hotter unit cells have lower OCV, and at a certain point, the difference in OCV between the hot and cold unit cells dominated the contribution indifference in overvoltage. This is shown in practice in 2.30. Two cells of different resistance are connected in parallel. As Cell 2 has a lower resistance, it initially has a higher current. As the cells near depletion at the 700 mark, their OCV starts to drop. But since Cell 2 has a lower SOC it drops more rapidly, and Cell 1 starts to contribute with more current. The difference in SOC can be seen at the 700 mark when there is no external current. Since Cell 2 has a lower SOC and therefore a lower OCV than Cell 1, Cell 1 charges Cell 2 until they have the same SOC.

In figure 2.31 we see Dondelewski et al. [7] illustrates the usable capacity for a LiB with two different cooling systems, one where the pouch is cooled on one side and the other where the tabs are cooled and thereby cooling the cell internally. It can be seen from the illustration that the usable capacity of two cells with the same average temperature differs. A hotter cell will have more useable capacity, but because this relationship is not linear, the gained capacity from having parts of the cell at a hotter temperature and parts at a colder temperature is out weight by having the entire cell at the same average temperature.

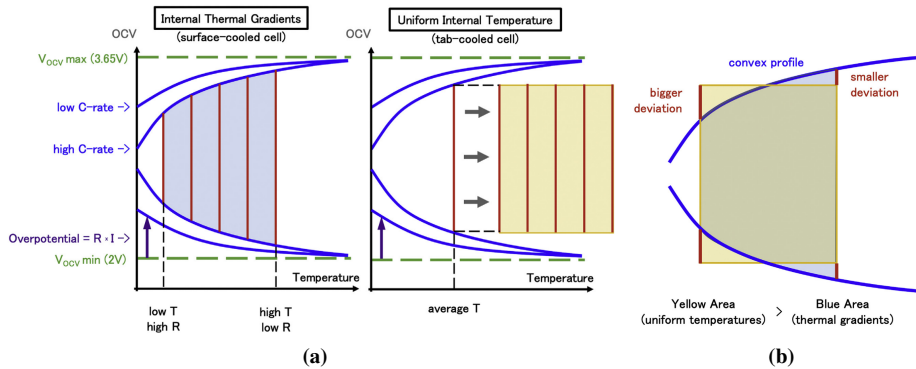


**Figure 2.31:** Effect of temperature gradients in cells. Figure (a) shows the available capacity of two cells with the same average temperature and different cooling systems. The blue area illustrates the usable capacity in a one-side surface cooled cell, with a temperature gradient thru the cell. And the yellow area is the a representation of a tab cooled cell held at the same average temperature, the yellow area is folded out to see the available capacity as an area. Figure (b) shows the overlap, and the extra capacity available in the tab cooled cell due to the convex relationship between overpotentials and temperature. Reprinted from Dondelewski et al. [7]

## 2.5.4 Heat rejection from Lithium-ion batteries

To compare the cooling capabilities of different LIB's is a challenging task. The heat generation, geometry, and material properties all take part in defining how much heat can be transferred out from a surface of a cell. Hales et al. [8] developed a method to evaluate the heat rejection of a LiB thru a single number defining the heat rejection thru a single surface of the cell. The coefficient is called the Cell Cooling Coefficient (CCC) with the units  $\frac{W}{K}$ . While the Biot number, thermal conductance number, and the thermal resistance parametrize a body's ability to conduct heat from one plane to another, it is not suitable for bodies that produce heat or have uneven thermal conductivity like the layered structure of LIB's have.

$$CCC_i = \frac{\dot{Q}_i}{\Delta T_{cell}} \quad (2.20)$$

To evaluate the heat transfer and cooling capability of a Lithium-ion battery it is usually necessary to know the thermal conductivity of all the materials the electrodes, separator, and current collectors, these properties are dependent on the electrolyte composition and aging of the cell. These values differ from cell to cell and require extensive material testing to get accurate values. [60]

$$CCC = \frac{\dot{Q}}{\Delta T} \quad (2.21)$$

The papers of Hales et al. [8, 93] introduces the  $CCC_{Tab}$  and  $CCC_{Pouch}$  these coefficients describes the temperature difference needed from the hottest part of the cell to the temperature of a specific cooled side of the cell needed to transfer a amount of heat. The CCC is defined in equation 2.21 where  $\dot{Q}$  is heat rejected from the measured surface,  $\Delta T$  is the temperature difference from the hottest part of the cell to the cooled surface. This definition gives a possibility to compare different cells without taking into account the different geometry of the cells.

Since the CCC is defined as the heat transferred from a cooled surface it is independent of the cell geometry and cooling method. Giving a possibility to compare different cooling systems for a single cell, or compare what temperatures you must have available for a set cell to be used in a pack with a cooling system.

The CCC method for characterizing the thermal properties of LiBs was adapted and used in this thesis. The work of Hales et al. [8, 93] were used as a baseline. And the method were adapted and used to characterize the cells during ageing. The method used is described in section 3.4.

### **Different cooling strategies, with advantages and disadvantages**

The heat production of LiB and the quite narrow working temperature range usually demands a cooling system for a battery pack. A cooling system must keep the cells in a safe working temperature, usually below 60°C for charge and discharge and over 10°C for charging, a thermal management system should be able to keep the cells within the optimal range of 15-35°C [94] while keeping the difference between cell temperature as low as possible. Keeping the temperature gradients as even as possible is an important aspect to not get uneven degradation and SOC distribution in the pack. [91].

Battery thermal management systems can be categorized after the cooling medium used, where air and liquid cooling is the most common. Phase Change Material (PCM) solutions has been suggested as alternatives [95, 96], these can rely on the latent heat in the phase change from solid to liquid or liquid to gas. Passive systems that rely solely on taking up the produced heat in the thermal mass of the batteries is also used.

The liquid cooling systems is generally more effective than air cooling due to the higher ability to take up and transfer heat, but is usually heavier and more complex than air cooling systems. Both can work either directly where the liquid or gas cools the cell by passing over the surface. Or indirectly thru cooling blocks or radiators. A pouch cell can be cooled either thru the pouch or the tabs of the cell [97]. The geometry of the cell plays a huge role when choosing if the cell can be cooled best thru the pouch surface or the tabs [7].

## 2.6 Melasta SLPBB042126

The cell used in this thesis is a Lithium Cobalt Oxide (LCO) produced by Shenzhen Melasta Battery Co. Ltd. The cell is high power and energy density. The cell's key characteristics can be found in table 2.2 and the rest of the manufacturer's info can be found in the datasheet in appendix A.

**Table 2.2:** Values from the Melasta SLPBB042126 Datasheet, the complete datasheet could be found in Appendix A, [98]

Cell Cathode Material		$LiCoO_2$
Typical Capacity		6550mAh
Nominal Voltage		3.7V
	Maximum voltage Cut of voltage	$4.2 \pm 0.03V$ 3.0V
Charge condition	Max continuous charge current	13.1A(2C)
	Peak charge current	64A(< 0.5s) 54A(< 1s)
Discharge condition	Max continuous discharge current	65.5A(10C)
	Peak discharge current	98.25A(15C)(< 5s)
AC Impedance		< 1.5mOhm
Operating temperature	Charge	0°C – 60°C
	Discharge	-20°C – 60°C
Cell Dimensions	Thickness	$10.3 \pm 0.3mm$
	Width	$42 \pm 0.5mm$
	Length	$127.5 \pm 0.5mm$
	Distance between tabs	$2mm \pm 1mm$
Cell Tab Dimensions	Tab width	12mm
	Tab thickness	0.2mm
	Tab length	30mm
Weight		$128.5 \pm 3.0g$



# Characterization and ageing cycles

This chapter aims at describing the methods used. Ageing cycles and set-up is explained, as well as how and which characterizations were done. The chapter is split into the following sections:

- Degradation cycles
- Degradation setup
- Degradation mechanisms
- Cell Cooling Coefficient (CCC)
- Heat generation
- Capacity analysis

## 3.1 Degradation cycles

Two categories of ageing cycles were discussed; constant current discharge and charge and cycles that resemble a car with regenerative braking. The latter was more applicable for a real-life automotive application. However, cycles with constant current discharge and charge were decided for due to most research using this kind of cycling, and this gave a more extensive set of research that could be used to understand the degradation mechanisms in this thesis. In addition, running parallel to the thesis, other research on the same cell was in progress at the same institute at Norwegian University of Science and Technology (NTNU). This research used constant current discharge but at different thermal conditions. A similar cycle was seen as beneficial as later research could build upon the two datasets which were created.

A high C-rate was seen as beneficial due to two main factors. Firstly, higher C-rates would create higher thermal gradients, and it was hypothesised that this would increase the

difference in degradation between tab and surface cooling. The high C-rate would allow to easier identify the degradation differences between tab and surface cooling, at the cost of measuring the magnitude of each of the degradation mechanisms in an automotive application. Secondly, there were concerns regarding the possible lack of degradation of the cell within the time frame. As discussed in 2.4, high C-rates would increase degradation rates, as well as allow for more cycles in the same time frame.

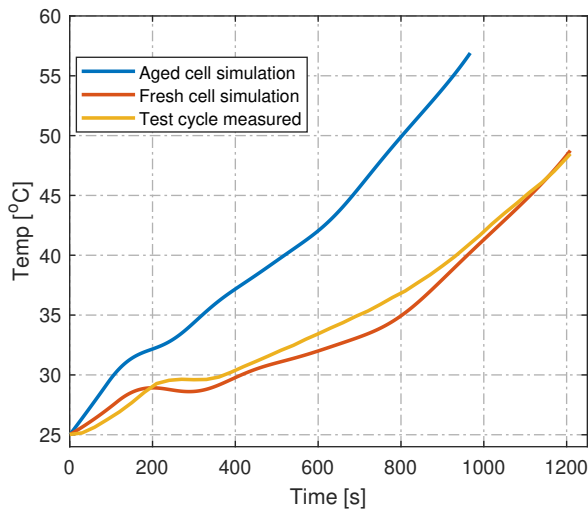


**Figure 3.1:** The simulated temperature at EOL at 3C. In addition the first cycle simulated and the first cycle measured is plotted.

A high C-rate also gave concerns regarding the temperature throughout ageing cycles. As impedance increases, the total heat generation increases. The impedance increase could inhibit the cell from cycling without entering over temperature. Trandem [29], MacDonald [83] developed a thermal model for the cell in question in an adiabatic system. An assumption was made that charge transfer and ohmic resistance tripled at EOL and reversible heating was stable. The model showed that a 3C would allow for cycles without entering over-temperature. A higher C rate was not desirable because it would be too far away from most real-world applications. 3C constant current cycle was chosen. The degradation cycles were stepwise as follows:



- CCCV of 3 C and shut of current of 1 C at 4.195 V
- Rest for 15 minutes and temperature under 27/19°C (Setup 1/Setup 2)
- Discharge at 3 C and shut of voltage of 3.05 V
- Rest for 5 minutes
- Characterization testing every 200 cycles or a decrease of  $\geq 2.5\%$  SOH since last characterization

The maximum allowed temperature was set 57.5°C during charge and 65°C during charge. If the temperature exceeded the temperature limit, cycling stopped for 5 minutes before returning to step 1.

Characterization testing was periodically done and are explained in the following sections.

## 3.2 Degradation setup

For the degradation setup, a cooling system was replicated. A cell within a battery pack would usually be surrounded by cells of the same temperature on all sides except the cooled one. As the temperature deviation is zero between cells, a heat transfer of zero is assumed. To replicate the surrounding cells, they were isolated in styrofoam. The cells were then placed in a thermal chamber. For cooling, a water bath connected to cooling blocks placed on the cooled surface were used. The water baths were kept at a constant temperature.

For the pouch cooled cell, the cooling block was directly placed on the pouch. For the tab cooled cell, an aluminium plate was connected to the tab to allow for a larger cooling block than the size of the tabs. Thermal paste was used between the cooling block and the pouch/aluminium plate to increase thermal conduction.

The temperature was measured at the middle of the pouch by a thermistor. Optimally more thermistor would be employed, but due to accessibility in the number of thermistors, a maximum of two was used for each cell.

To ensure good and replicable electrical contact at the tabs, two copper blocks were used to ensure uniform contact to the tab. A voltage sensor and current line were fastened to the copper blocks. The voltage sensor was placed closest to the cell due minimize the voltage drop through the copper block. For tab cooling, one of the two copper blocks were switched with an aluminium "plate", as discussed in the paragraphs above. Copper was seen as a favourable material due to its high electric and thermal conductivity. Due to material inaccessibility, aluminium had to be used for the tab cooling plate.

Two different cooling setups were used. First, one tab cooled and one pouch cooled cell was degraded when cooled with water at 25°C. However, due to its superior cooling abilities through the pouch, the pouch cooled cell had a significantly lower average temperature during cycling than the tab cooled. This setup is referred to as setup one. A second setup was also cycled. Here the pouch cooled cell was isolated with Nomex. The number of Nomex layers were adjusted until the tab and pouch cooled cell had the same average temperature at the end of discharge. A lower temperature on the tab cooled cell was desired, and the cooling water temperature was set to 12.5°C. An iterative process with a different amount of insulating Nomex between the cooling block and the cell was used to get the cells to end their discharge cycle at the same temperature. The tab and surface cooled cell was cycled, and the temperature on the cooled side and the insulated side of the cell were averaged and seen to match the temperature of the tab cooled cell. This setup is referred to as setup two.

The two different setups made it possible to study two different effects of the different cooling methods. Setup one allows studying the temperature and thermal gradients impact on the cell. With setup two, the smaller deviation in temperature can facilitate the study of the impacts of thermal gradients without the effect of temperature itself.

For setup one, the water bath was set to 25°C. For setup two, the water bath was set to 12.5°C. The aim for end temperature for setup 2 was halfway between Setup 1 pouch and tab cooled cells end temperatures, 37.5 degree C

### 3.3 Specific heat capacity (Cp)

To verify the results from the heat generation test, a simple model of the cell was developed. To get a more accurate representation of the cell, the Specific heat capacity (Cp) of the cell were tested since this is a cell-dependent property where the value is not in the datasheet of the cell.

To characterize the specific heat capacity of the LiB used in the thesis, a test where the cell was heated up and dropped in an insulated bath of water with known Specific heat capacity was done where.

The test was designed to be as simple as possible, still yielding a sufficiently accurate result to be representable in the test. The testing equipment consisted of an insulated water bath made of XPS foam plates with a hole for the cell covered in plastic for waterproofing. The cell tabs were cut off, and the cell was sealed in an additional cell pouch to keep it sealed from water to prevent a short circuit between the tabs of the cell thru the water. The mass of the cell with its new pouch was measured and can be found in 4.2. The cell was heated to 45 °C overnight to be certain it was isotherm at the start of the experiment. The distilled water used in the water bath was weighted and cooled down to 12 °C in a thermal chamber. The insulated bath was put in a thermal chamber at the expected end temperature for the mix of water and cell 17 °C. The Cp for the cell is calculated from equation 3.1 the

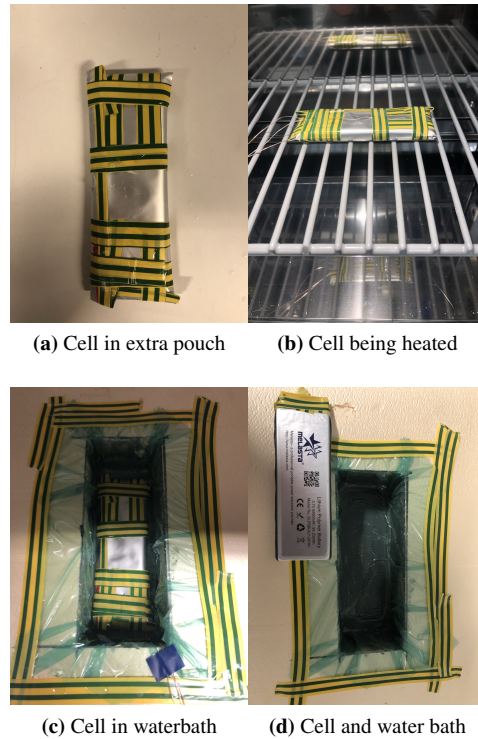


**Figure 3.2:** Pictures of the setup for measuring the specific heat of the cell

results can be seen section 4.5.1. To get the uncertainties of the test down, it should be repeated several times, adjusting the temperature of the insulation to the steady-state thermal temperature obtained until convergence is reached with expected and actual end temperature. For this thesis, the experiment was repeated three times, yielding sufficient accuracy.

$$C_{p_{cell}} = C_{p_{water}} \cdot \frac{m_{water}}{m_{cell}} \cdot \frac{T_{end} - T_{water}}{T_{cell} - T_{end}} \quad (3.1)$$

### 3.4 Cell Cooling Coefficient (CCC)

For characterization of the cells cooling potential, the cells Cell Cooling Coefficient (CCC) [8, 93] were tested before, during and after degradation cycling. The CCC is described in section 2.5.4. The CCC is a physical property of the cell and does not take into account the thermal resistance in the cooling system, e.g. the convective coefficient for air cooling or the thermal resistance between a cooling block and the cell [99]. The CCC can be measured for different surfaces of the cell and will be described accordingly.

**Table 3.1:** Values used for calculating the heat thru the CCC jig

Variable	Value	Unit
$k_{aluminium\ 6082}$	180	$\frac{W}{m \cdot K}$
$A_{pouch\ fin}$	$1.6 \cdot 10^{-4}$	$m^2$
$A_{tab\ fin}$	$7.2 \cdot 10^{-4}$	$m^2$
$n_{pouch\ fin}$	4	
$n_{tab\ fin}$	2	

### 3.4.1 $CCC_{Pouch}$

$CCC_{Pouch}$  or  $CCC_{Surface}$  which it is called in Hales et al. [93], is a measure of how much a cell will be cooled thru one of the pouch sides of the cell.

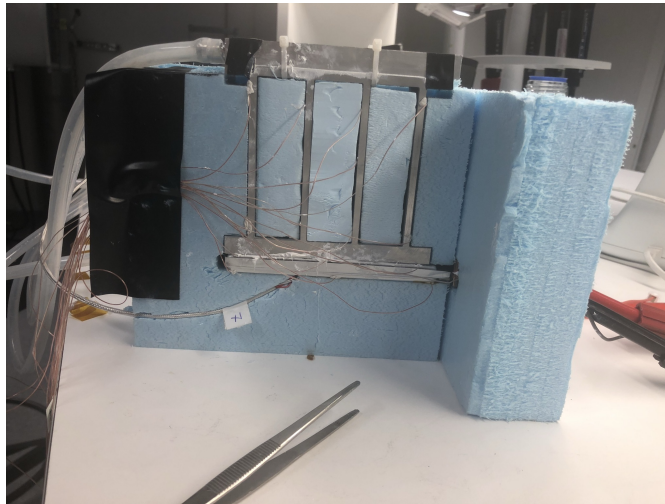


**Figure 3.3:** Picture of the  $CCC_{Pouch}$  setup with the insulation

The characterization cycles of the potential for cooling the cells by cooling the pouch surface was done by holding the cell insulated in a styrofoam encapsulation as seen in figure 3.3 to keep close to all heat rejection from the cell to the cooled surface. The cell is cooled thru a jig in aluminium with fins as shown in figure 3.5 and 3.3 where the temperature is measured with thermocouples as marked in figure 3.4. In total, 16 thermocouples were used, number 0-7 is used to measure the heat flux out of the cell, 8-13 measures the temperature gradient over the cell, 14 is a control measurement of the tab temperature. 15 is used to check that the heat flux over half a fin matches the whole fin to estimate the heat loss over the fins. The fins have a known thermal conductivity, so the heat flux thru each fin is calculated by equation 3.2 and the total heat flux by equation 3.3.

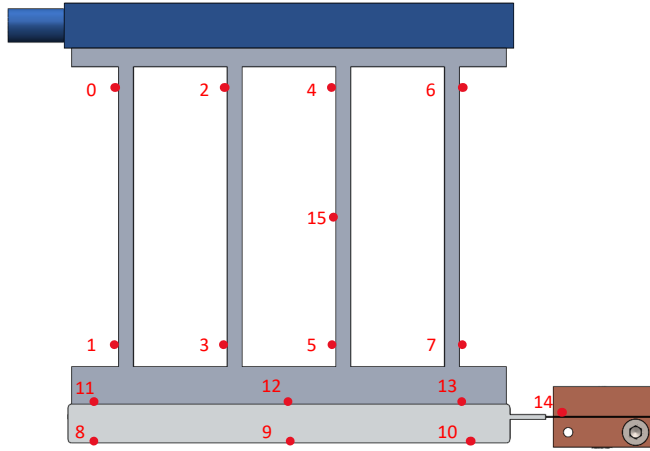


**Figure 3.4:** Sideview with thermocouple placements of  $CCC_{Pouch}$  Jig

$$\dot{Q}_{fin\ i} = \frac{k_{fin\ i}}{x_{fin\ i}} A_{fin\ i} \Delta T_{fin\ i} \quad (3.2)$$

$$\dot{Q}_{Pouch} = \sum_{i=1}^4 \dot{Q}_{fin\ i} \quad (3.3)$$

Where  $Q$  is the heat transferred,  $k$  is the thermal conductivity,  $x$  is the distance between the temperature measurement points,  $A$  is the cross-sectional area of each fin and  $\Delta T$  the temperature difference measured between the thermo-couples on each side of the fin.

The temperature difference over the cell is calculated by equation 3.4.

$$\Delta T_{Cell} = (T_8 + T_9 + T_{10})/3 - (T_{11} + T_{12} + T_{13})/3 \quad (3.4)$$

Where the temperature measurement points T is marked on figure 3.4.

$$CCC_{Pouch} = \frac{\dot{Q}_{Pouch}}{\Delta T_{cell}} \quad (3.5)$$

The heat flux and temperature difference over the cell is used to calculate the Cell Cooling Coefficient of the cell with respect to cooling the surface by equation 3.5. The top plate of the Jig is held at a constant temperature by a water cooling block connected to a cooling water bath held at a constant temperature of 25°C. The thermocouples shown in figure 3.4 is mounted with thermal grease for every characterisation and the relative position measured out with a digital caliper.

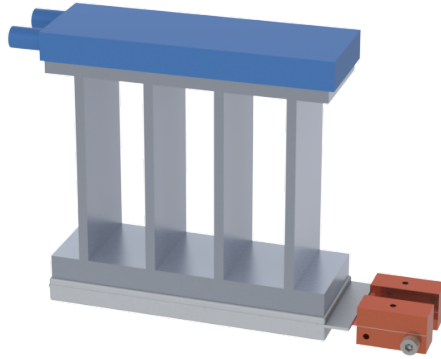


**Figure 3.5:** Render of the setup used to measure the  $CCC_{Pouch}$

The cell is charged then discharged to 50%SOC. The test is performed by charging and discharging the cell with a pulse at an average C-rate of 0, holding the cell at 50%SOC. The complete cycle and a zoomed-in snip can be seen in figure 3.6. The cycle is as follows:

- Constant Current-Constant Voltage (CC-CV) charge at 3C to 4.2V
- Constant Current (CC) discharge at 4.5C to 50% SOC
- 4.5C CC charge-discharge square pulses at 0.25Hz for 3.6hours
- Rest for 2 hours
- Repeated until desired amount of measuring points is gathered

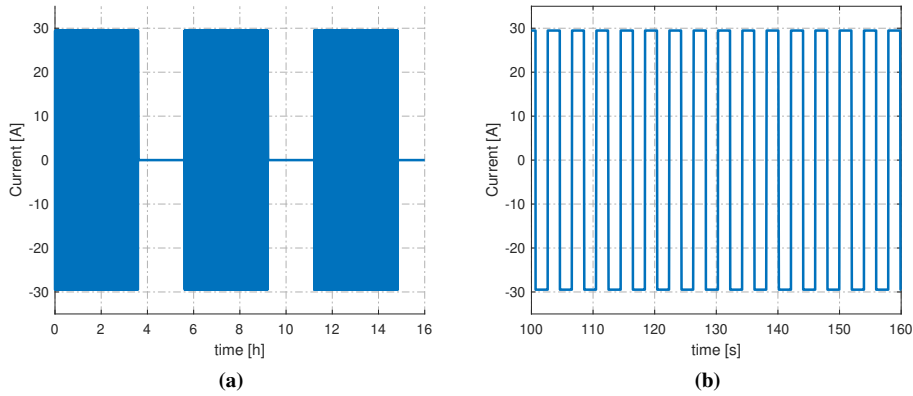


**Figure 3.6:** Current profile used for the CCC test

### 3.4.2 $CCC_{T_{abs}}$

The characterisation cycles for the  $CCC_{T_{abs}}$  follows the same cycles as for the  $CCC_{Surface}$ . Instead of cooling the cell pouch, the tabs were cooled thru busbars connected to the tabs. The end of the busbars which is seen in figure 3.9b, was cooled with water cooling blocks. The complete setup is seen in figure 3.8. The heat transported out of the cell thru the tabs is monitored by thermistors mounted on the busbars as shown in figure 3.7.

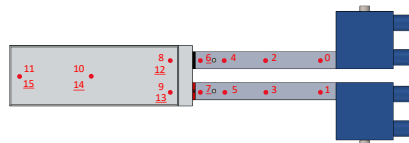


**Figure 3.7:** Top view of  $CCC_{T_{abs}}$  setup with placement of thermocouples. Underlined number is thermocouples placed underneath the cell

To prevent several paths for the heat from the tabs and out, the battery cyclers were connected to the busbars after the thermocouple measurements, underneath the cooling blocks. The Ohmic heating of the busbars caused by the resistance in the busbars could be accounted for in the measured heat flux. By calculation of the heat produced in the busbars, it was seen as negligible compared to the heat transfer. The area of the busbars where the heat and current are transferred thru is shown in table 3.1. The thermocouples are placed out between every new characterization and the relative position measured out with a digital caliper. The cooling water holds a temperature of 12.5°C.

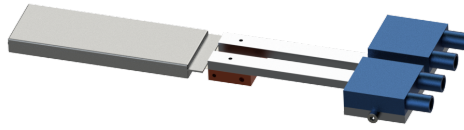


**Figure 3.8:** Render of  $CCC_{Tab}$  setup without isolation.

The cycle run is the same as for the test run with the cooling on the surface as seen in section 3.4.1 and figure 2.30.

$$\dot{Q}_{Busbar\ i} = \frac{k_{Busbar\ i}}{x_{Busbar\ i}} A_{Busbar\ i} \Delta T_{Busbar\ i} \quad (3.6)$$

$$\dot{Q}_{Tab} = \sum_4^{i=1} \dot{Q}_{Busbar\ i} \quad (3.7)$$

$$CCC_{Tab} = \frac{\dot{Q}_{Tab}}{\Delta T_{cell}} \quad (3.8)$$

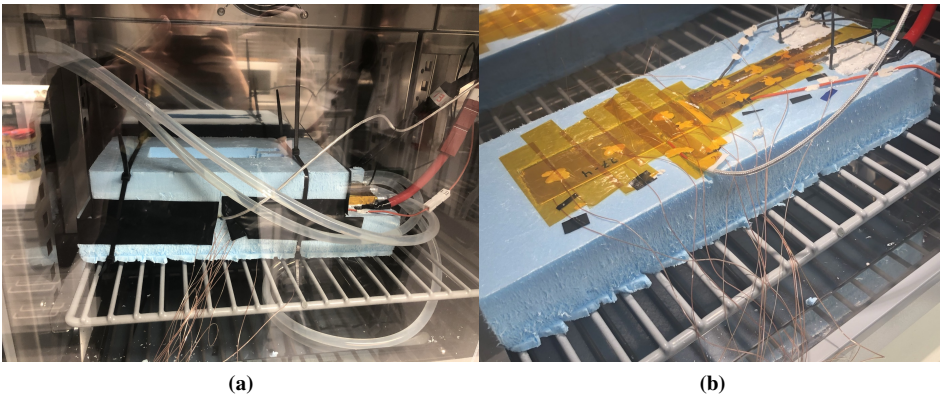


**Figure 3.9:**  $CCC_{Tab}$  setup with. (a) in thermal chamber, (b) without top isolation.



## 3.5 Visual and mechanical inspection

To keep track of potential changes in the LiB's, a visual inspection and mechanical measurements were done before, under and after ageing of the cell.

### 3.5.1 Opening of cell

A cell of the same type and manufacturing batch was opened by Trandem [29], and electrodes were sorted, visually inspected and measured. To see the changes internally on the electrode, a cell cycled to 50% SOH were opened, and the electrodes sorted and visually inspected before measurements were made of the electrode thickness.

The cell was fully discharged and introduced into a LabMaster Pro Eco glovebox [100] with inert Argon atmosphere. The cell was opened, and visual inspection of the electrodes and measurements were done.

### 3.5.2 Thickness

As discussed in 2 the thickness of the cell can increase due to the degradation mechanism. These degradation mechanisms lead to either increase in electrode thickness or the creation of gas, leading to the increased thickness of the entire cell.

Before cycling, every cell was marked at three points on the pouch, close to the tabs, in the middle and on the far side from the tabs. Before every CCC measurement of the cell was done, the thickness at each point was measured with a micrometre of type Mitutoyo QuantuMike. As the thickness of the cell changes with SOC [6, 12, 14, 15, 33, 37], all measurements should be done at 50 % SOC.

As a thickness change in the full cell can be caused by either gas or electrode swelling, the electrode was measured after opening a cell. The measurements were done at approximately the same points on the electrodes. Due to safety concerns, the cell was opened at 0 % SOC, and the full cell was measured before opening and also after "puncturing" the pouch to let potential gas escape.

The electrode thickness was measured after the cell was opened. This was done on ten different samples from each electrode. Three independent measurements were done on each sample, the standard deviations were calculated from these measurements.

### 3.5.3 SEM

Scanning electron microscope (SEM) pictures are a common tool for inspection of electrode degradation. It allows a study of each electrodes particles, and physical changes such as cracking and delamination can be seen. [101] Due to time-restraints a SEM picture was taken of a new cell and a 3C aged cell at 50 SoH. However, this was a cell from the same

batch that was cycled in a parallel study. The only difference to the cells cycled in this study was the applied cooling system: free-air convection at 25°C. The ICA curve (IC) curves, as well as degradation rate, were similar between the free-air convection cells and the cell studied in this thesis, and it was therefore concluded that it was likely that the same degradation mechanisms were dominating. This meant that pictures from a SEM would be beneficial to determine the degradation mechanisms in the pouch and tab cooled cell.

### **3.5.4 Density**

The density of the electrodes was calculated from the thickness measurements of the electrodes described in section 3.5.2. Round samples of 21.18mm were stamped out and weighted on a lab-scale, and the density is calculated. The densities reported is active material, including the current-collector. The change in density of the electrode from a fresh cell to an aged cell is also reported, including the current-collector. It is not thought that the density of the current collector itself changes with ageing, so the entire difference is thought to be in the active material.

The average of ten samples builds up the density, the standard deviation is added together with the standard deviations from the thickness measurements.

### 3.5.5 Thermal conductivity

The thermal conductivity of the electrodes active material was measured in a Jig made for thermal conductivity measurements. In this thesis, measurements were done on aged electrodes at 50% SOH. In Trandem [29] the same measurements were done in the same jig for fresh electrodes, and these results will be used as a baseline for comparison of the ageing effects. A more comprehensive explanation of how the measurements were done can be seen in Trandem [29].

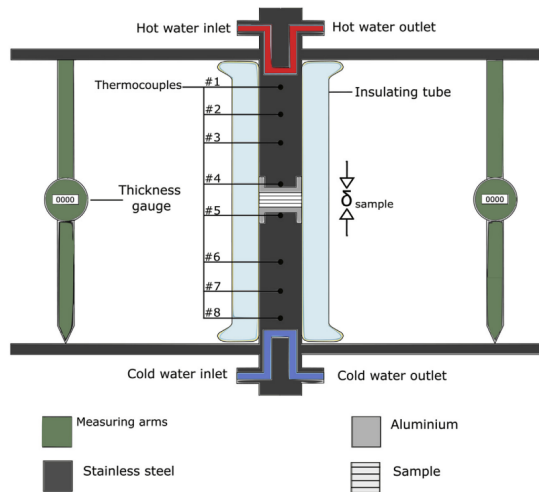


**Figure 3.10:** The thermal conductivity meter used. Reprinted from Richter et al. [61]

The thermal conductivity meter used was a constant heat flux meter which can be seen in figure 3.10. The temperature over and under the sample is held at constant temperature and the heat flux over the samples is calculated from measurements with thermocouples along steel rods. The samples are put between the rods and stacked in different thicknesses to produce a graph for the thermal resistance, which from the thermal conductivity can be calculated as the inverse of the slope. Electrode samples were stacked from one to four giving measurements for the standard deviation to be calculated. Since the current collectors have a thermal conductivity two magnitudes greater than the active material their contribution to the resistance can be neglected, the same goes for the contact resistance between the samples. [29, 61, 102, 103]

Measurements of the thermal conductivity were done on the electrodes with active material. These measurements were done by Trandem [29] for a fresh uncycled cell and were repeated with the same procedure here for aged cell (cell 26-5). The aged cell was at about 50% SOH when it was opened. Both the fresh and aged cell were drained to 0% SOC before the measurements were done.

### 3.6 ICA

Incremental Capacity Analysis (ICA) is an analysis method that helps identify ageing modes through the study of a voltage curve. Through a low C-rate discharge, the quasi-OCV of the cell can be obtained as a function of SOC. An ICA curve (IC) is a plot of  $\frac{dQ}{dV}$  as a function of OCV. An example can be seen in 3.11. Each chemistry has its own distinct graph, usually with one or more peaks and dips. The dips indicate a transition in the structure of one or both electrodes. [104]

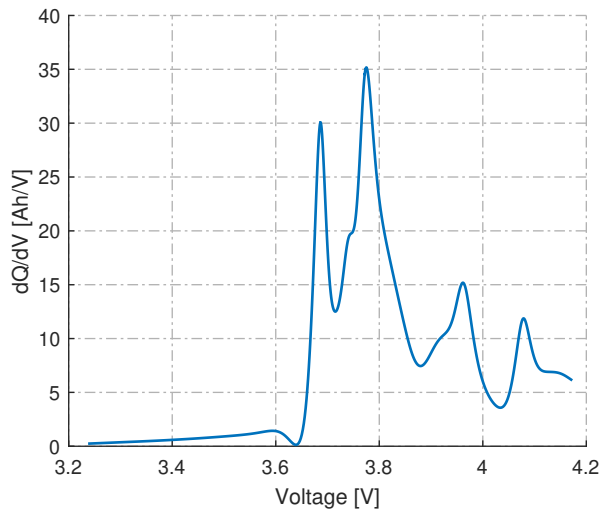


**Figure 3.11:** IC of the Melasta cell at 100 SOH.

For a full cell, the IC shows the deviation between the electrodes. It can therefore be hard to identify if the degradation occurs in the anode, cathode or both. [105] To separate each electrodes contribution to the IC, a half cell has to be made from each electrode. Figure 3.12 and 3.13 shows the IC of a LCO and a graphite half cell. By estimating the voltage as a function of SOC two half cell IC can predict the IC of the full cell made up of the two materials.

Note that as a full LCO cell is discharged, the LCO cathode is lithiated and decreases in voltage versus lithium. The anode is de-lithiated, and the voltage increases versus lithium. A full cell "top" at 3.6 V is created due to the top at 0.2 V anode. The tops at 3.67 and 3.77 V is mainly created by the tops at the anode at 0.1 and 0.16 V. While the tops at 3.95 V and 4.1 V is created by the cathode. Note that even though the different electrodes "define" the tops, a lower top can still be attributed to changes in the other electrode. The changes in the top themselves are therefore not as important as the difference in changes between the tops.

As each electrode has a unique IC, the same change for two different electrode materi-

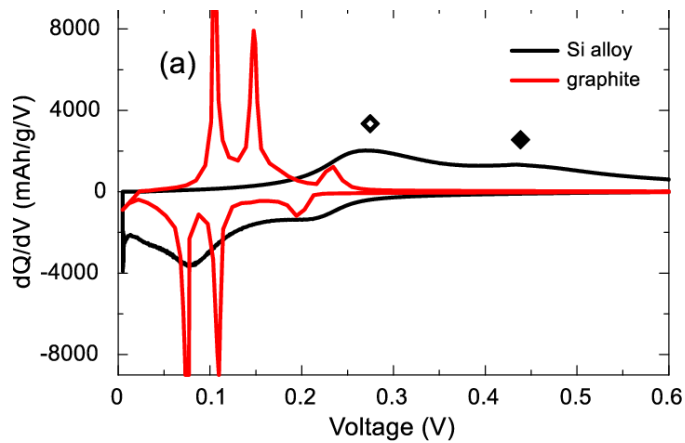


**Figure 3.12:** The figure shows the IC of a graphite and Si/graphite half cell. Voltage indicates the potential difference between Si/graphite and pure Lithium metal. Positive Y values indicate charging, while negative discharge. Reprinted from Krause et al. [106]

als does not necessarily mean the same degradation mechanisms. However, some changes indicate the same degradation regardless of electrode materials. An increase in impedance will increase the deviation between the terminal voltage and OCV, as seen from 2.11. This will manifest itself as a drift in the whole IC curve. A "smoother" curve indicates uneven degradation of the unit cells. This can be explained by the different unit cells reaching the structural changes at a different point in time. Lastly, a capacity loss during low C-rate cycling indicates LAM and/or LLI. This is because the low current will not give a significantly higher  $\eta$ , regardless of the impedance increase. Therefore, the cut-off voltage is mainly due to the cell not being able to cycle more electrons/ions. [105]

The IC were acquired through a C/10 cycle. This is relatively high compared to the majority of other similar research. However, as the Melasta cell is a power cell with low impedance, a higher C-rate can be applied because the following overpotential is negligible.

The characterization was done with the following schedule:

- CCCV: CC of 1 C and shut of current of 0.1 C at 4.195 V
- Rest for 15 minutes
- Discharge with 0.1C until 3.05 V
- Rest for 15 minutes
- Charge with 0.1C until 4.195 V

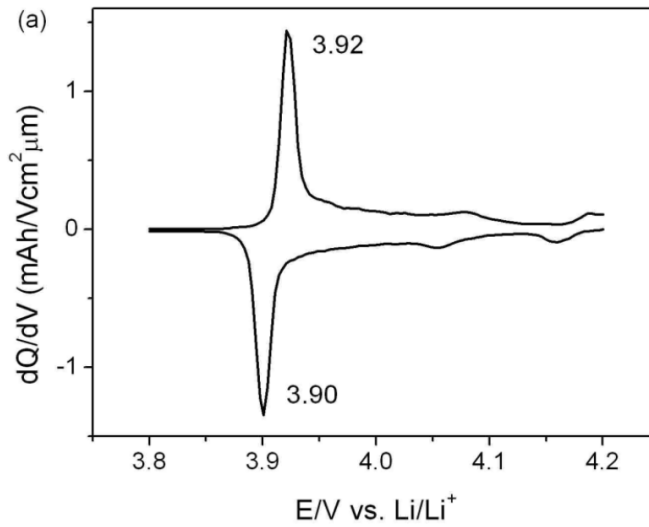


**Figure 3.13:** IC of a LCO half cell. Reprinted from Xia et al. [107]

Measurements were done every 5 seconds and not more frequent to keep the files at a manageable size. The voltage measurement was moving averaged with a window size of 7 data points, this due to the oscillation of the measurement. The graph was then calculated by the following equation:

$$\frac{dQ}{dV} = \frac{Q(t+1) - Q(t)}{V(t+1) - V(t)} \quad (3.9)$$

where  $Q(t)$  is the total charge/discharge in Ah at time  $t$ , and  $V(t)$  is the voltage at  $t$ . The graph is then smoothed by the use of smoothing spline in MatLab.

### 3.7 Overpotentials

There are two main methods of identifying overpotentials; Electrochemical Impedance Spectroscopy (EIS) and Hybrid pulse power characterization (HPPC) method. EIS gives a more thorough measurement of the full impedance spectre. However, EIS is impractical for the ageing setup, as it requires the connection of an additional measurement instrument. The HPPC method is giving relatively good measurement and has low complexity since the battery cyclers can do the tests. [76] Therefore the HPPC method is the chosen method.

The HPPC method uses the voltage response to a change in current, known as the current step response, to calculate the internal resistance as well as the charge transfer resistance. This is illustrated in 3.14.

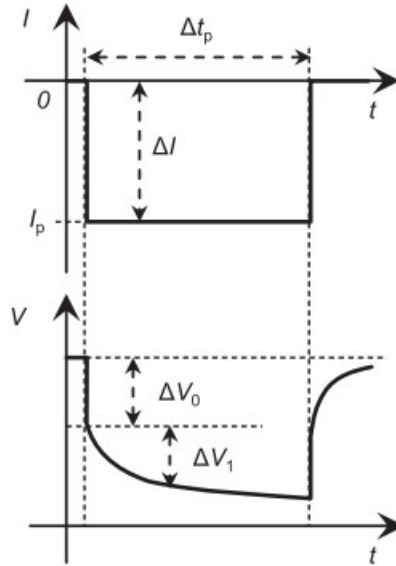


**Figure 3.14:** Illustration of a current step test. Upper figure shows the current and lower figure shows the voltage response. Reprinted from Barai et al. [76]

As the internal resistance is an Ohmic resistance, i.e. it follows Ohms law, the overpotential due to the internal resistance occurs instantaneously. Other overpotentials, both inductive and capacitive, also occur after a few milliseconds. However, the ohmic overpotential is dominating in this time frame and is neglected in this thesis [76]. The ohmic overpotential is calculated as follows:

$$R_{IR} = \frac{\Delta V_0}{\Delta I_0} = \frac{V_{0ms} - V_{50ms}}{I_{0ms} - I_{50ms}} \quad (3.10)$$

where  $\Delta V_0$  and  $\Delta I_0$  are shown in 3.14. The measurement point to calculate  $\Delta V_0$  was chosen to be taken 50 ms after the current was applied. A measurement of 50 ms is equal to a measurement of a 20 Hz signal, which means that a small capacitive overpotential is probably occurring [76]. However, the measurements at higher frequency showed some inconsistencies, and those were deemed larger than the small capacitive overpotential.

For the calculation of charge transfer resistance, the following equation is applied:

$$R_{CT} = \frac{\Delta V_1}{\Delta I_1} = \frac{V_{50ms} - V_{5000ms}}{I_{50ms} - I_{5000ms}} \quad (3.11)$$

3.11 takes use of that the overpotentials occurring in this time frame are dominated by the charge transfer resistance, as discussed in 2.

The overpotentials were calculated at the removal of the current instead of when it is applied. This removes the change in voltage which comes due to change in OCV, which would occur if the measurement is done after the current is applied.

The HPPC schedule is shown in 3.7:

- Apply discharge current for 7 seconds
- Rest for min 30 seconds and until a maximum 0.005 mV/s
- Apply charge current for 7 seconds
- Rest for min 30 seconds and until a maximum 0.005 mV/s
- Repeat with next current

The schedule was run at 90%, 50%, 15%. Several SOC were needed as the charge transfer resistance is a function of SOC. 0.0025 mV/s were chosen, so it would give a maximum error of 5% given our assumption that the initial charge transfer resistance was greater than 0.2 m $\Omega$ . Three currents were applied: 15A, 20A, 25A. Several currents enable us to see if the observed overpotentials are linear with the applied current. For the ohmic resistance, this is expected. Charge transfer resistance should not be linear but follow the Butler-Volmer equation 2.14. However, if other overpotentials also occur, the calculated overpotential could behave as a regular resistance. After the CCC tests at every 10% SOH the tests were done at 45, 30 and 15°C.

### 3.8 Capacity analysis

As one of the most important factors for a battery, an analysis of the capacity was done on the cells. There was done two different types of capacity tests; one where the cells are in their respective Jiggs and one where the cells are in quasi adiabatic conditions.

The tests in the respective cooling Jiggs were done to have data for the performance of the cells in what would be their environment in a real-world application. Due to less gradients for tab cooling than surface cooling, it is expected that in a one cycle perspective, tab cooled cells should have a higher capacity.[4, 89, 90]. An increase in the gap between the two cooling methods is in this studies setup amplified by the higher average temperature in the tab cooled cells, where a higher temperature gives better efficiency. However, a higher temperature will also increase ageing. This means that at some point, the ageing of the tab cell will have a higher impact than the advantage of the tab cooling method and that at some point, the surface cooled cell will have a higher capacity. [4, 7] This is illustrated in figure 3.15.

The tests in the quasi adiabatic environment were done to get comparative data between the cells. As the cells are in the same environment, the capacity is decoupled from



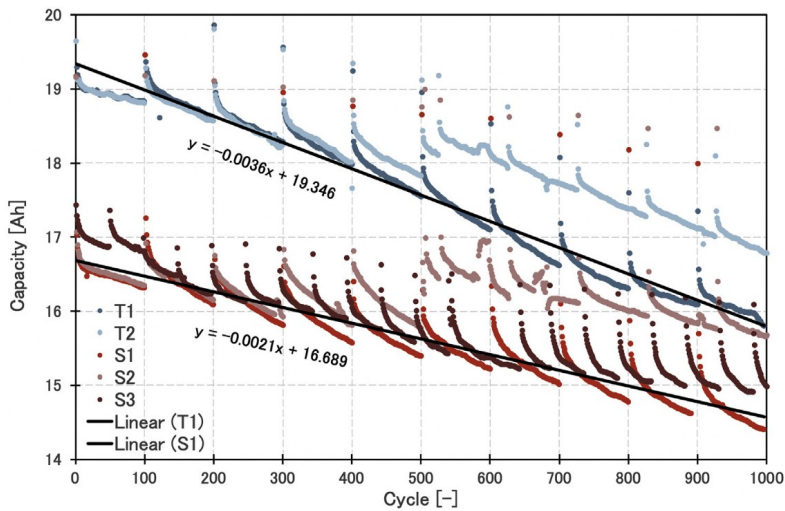


**Figure 3.15:** Capacity as a function of cycles. Blue datapoints are tab cooled cells, red pouch cooled. The periodical increase comes due to the cell is being characterized. This lets the cell relax and reach equilibrium. Reprinted from Dondelewski et al. [7]

the cooling method, and only the cell and its ageing will affect the results. Due to the more rapidly aged tab cell, one expects the tab cooled cell to have a lower capacity when in the same environment as the pouched cell.

The capacity analysis is at three different currents, 0.25C, 1C, and 3C, and done with the following procedure:

- CCCV CC of 3 C and shut of current of 1 C at 4.195 V
- Rest for 15 minutes and temperature under  $27^{\circ}C$
- Discharge at the given C and shut of voltage of 3.05 V
- Rest for 5 minutes

Different currents were chosen as different degradation modes will give different capacity fade at different C-rates, where higher impedance will give higher capacity fade at higher C-rates.

### 3.9 Entropy

There are two main categories of methods for measuring the entropic coefficient  $\Delta S$ ; calorimetric and potentiometric.[81] Calorimetric methods measures the heat generation due to entropy and determines  $\Delta S$  from this. While potentiometric methods make use of that  $\Delta S$  is proportional to the potential change due to temperature ( $\frac{dV}{dT}$ ). In this thesis, potentiometric is chosen due to higher accuracy [72] and available equipment.

The following formulas give the correlation between the potential and temperature:

$$\Delta G(x) = \Delta H - T \times \Delta S(x) \quad (3.12)$$

$$\Delta G(x) = -n \times F \times E(x) \quad (3.13)$$

$$\Delta S(x) = \frac{\delta \Delta G(x)}{\delta T} \quad (3.14)$$

$$\Delta S(x) = n \times F \left( \frac{\delta E(x)}{\delta T} \right)_{SOC,p} \quad (3.15)$$

where G is Gibbs free energy, H is enthalpy, T is temperature, n number of electrons, F Faraday's constant, E the electromotive force and p pressure.

3.15 shows that the only unknown is  $\frac{\delta E(x)}{\delta T}$ . With the cell in voltage equilibrium, the temperature of the cell can be changed, and the resulting potential change can be measured.

However, potentiometric methods pose several challenges. The first and biggest one is that it is time-consuming, as the cell has to both reach temperature and voltage equilibrium. As a cell never reaches truly a voltage equilibrium, a quasi-equilibrium must be used. Papers report anywhere from 3 to 60 hours to reach equilibrium. [72] Due to the cells thin electrodes it can be assumed that the cell used in this thesis is in the lower range. Another challenge is that the entropy coefficient is strongly correlated to SOC as illustrated in figure 2.28. This means that several measurements are needed to approximate the curve, which can lead to the test lasting weeks.

In this thesis, a method is chosen where the cell is only partially relaxed, and the voltage change due to relaxation is corrected for. This is done through a interpolation of the voltage relaxation. The interpolation was done with a logarithmic fit in MatLab. This is illustrated in 3.16. The method is similar to the one reported in [72]. The method cuts the measurement to only 35 hours for 11 data points (every 10% SOC).

From 3.16 it can be seen that the voltage is not fully relaxed at the time of the temperature change. This indicates that without the correction term, there will be errors.

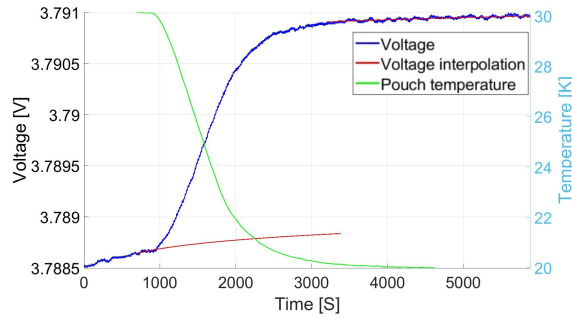


**Figure 3.16:** Shows the temperature change and voltage response of the cell. Note that the voltage change is due to temperature change. The red line shows the interpolation of the voltage if the cell was kept at a constant temperature. Reprinted from MacDonald [83]

For this method, the following was done to find  $\frac{\delta E}{\delta T}$ ;

$$\frac{\delta E}{\delta T} = \frac{E_{30^{\circ}C,interpolated} - E_{20^{\circ}C,interpolated}}{30^{\circ}C - 20^{\circ}C} \quad (3.16)$$

where the terms are:

- $E_{30^{\circ}C,interpolated}$ : The interpolated voltage at  $30^{\circ}$  at the halfway point between the cell was last  $30^{\circ}C$  and  $20^{\circ}C$
- $E_{20^{\circ}C,interpolated}$ : The interpolated voltage at  $20^{\circ}$  at the halfway point between the cell was last  $30^{\circ}C$  and  $20^{\circ}C$










# Results & Discussion

This chapter will present the results and discuss these. Note that unless specified, the SOH presented in graphs are always the SOH at 3C. Due to the cells having a higher life span than expected and some issues with uptime for the battery cyler, the cells for setup two did not manage to degrade further than 90% SOH. Due to this and the limited time frame between the cells reaching 90% SOH and the delivery date, the cells for setup two will only be discussed in regards to CCC and capacity fade.

## 4.1 Results labeling

The results in this chapter, unless otherwise mentioned, the different cells tested are plotted with a unique colour for recognition between datasets. The cells names are as given by Melasta Battery during sorting. Information of the cells cooling system during the cycling and the colour the data is plotted with can be seen in table 4.1

**Table 4.1:** For identification of each cell, all plots for a cell keep the same colour

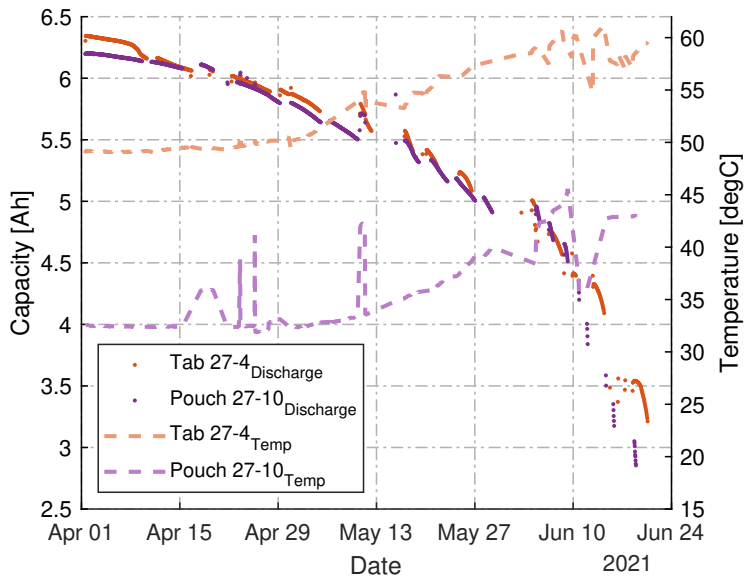
Cell number	Cooling method	Colour
$\bar{X} X - \bar{X}$	XXXX	
26 - 5	Ambient aged	
27 - 4	Tab cooling 1	
27 - 10	Pouch Cooling 1	
24 - 8	Pouch Cooling 2	
16 - 8	Pouch Cooling 3	
25 - 2	Tab cooling 2	

## 4.2 Ageing

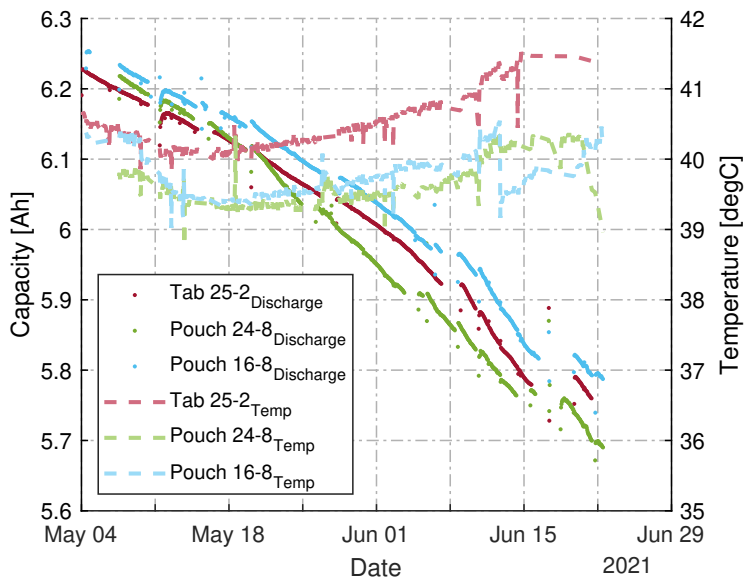
This section describes the main results and trends seen during the ageing-cycling of the cells studied. The effects of the different cooling systems and temperatures experienced by the cells

### 4.2.1 Ageing by different cooling methods

Figure 4.1 shows the cells cycled and the time they were cycled. The first batch seen in 4.1a was started first and cooled with water cooling blocks directly mounted on the cells pouch with thermal grease for 27-10 and to the tab for 27-4. The temperature shown in the graphs is from thermistors mounted to the pouch at the middle of the cells uncooled side. The two cells were cooled with water at 25 °C. In figure 4.1b the cells were cooled to be at the same end temperature. The two pouch-cooled cells were insulated with Nomex towards the cooling blocks to match the tab cooled cell's temperature. The water in the cooling blocks was 12.5°C. The plotted temperature for the pouch cooled cells in figure 4.1b is the average of a thermistor placed underneath the cell and one placed between the cell and the cooling block. All thermistors were placed on the cells pouch with thermal grease. The differences will be discussed in the following subsections.



(a)



(b)

**Figure 4.1:** Ageing cycles with SOH and temperature for all cells.(a) shows cells in setup 1 and (b) shows cells in setup 2.

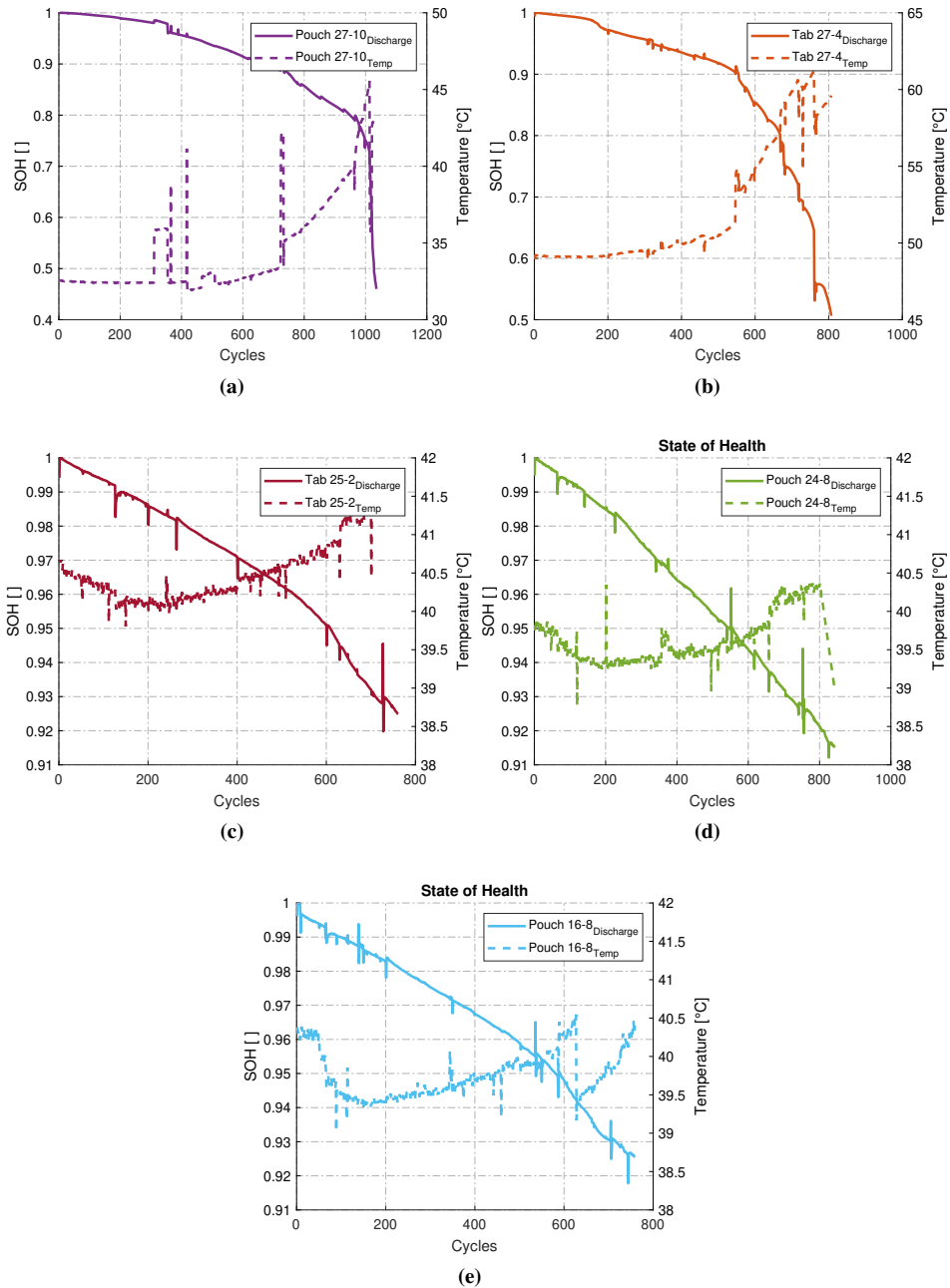


**Figure 4.2:** Ageing cycles with SOH and temperature for all cells. Sudden and brief increases in capacity are due to the cells having been characterised, therefore being relaxed and reaching equilibrium.



## 4.2.2 Capacity during cycling

One interesting aspect that was evaluated during the work with the thesis was how the available capacity in the cell is affected by the cooling method. As stated in 2.5.4 Dondelewski et al. [7] reports that tab cooling will give more usable energy from the cell at the beginning of the life of the cell because of smaller thermal gradients in the cell, which is explained in figure 2.31.

When looking at figure 4.1a it can be seen that the pouch cooled cell 27-10 had a higher initial capacity than the tab cooled cell 27-4 when tested under the same insulated conditions at 3C discharge. However, when cycling with the cooling system turned on, the tab cooled cell shows a higher usable capacity at the start of its life. Due to the difference in the CCC of the two cooling methods, the Tab cooled cell ended up at a higher temperature after the discharge giving it favourable conditions in regards to internal resistance. It is hard to differentiate between the two cooling methods if the extra capacity comes from the thermal gradients being favourable or just that it has a higher temperature.

In batch two with cells, the cells cooling were tuned until they had the same end temperature after the discharge. The goal was to isolate the cooling strategies effect on the available capacity without having the effects of the cell running at different temperatures. As can be seen in figure 4.3b all the three cells had similar capacity when tested isolated under the same condition with 3C discharge. Under the ageing study, the three cells also show similar capacity and degradation. There was not seen any significant difference between the tab-cooled and the two pouch-cooled cells when they were cooled to the same temperature.

When evaluating the effects the cooling system and strategy have on the cell's capacity and degradation, it seems that the temperature the cell holds plays a far more significant role than if the cooling is performed with tab- or surface-cooling. Furthermore, in terms of available capacity, the end temperatures are the most important variable in choice of the cooling system. Higher temperatures give a higher available capacity but a shorter lifetime for the cells.

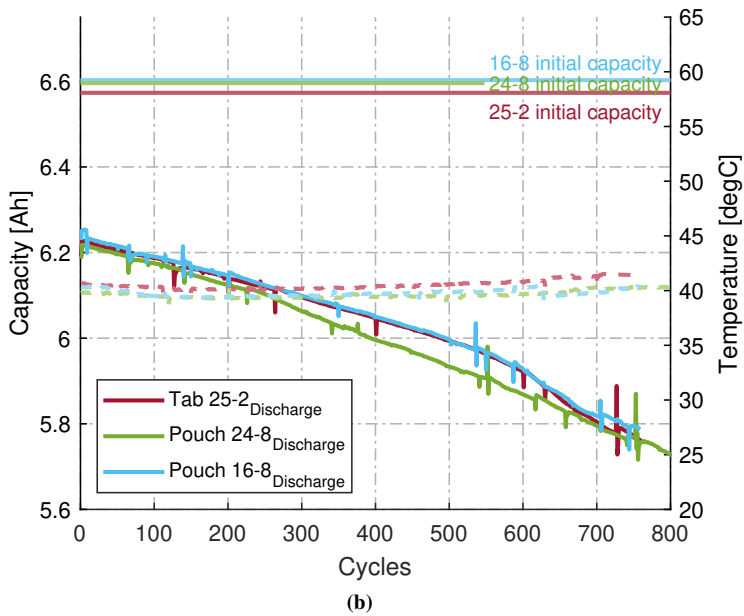
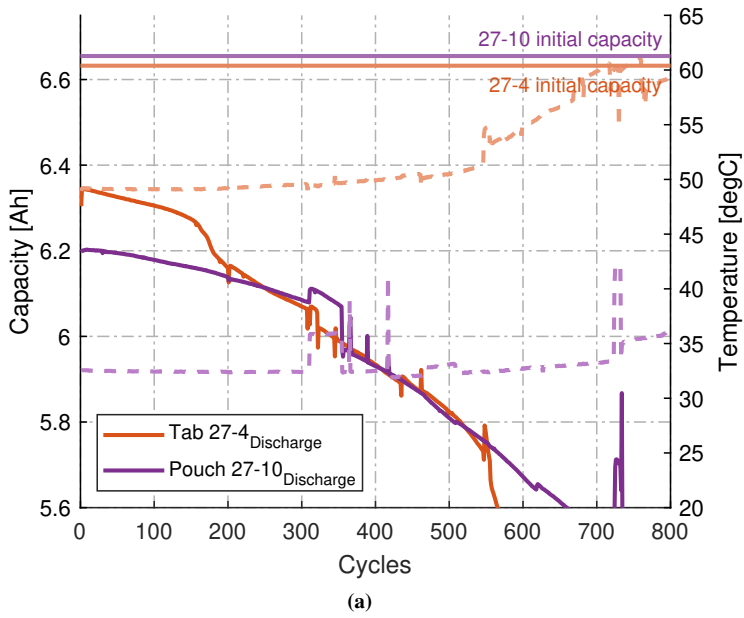


**Figure 4.3:** Ageing cycles with capacity and temperature for all cells

### 4.2.3 Isolated tests

Insulated tests were done with the cells to differentiate between the difference in performance and the degradation rate. Figure 4.4 shows both capacity and energy from these results at different C-rate. Note that all SOH are calculated with the use of the first ageing cycle in the cooling jig. This is why certain data points have higher than 100 SOH as SOH decreases, the difference in capacity increases between the different C-rates. The increase in impedance can explain this. This is amplified when looking at eSOH as impedance both lowers the average voltage and the capacity.

For the pouch cell, a higher capacity can be observed for 0.25C than 0.1C. Due to the cells' low impedance, similar results would be expected between the two C-rates, as found with the tab cell. However, no clear explanation was found as to why the capacity was higher for a higher C-rate.

4.5 shows both the ageing cycles and the isolated tests. The isolated tests gives a better tool for comparing the degradation rate between the tab and pouch cooled cell.

4.5 confirms the statement in 4.2.2; that the tab cooling system would initially give higher capacity, but that the degradation rate would be higher. It can also be seen that this extends to lower SOH as well, as there is a higher deviation between the cooling jig capacity and isolated test for the pouch cell than for the tab cooled cell.

The last two isolated tests for both cells show significant deviation and inconsistent results. However, at a SOH under 50% the cells are way past EOL, and the results are therefore not relevant for most real-world applications.

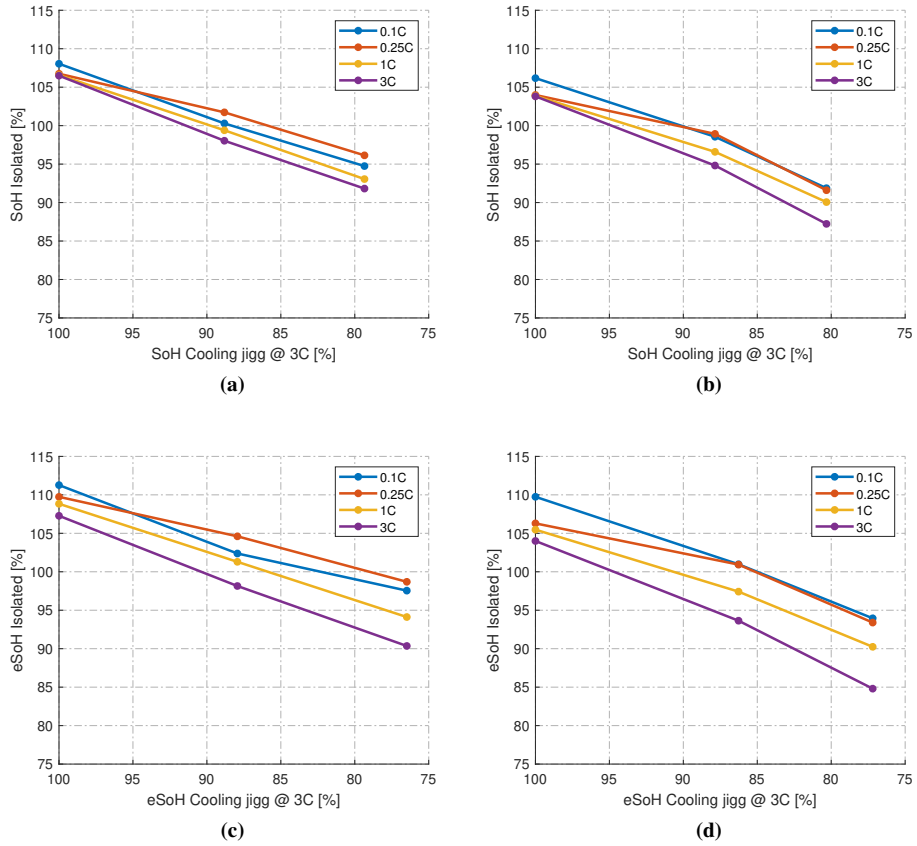


**Figure 4.4:** Shows the SOH and eSOH for the two aged cells in setup 1. The x-axis shows SOH at the last cycle in the cooling jig before the isolated tests, while the y-axis shows the capacity in an isolated setup. Note that all SOH is calculated by the capacity at the first cycle in the cooling jig. (a) and (c) shows the pouch cooled cell, while (b) and (d) the tab cooled cell.

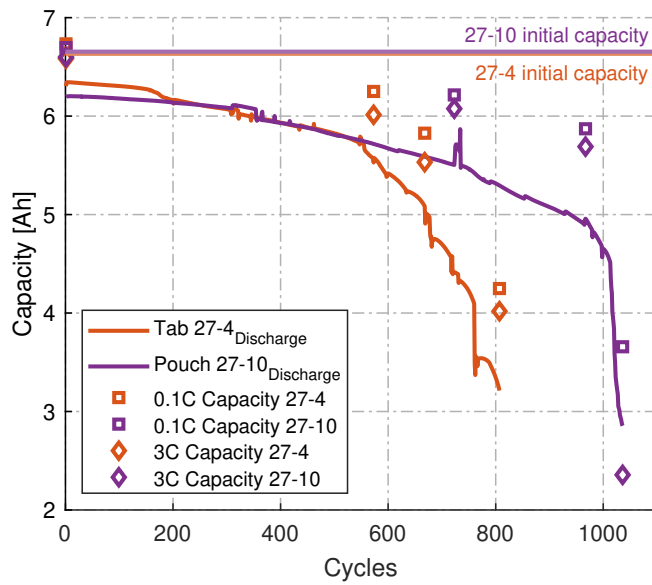


**Figure 4.5:** Capacity as a function cycles. The single points are data points from the isolated tests.

#### 4.2.4 Temperature effects on cycle life

When looking at the effects of temperature and cycle life has on the degradation of the battery cells Accumulated thermal unit (ATU) were used as a unit to compare the temperature experienced by the cells thru the cells life. 1 ATU is 1 °C for one day (24hours), meaning something held at constant 20 °C for 10 days will have accumulated 200ATU. Figure 4.6a shows SOH plotted against ATU, only the temperature experienced by the cell during normal age-cycling and the characterizations done during this cycling is accumulated. Moments of longer rest time, as when the cycler has been out of service, or the cells have been CCC characterized, is not accounted for.

The tab cooled 27-4 cell is the cell that has been cycled at the highest temperature, which can be seen in figure 4.2b where the end of discharge temperature is plotted. In figure 4.6b it is seen that the same cell (27-4) is also the cell that degrades the fastest seen against the number of cycles, this is also expected since it is the cell getting the worst cooling. However, if we instead look at the ATU as a measure for the lifetime of the cells, we can see that the cells behave more similar, and the 27-4 cell follows the other cells better in degradation and degrades slower with ATU than the 27-10 cell.

To estimate the future degradation of cells, the ATU could be a helpful tool to look at when predicting degradation of a cell if the C-rate is constant but the temperatures are changed.

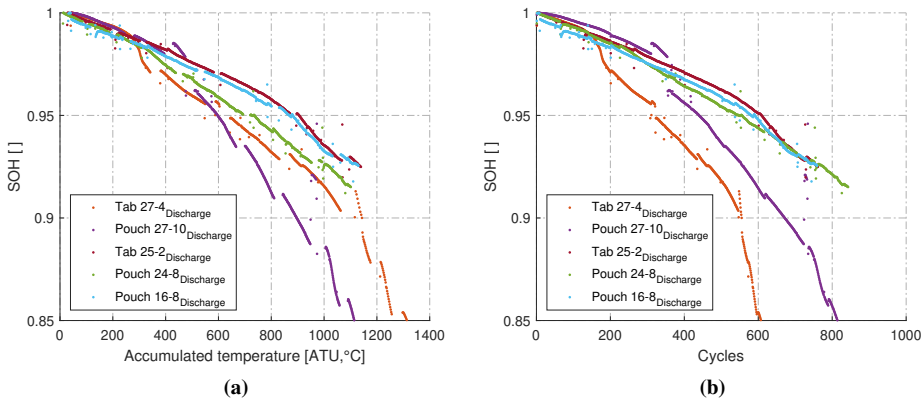


**Figure 4.6:** In (a) State of health is plotted against the accumulated temperature the cells has experienced during the cycling in the unit Accumulated thermal unit (ATU) where 1 ATU is 1 degree Celsius for 24 hours. The temperature during external characterization or periods at rest where the battery cycler has been off is not counted in. (b) for comparison shows the state of health against full cycles.

### 4.2.5 Calibration error in battery cyclers

There is an offset in the data from the battery cycler. When starting the cycling of the cell, one cycler was used where the data seems reasonable. This can be seen in figure 4.7a, where the data points that can be seen between April 1st and April 20th have a Columbic efficiency of the cell in the expected range of around 99.95%. April 20th, the cells were switched from the first cycler to a new one, this cycler was badly calibrated, which can be seen in the Columbic efficiency of the rest of the data in figure 4.7a and all the data in 4.7b which lays in the range of about 100.4% efficiency which is clearly not right. A slight offset can also be seen around April 20th in the data in figure 4.1a. It showed to be difficult to get the cycler recalibrated even tho a few attempts were made. No further actions were taken with the error in capacity measurements in the data-sets since the error it is thought to produce lies in the range of 1%. This offset would not affect the final conclusions.

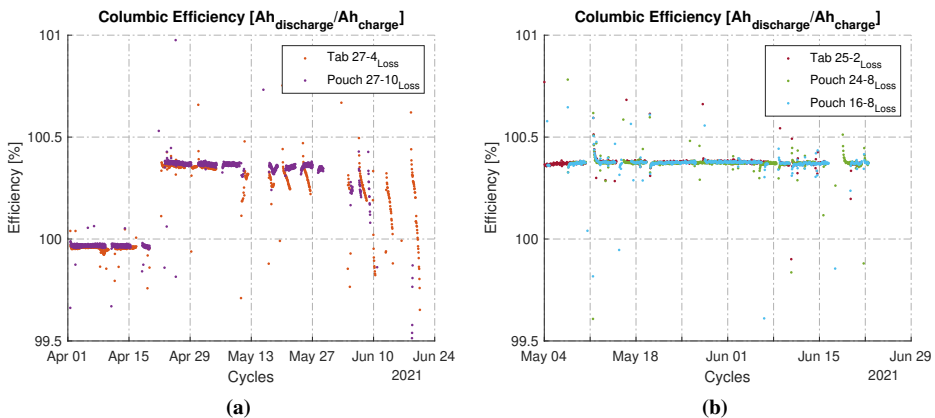


**Figure 4.7:** The columbic efficiency measured by the Arbin battery cycler

### 4.3 CCC characterization

As described in section 3.4, the Cell Cooling Coefficient (CCC) of the cells were characterized first before the cycle-ageing of the cells started and then at about every 10% drop in capacity measured at 3C discharge.

In the first part of the work with the thesis, two cells were characterized one cell 27-10, for  $CCC_{pouch}$  and the other cell 27-4, for  $CCC_{tab}$ . The cells would in the cycle ageing be cooled with water at the same temperature, 25°C. The goal was to identify if and by how much the CCC changes when the cell degrades.

The second batch of cells that were tested and cycled had two surface cooled and one tab cooled cell. In this batch, the cells were cooled to have the same average temperature thru the cycles, so the pouch cooled cells were insulated from the cooling blocks until they obtained the same average temperature as the tab cooled cell. The cells were cooled with water at 12.5°C. In this batch, the goal was to isolate the ageing effects of the cooling system and keep the temperature independent. These cells were only CCC characterized at 100% and 91% SOH.

In the plots coming in this section, the period of the CCC measurement where the current is pulsed is marked in blue, while the rest periods is unmarked. The CCC measurement is only valid in the periods of heat generation.

#### 4.3.1 $CCC_{pouch}$

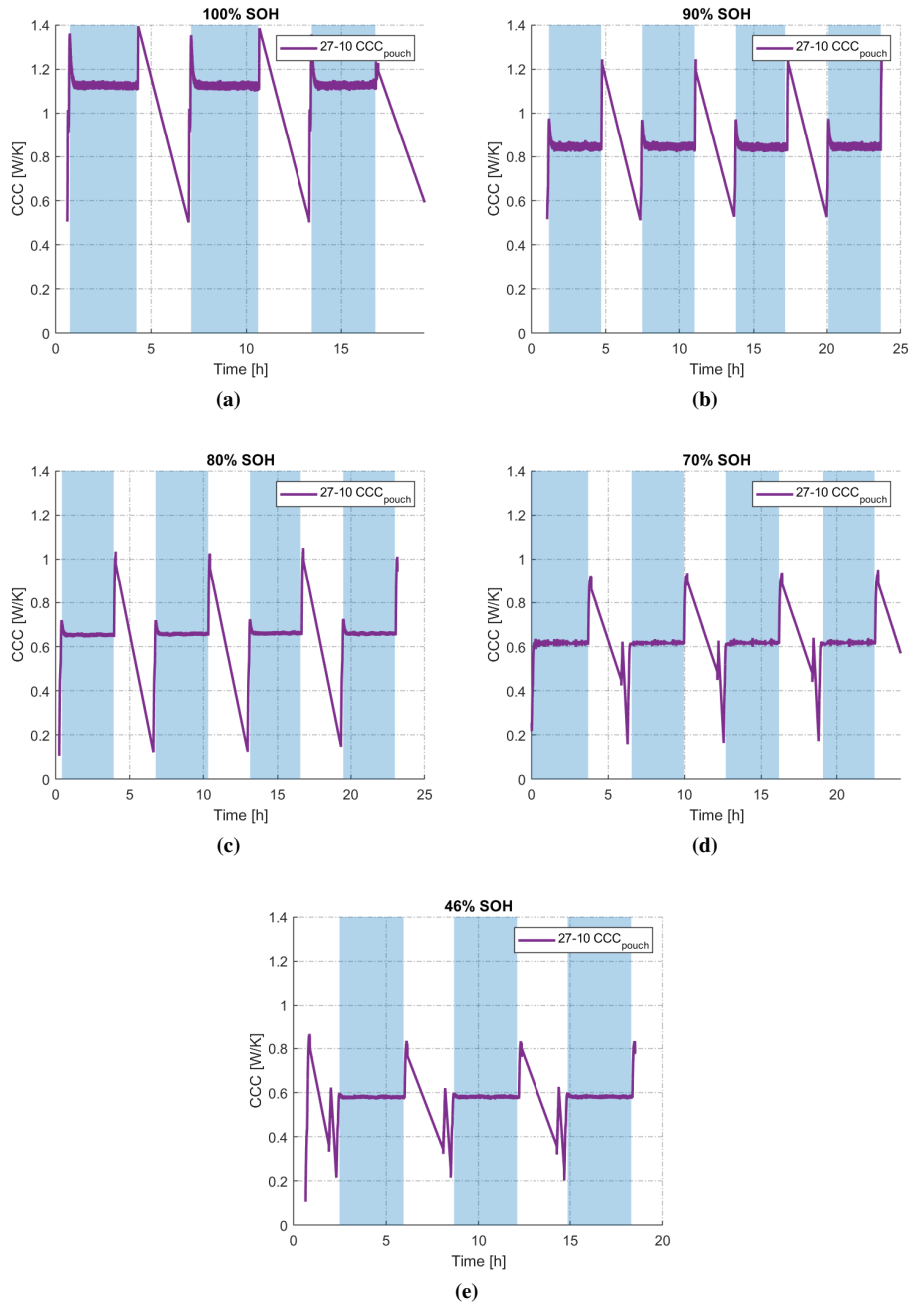
In figure 4.8 all CCC characterisations done for cell 27-10 can be seen. The measurements where the pulse currents are drawn is marked in blue. When the temperature difference over the cell is approaching 0 in the rest periods, the CCC goes to infinity as can be seen in equation 3.5 so all measurements where the  $\delta T$  is less than 1 °C or the calculated CCC is at unrealistic values between the measurements is removed.

After the current pulse is started, the cell comes to a steady state CCC value relatively fast. From the measurements, during the life of the cell, it can be seen as the cells SOH degrades the CCC also goes down. From its start point at 1.25 down to 0.58 at 46% SOH.

Figure 4.9 shows the CCC measurements for the two cells in the second ageing batch. Because of limited time, it was only possible to age them down to 90% SOH so only two measurement points were gathered for the CCC degradation on these cells.

The same trends can be seen on these cells as 27-10. The CCC goes down with the cell degradation.



**Figure 4.8:** CCC measurements done on cell 27-10

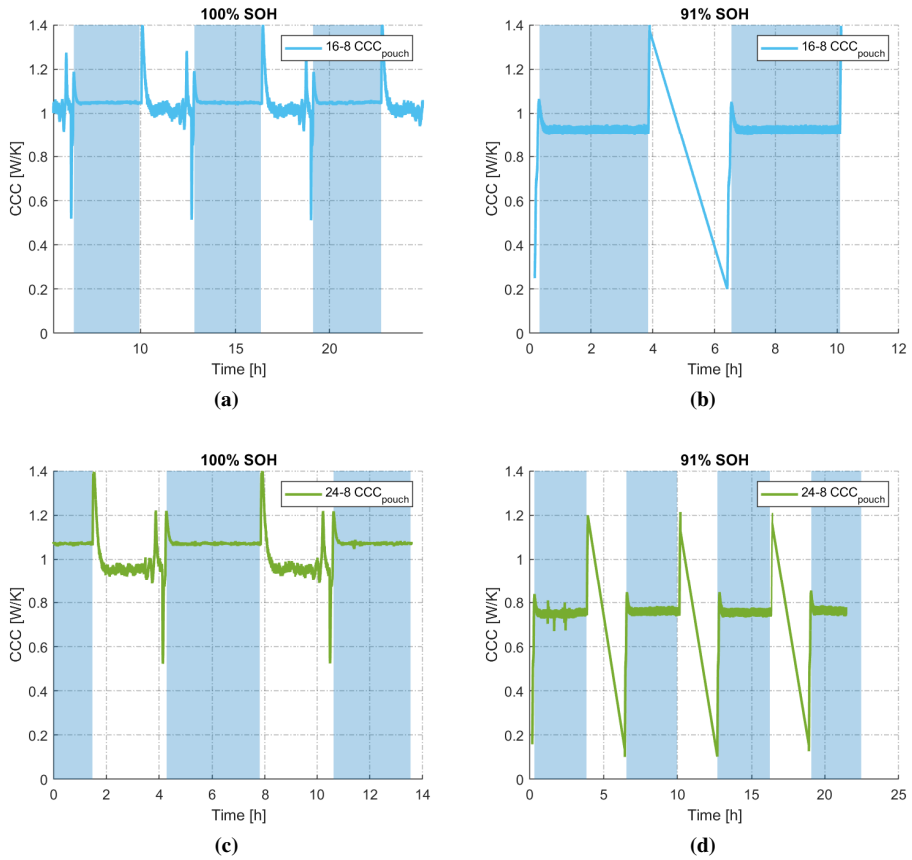


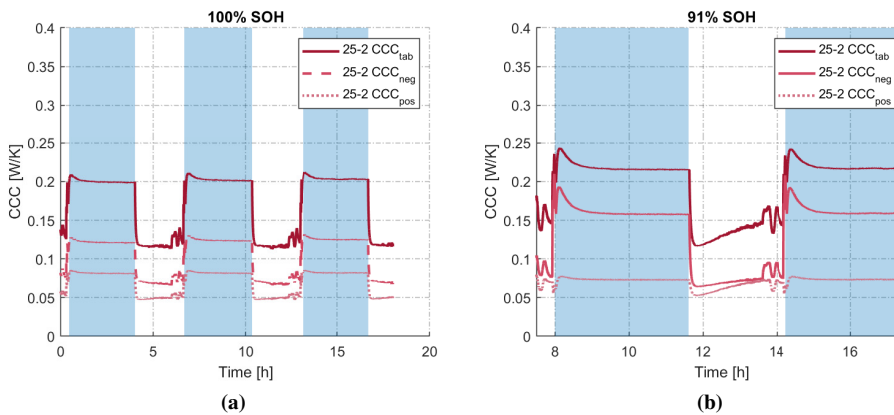
Figure 4.9: CCC measurements done on cell 16-8 and 24-8

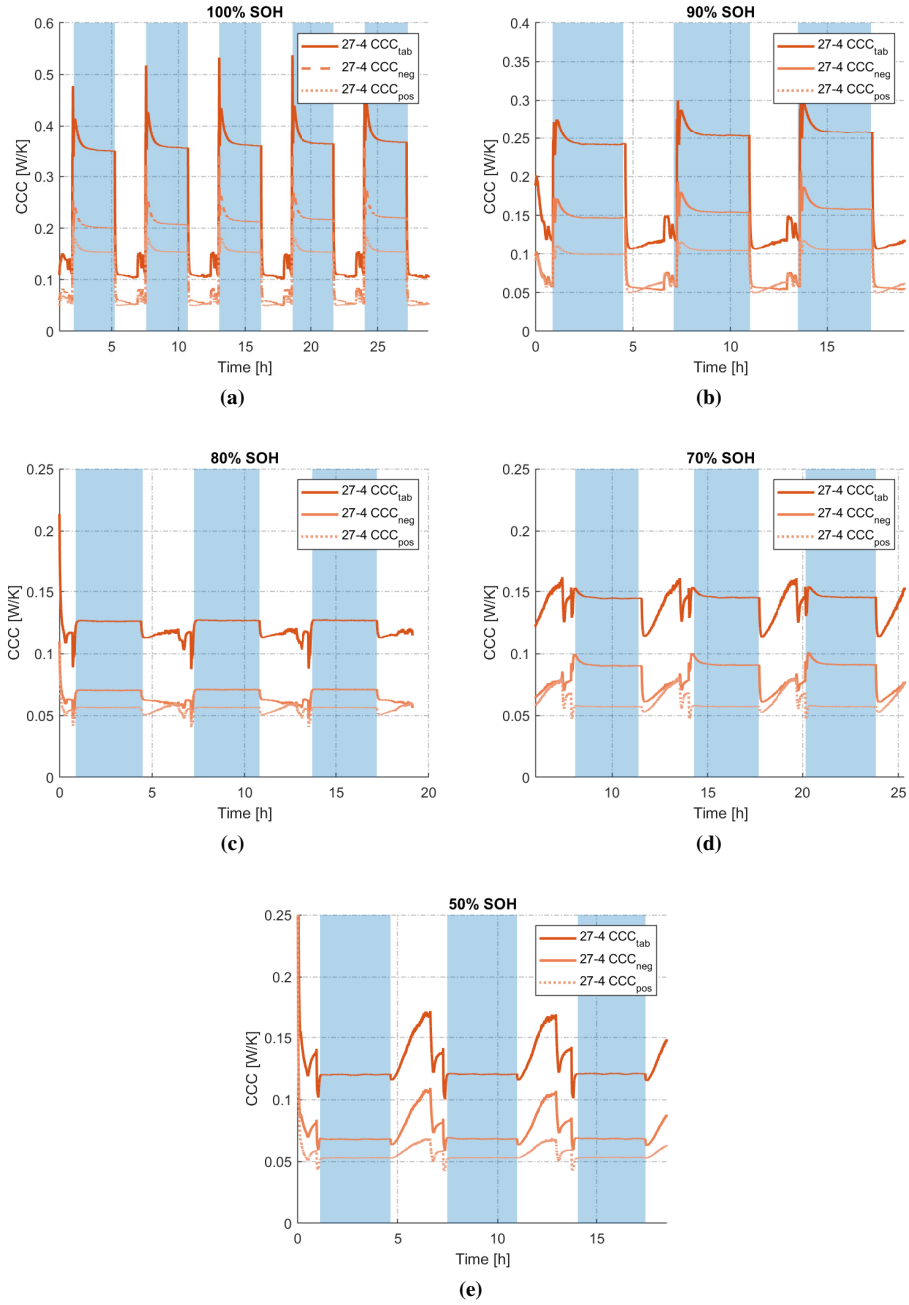
### 4.3.2 $CCC_{tab}$

Figure 4.10 shows the CCC characterization cycles run for the tab cooled cell 27-4. In the first series 4.10a at 100% SOH six runs were tested over 26 hours. The CCC measurement was steadily increasing thru the measurement series from 0.352 at the first measurement to 0.375 in the sixth measurement. No conclusive reason for this stepwise increase in the  $CCC_{tab}$  was found, and it was not seen in the  $CCC_{pouch}$  measurements. It could be that the styrofoam insulation got heated slightly, and the rest period should have been longer. A hotter insulation could lead to a lower  $\Delta T$  in equation 3.8 and therefore increasing the CCC. The error from this is quite small, and no further effort was made to get rid of it.

Since the in-plane thermal conductivity is relatively unchanged with the change of thermal as can be seen in 4.6.3 It was thought that the  $CCC_{tab}$  also would be less sensitive to degeneration and should stay more or less unchanged. Looking at the measurements from cell 27-4 in 4.10 it starts lower than the  $CCC_{pouch}$  and percentwise change shows similar behaviour to the  $CCC_{pouch}$  of cell 27-10. Cell 25-2 has a flat development and does not change a lot between 100% SOH and 90% SOH in fact, a slight increase is seen.

The gathered results from the  $CCC_{tab}$  measurements makes it hard to make any concise conclusions, and a bigger sample of cells would be needed before we can say anything about the general behaviour of the  $CCC_{tab}$  with ageing.





**Figure 4.10:** CCC measurements done on cell 27-4

### 4.3.3 Change in CCC as function of SOH

In figure 4.11 all CCC measurements done on the cycled cells is plotted together against State of health. In the Pouch cooled cells a clear trend is seen in the CCC development. The CCC is decreasing, most drastic in the start and from the look at the development of cell 27-10 and the one measurement done on cell 26-5, it seems to stabilize.

Again looking at the results from cell 27-10, the CCC has halved, from the cell being pristine to being at the end of its life. The halving of the CCC thru the cells lifetime imposes a challenge for the cooling system designers. The same cell, thru its lifetime, need to more than double the  $\Delta T$  from cooled to hot surface to get rid of the same amount of heat. The fact that cells produce more heat when degraded combined with the lower CCC means the cell cooling system towards the end of the cells life must cool with a lower temperature or allow the cell to come to a higher temperature.

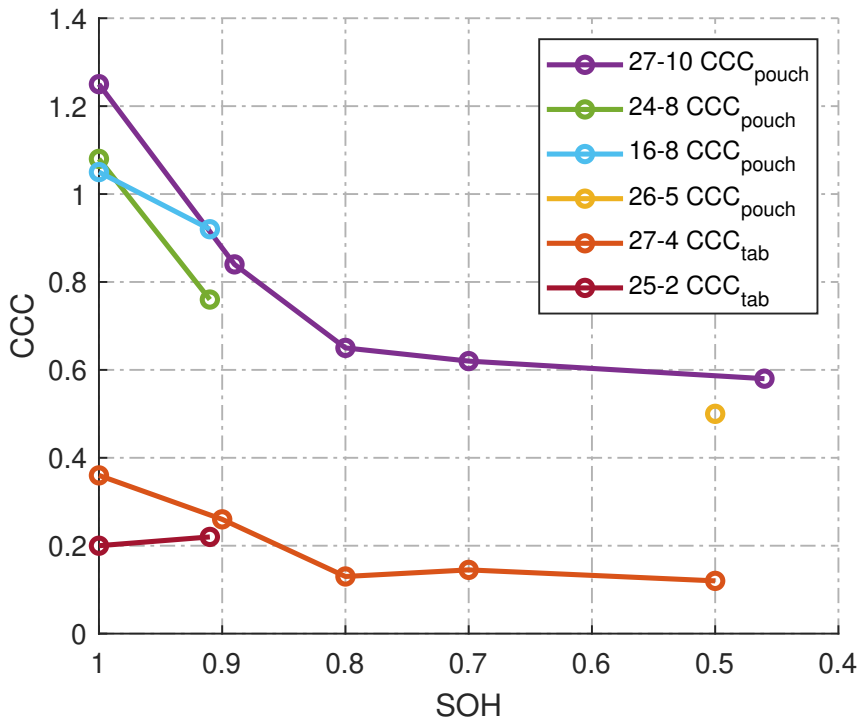


**Figure 4.11:** CCC as a function of SOH for all cells. Note cell 26-5 is only measured after ageing. The  $CCC_{tab}$  is a lot lower than  $CCC_{Pouch}$  from before the ageing is started

### 4.3.4 Independence of C-rate

To check the independence of the C-rate for the CCC jig, several CCC measurement series were done one after another on the same cell. In figure 4.12 plot (a) shows the CCC measurements done and (b) shows all temperatures recorded on the cell and on the cooling jig. The colour codes represent the different C-rates the measurement series is run at, Cyan 2C, Magenta 4.5C and Green 3C. And it can be seen that independent of temperature on the cell and the C-rate, the battery is cycled at the CCC is almost unchanged. This confirms the claims discussed in section 3.4 where it is stated that the CCC should be a cell-dependent coefficient, independent of external factors such as cooling temperature and heat generation. As seen, the higher the heat generation in the cell, less fluctuations are seen in the measurement, and the CCC is less sensitive to small changes.

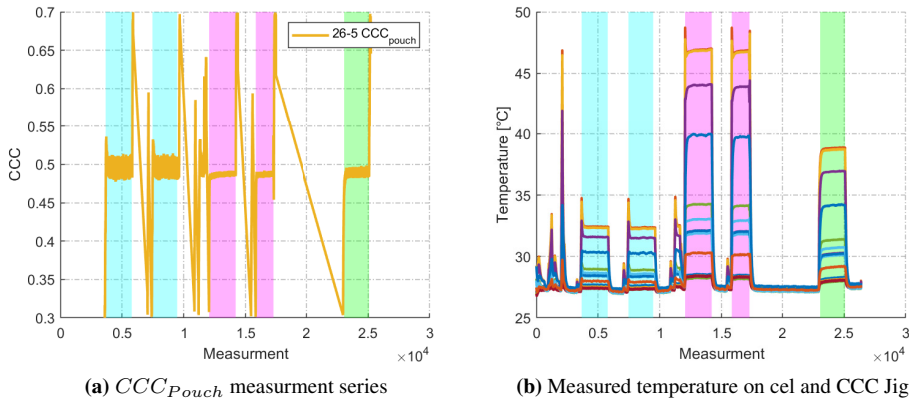


**Figure 4.12:** Colour sections represent measurement series taken at different C-rates. Cyan 2C, Magenta 4.5C and Green 3C

The results shows that the CCC should be able to predict the cooling potential of a cell. Given the heat generation and the CCC of a cell together with a maximum allowable temperature, the cooling system needed could be designed.

### 4.3.5 Error estimates

Looking back at equation 3.2 it can be seen that errors in all physical measurements scale linearly with the results, meaning an error of 1% in the measurement gives the same percentwise error the heat flux in the actual fin. The geometry of the CCC Jigs was measured out once, so any error in that measurements is constant for all tests done. The placement of the thermocouples is measured out before each measurement series, so this could change between each measurement. The distance is measured with a caliper, and all distances lie in the range 50-75mm. The measurements should be accurate at least to the nearest millimetre, giving an uncertainty of up to 2%. The uncertainty in the thermal interface

between the thermocouples, jig and cell is harder to quantify, but everything is connected with thermal grease for good conductivity. The heat loss is estimated by using thermocouple  $T_{15}$  as seen in figure 3.4. The heat transferred between  $T_5$  and  $T_{15}$  and  $T_{15}$  and  $T_4$  is compared to the heat between  $T_5$  and  $T_4$ . The result from that can be seen in figure 4.13 where the heat in fin two from 4.10b is plotted and seen to match well. The same study was done for the Tab jig.

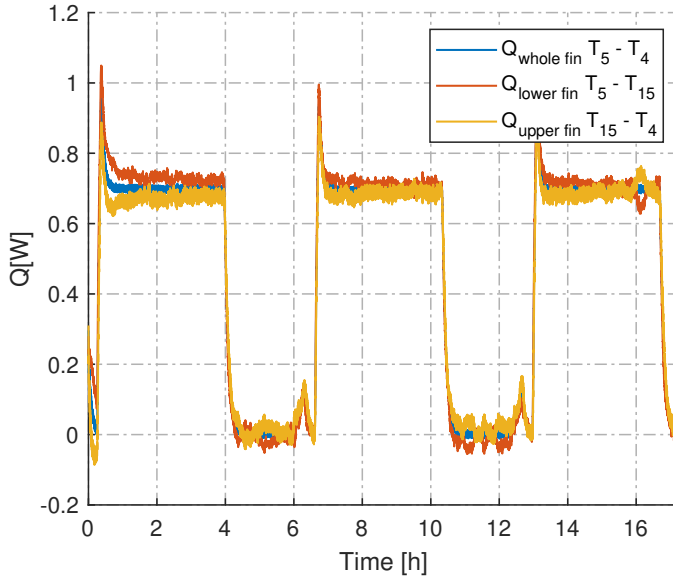


**Figure 4.13:** Heat transfer in fin 2 of the  $CCC_{Pouch}$  Jig

## 4.4 ICA

Figure 4.15 and 4.14 shows the discharge IC for the two cells of setup one at an interval of 5% SOH. The figure shows only 3.6-4.2V as there are no tops in the range 3-3.6V, and there was not any change in this section throughout ageing.

It is clear that for both cells, the largest drop in capacity comes due to the top at 3.78 V. With some loss at the peaks at 3.67V and 3.96 V. The reduction in all peaks indicates LAM, however, a loss in the peak under 3.78V indicates LLI [108]. The top around 3.78V was defined as the area between 3.75 and 3.81 V, and the capacity in this range was analysed. Both cells showed that the capacity decrease inside the range was nearly 67%. While outside the range was 25%. If an assumption is made that LAM gives an equal decrease in capacity through discharge, an additional capacity loss of 42% in the 3.75 to 3.81 V range was due to LLI. This equals 33% of the total capacity loss, the rest due to LAM. Note that this is at a 0.1C. The voltage range for these calculations could give uncertainties, especially due to the tops at 70% SOH is not as defined as at higher SOH.

At some voltages, both cells show a higher  $\frac{dQ}{dV}$ . This is not due to impedance increase, as can be seen from other otherwise matching tops. This could be explained by different parts of the electrodes reaching different OCV at different time. This could occur due to the non-homogeneous ageing of the cell. It was hypothesised that this effect would be more visible in the pouch cooled cell due to larger thermal gradients. However, from 4.16 it can be seen that the effect does not more predominantly affect the pouched cooled cell than the tab cooled cell. Which either could indicate that the "smoothing" of the curve is not due to homogeneous ageing or that, in fact, the tab cooled cell also is inhomogeneous aged. The thermal gradients during tab cooling are only available from CCC testing, where a temperature difference of 4.5°C was measured at the initial test. This is 50% of the thermal gradient which the pouched cool cell reached during ageing. However, still a significant thermal gradient which could lead to inhomogenous degradation.



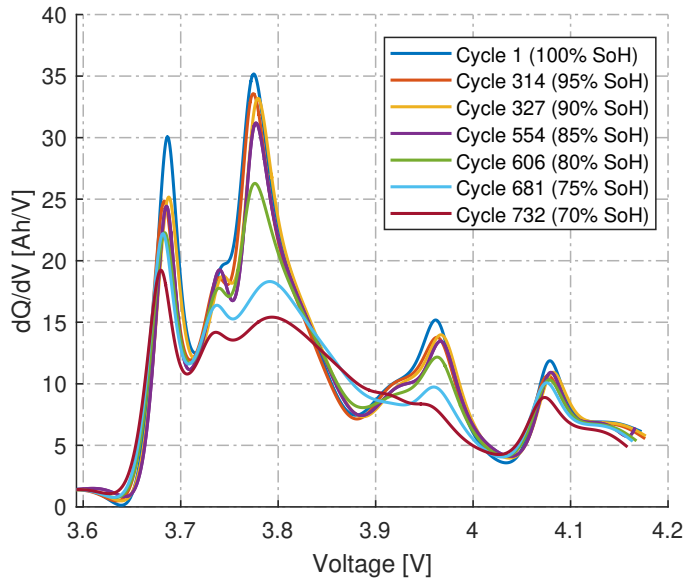


Figure 4.14: IC for 27-4.

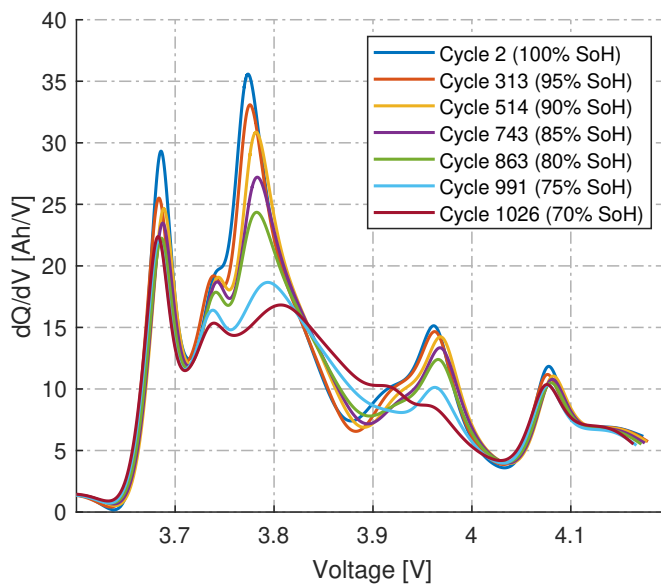
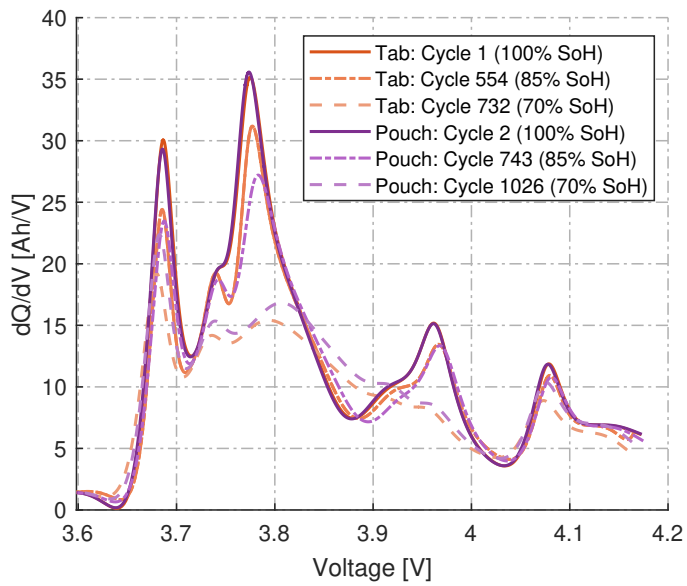


Figure 4.15: IC for 27-10.



**Figure 4.16:** IC for cells in setup 1.

## 4.5 Heat generation

### 4.5.1 Specific heat capacity (Cp) test results

To validate the results in the rest of this chapter a point mass thermal model of the cell were used. To get sufficient accuracy in the model the cells Specific heat capacity (Cp) were measured, since this is a property which is not obtainable solely from data-sheet values.

In section 3.3 the test done to characterise the cells Specific heat capacity (Cp) is described. The test was made to be simple, still yielding accurate enough results. The result from the test is presented in 4.2 and the measurement series leading to steady-state can be seen in figure 4.17. The specific heat of the tested cell were found by equation 3.1 to be  $Cp_{Cell} = 989.48 \frac{J}{kg \cdot K}$ .

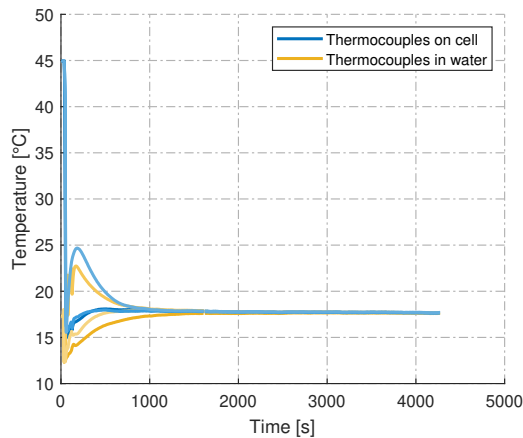


**Figure 4.17:** Results from the cell dropped into the water until steady state is reached. Three thermocouples were attached to the cell (shades of blue) and three in the water bath (shades of yellow). The cell was placed in the water bath right after  $t = 0s$ . The initial increase in temperature of two of the thermocouples is due to them being placed under the cell in the water bath.

**Table 4.2:** Measured and calculated variables for specific heat from test.  $Cp_{cell}$  calculated from equation 3.1 and  $Cp_{water}$  tabulated the rest measured

Variable	Value	Unit
$Cp_{water}$	4186	$\frac{J}{kg \cdot K}$
$m_{water}$	149.915	kg
$m_{cell}$	131.017	kg
$T_{water}$	12	$^{\circ}C$
$T_{cell}$	45	$^{\circ}C$
$T_{end}$	17.65	$^{\circ}C$
$Cp_{cell}$	989.4817	$\frac{J}{kg \cdot K}$

## 4.5.2 Overpotentials

The results for the overpotentials are split into two; internal resistance 4.18b and charge transfer 4.19a. Due to a scheduling error, only data for 45°C was obtained for the tab cooled cell at 80% SOH.

The results for internal resistance were in line with the hypothesis in terms that it increased with ageing and with the reduction of temperature. However, the two cells differ in the magnitude of increase. At the same SOH the internal resistance is higher for the 27-4. This indicates a small difference in degradation modes and, therefore, mechanisms.

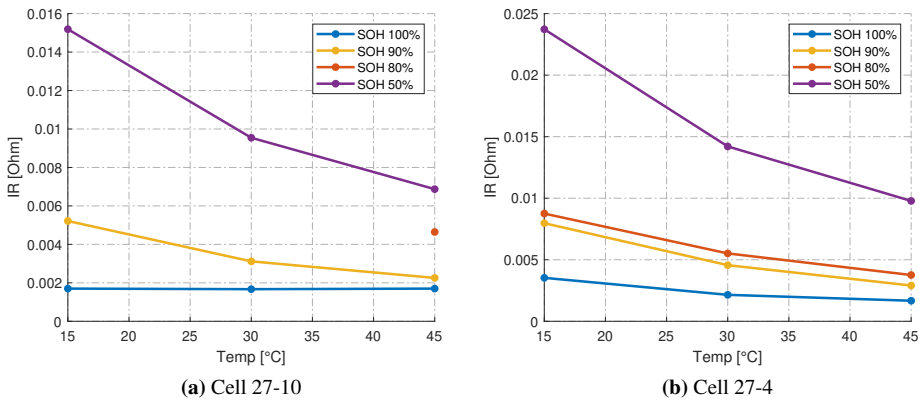


**Figure 4.18:** Internal resistance as a function of temperature at different SoC.

The charge transfer resistance measured showed itself to be independent of current, and therefore the results are shown as resistance. As this is not in accordance with the Butler-Volmer equation 2.14, the measurements done are not only for charge transfer but also other overpotentials.

The same tendencies can be found between the two cells for the charge transfer as for the internal resistance; that 27-4 has a higher impedance than the tab cooled cell. A higher charge transfer overpotential indicates a higher growth in SEI [76]. However, as the HPPC method did not manage to isolate the charge transfer overpotential, a conclusion can not be made only based on this evidence.

4.20 shows the charge transfer resistances dependencies on SOH. A slight reduction can be seen at 50% SOH compared to high and low SOH. This in accordance with theory.

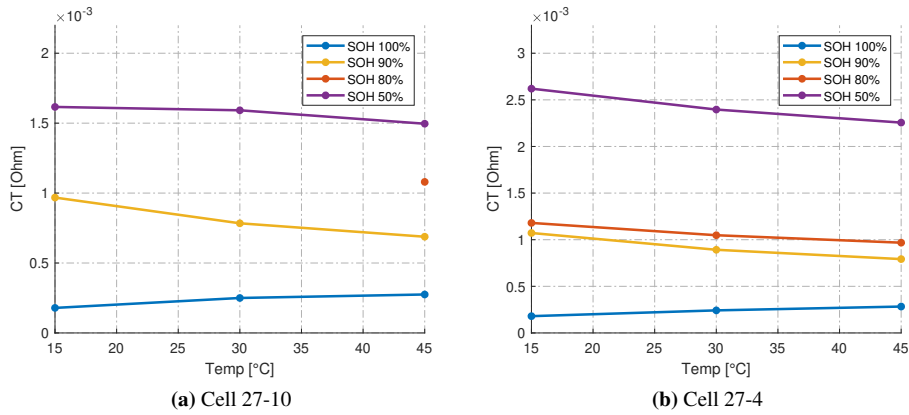


Figure 4.19: Charge transfer resistance as a function of temperature at different SoC.

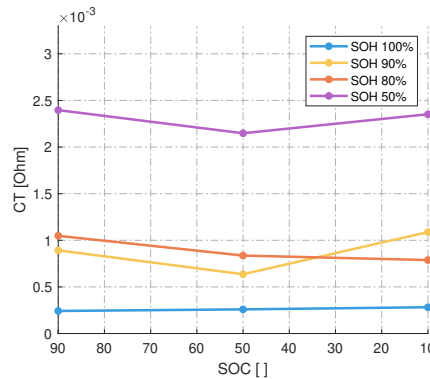
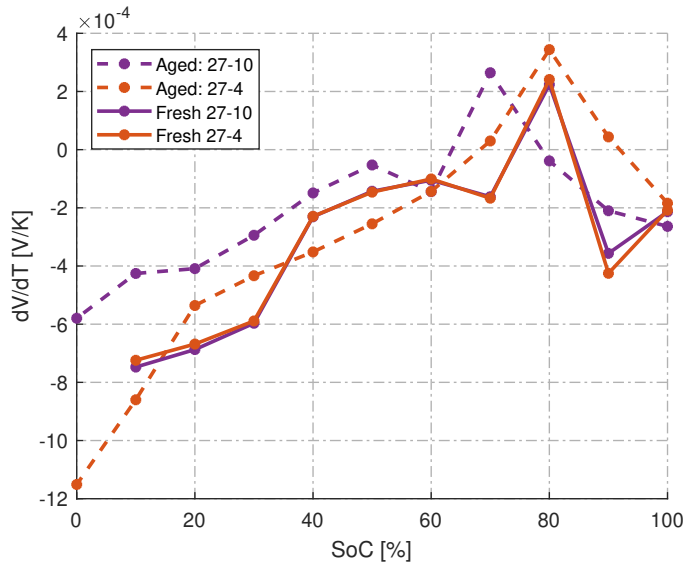


Figure 4.20: 27-10 at 30°C.

### 4.5.3 Entropy

For the pre-ageing measurements, both cells show a very similar curve. During a discharge from 100 to 0 % SOH the measurements would suggest only a 2.7% difference in reversible heating. This small deviation could be caused by both measurement inaccuracy or the cells being different. However, the small deviation suggests both a high accuracy as well as similar cells. The only significant deviation is found at 90 % SOH. Note that for 0 % SOH only cell 27-4 had measurements due to an error in scheduling.

For the aged cells  $\frac{dV}{dt}$  was much higher than for the new cells. This meant that the correction term was much bigger than for the new cells. This could lead to a bigger source in error with the method of choice, where a correction term for  $\frac{dV}{dt}$  is introduced. 27-4 followed a similar same shape as when it was new, but the magnituded change somewhat. 27-10 also kept the same shape, but shifted towards lower SOC.



**Figure 4.21:**  $\frac{dV}{dT}$  of the aged (50% SOH) and fresh cells.

#### 4.5.4 Validation

For validation of the heat generation, a simple single-point model was created. The model estimated the heat generation for a given current profile, and the results could be compared to those of test data.

The model has the following inputs and outputs:

##### Inputs

- Internal resistance as a function of temperature
- Charge transfer resistance as a function of temperature and SOH
- Entropy constants as a function of SOC
- Start temperature
- Heat capacity
- Heat loss
- Current profile

### Outputs

- Heat generation from the different contributors
- Temperature change

The model ran as following:

- Estimate heat generation as a function of temperature, SOH and current
- Estimate heat loss
- Estimate new cell temperature as a function of last temperature and heat generation and heat loss
- Estimate new cell SOH as a function of last SOH and current
- Repeat

Reversible heating is proportional to  $I$  (current). And charge transfer and Ohmic heating proportional to  $I^2$ . Therefore a growing deviation between the model and data as the C-rate increases suggests that the error lies in the ohmic and charge transfer resistance measurements. It must be noted that at higher C-rates and higher temperature, the charge transfer and internal resistance decrease, which would make them less predominant. .

4.22 shows that for the new cell the model and measurement fit well for all C-rates for 27-10. This indicates that both irreversible and reversible heating has been measured with high accuracy. For the aged cells the accuracy is low for lower C-rates. This indicates that the entropy measurements were off. This could be due to the  $\frac{dV}{dt}$  being high, and the correction term not able to give high enough accuracy. In addition the "tops" around 95-85% is shifted towards lower SOC. This is clearly showed in 4.22a. This could indicate that there was a problem with the SOC estimation during the entropy measurements.

4.23 shows that both initial measurements and measurements for the aged cells fit for 27-4. A slightly larger error in reversible heat can be seen for the aged cell in the 95-85% SOC range.

During the measurements of entropy the aged cells 27-10 showed a higher  $\frac{dV}{dt}$  compared to 27-4. As 27-4 measurements had a higher accuracy, while 27-10 had low accuracy, it can be hypothesised that the accuracy of the method used in this thesis has its accuracy severely compromised if  $\frac{dV}{dt}$  becomes too high.

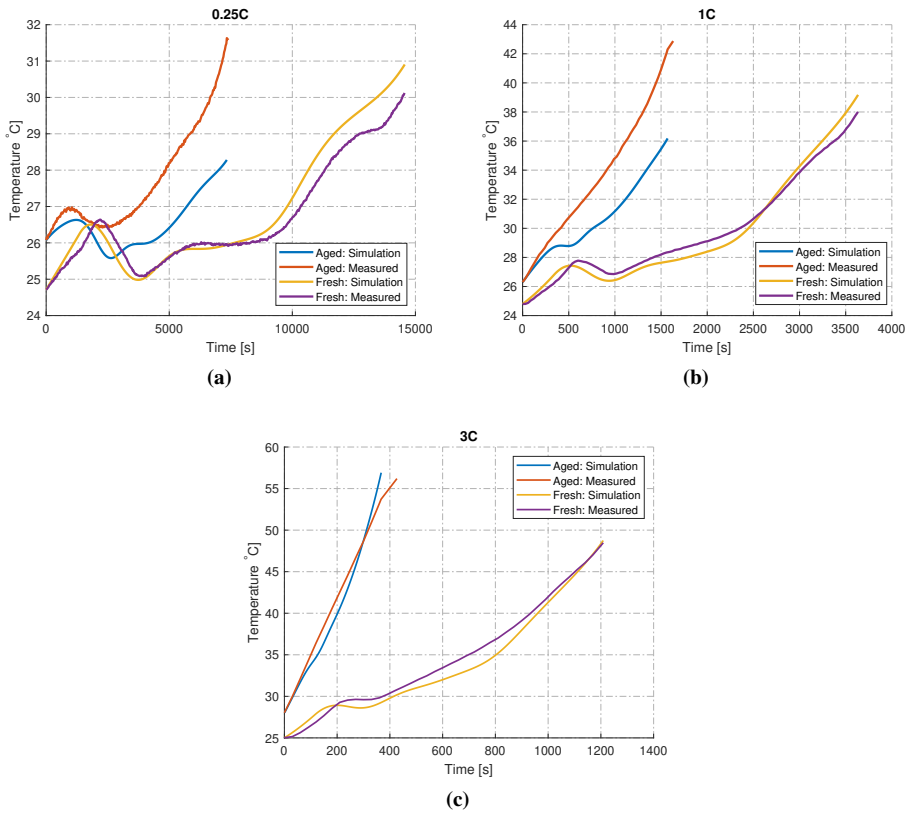
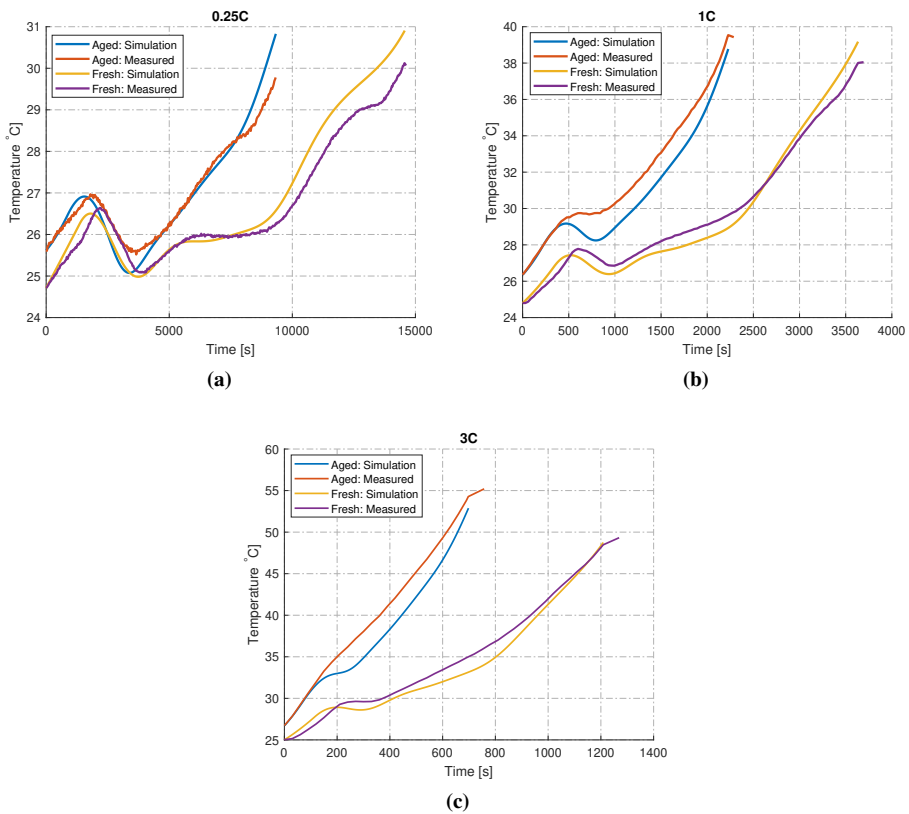


Figure 4.22: Temperature profile of model and point mass model 27-10.





**Figure 4.23:** Temperature profile of model and point mass model for 27-4.

## 4.6 Visual, mechanical and thermal inspection

### 4.6.1 Thickness

Introduction of the cell to the glovebox before it could be punctured to measure the thickness without eventual gas build-up means taking it thru a vacuum chamber to get rid of atmospheric air. Before the cell was introduced to the glovebox, it seemed inflated, being a bit bulky. When the cell was taken thru the vacuum chamber, it was seen to shrink 0.1mm and end up with some flat and bulky spots, suggesting some build-up of gas that may have escaped from the cell during vacuum. The measurements taken in the glovebox before and after the puncture of the cell were almost the same thickness, suggesting that if it were any build-up of gas, it escaped before the cell was punctured by us. As can be seen in table 4.3 the complete cell had grown more than 4mm from being pristine to ending up at 50% SOH. A comparison of a new and the aged cell opened is shown in figure 4.24

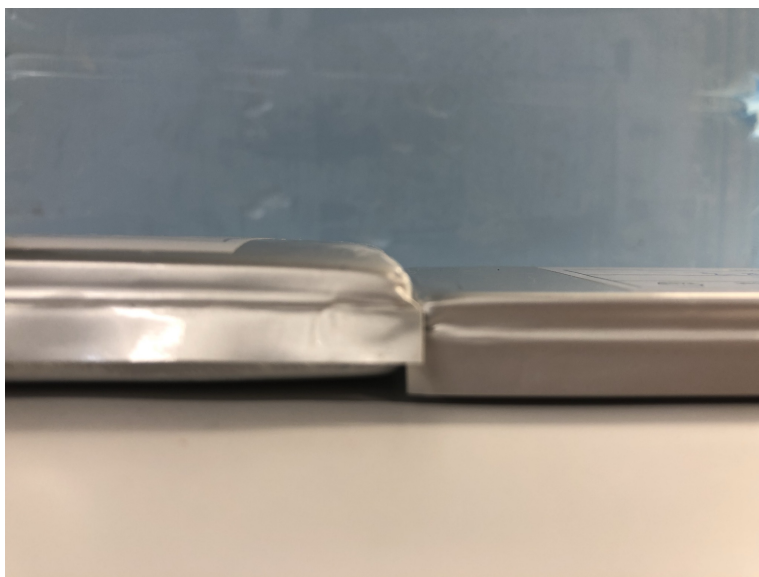


**Figure 4.24:** Visual comparison of the thickness of a aged and new cell. Side-view at the end furthest away from the tabs

The electrodes were seen to have grown considerably in thickness during the ageing process. As seen from the data in table 4.3 each cathode has grown  $4\mu\text{m}$  and the anode  $82\mu\text{m}$ . Seeing there are 43 layers of cathode and 44 layers of anode in the cell, this swelling sums up to  $4\mu\text{m} \cdot 43 + 82\mu\text{m} \cdot 44 = 3.78\text{mm}$ . So most of the cell growth can directly be put to the electrode layers growing.

**Table 4.3:** Measurements done on the battery cell and electrodes (current collector with active material) on pristine and aged cell. All number reported with double standard deviation  $2s$

Component	Pristine cell 100% SOH [29]	Aged cell 50% SOH
Complete cell atmospheric conditions	$10.15 \pm 0.18mm$	$14.38 \pm 0.17mm$
Complete cell in glovebox	-	$14.28 \pm 0.05mm$
Complete cell in glovebox punctured	-	$14.25 \pm 0.08mm$
Anode	$105.1 \pm 0.8\mu m$	$187 \pm 22\mu m$
Cathode	$90.0 \pm 1.9\mu m$	$94 \pm 5\mu m$

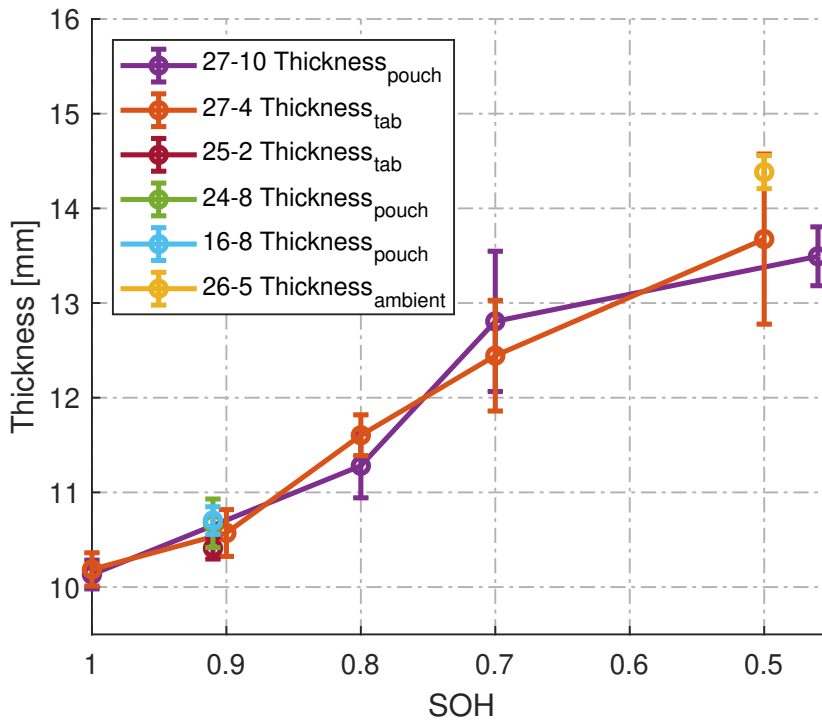


**Figure 4.25:** The thickness of the cells was monitored during ageing and was measured right before the cells were CCC characterized. How the cells were cooled is noted in subscript

## 4.6.2 Density

The density changes in the electrodes of the cell before and after ageing were calculated as described in section 3.5.4 and the results can be seen in table 4.4. There were not seen a substantial difference in weight of the samples before and after ageing, so the density change is mainly seen as a function of change in thickness.

**Table 4.4:** Measurements done on the electrodes (current collector with active material) on pristine and aged cell. All number reported with double standard deviation 2s

Component	Pristine cell 100% SOH [29]	Aged cell 50% SOH
Anode with Current Collector	1990 $\frac{kg}{m^3}$	1150 $\pm$ 120 $\frac{kg}{m^3}$
Cathode with Current Collector	3270 $\frac{kg}{m^3}$	3118 $\pm$ 155 $\frac{kg}{m^3}$

## 4.6.3 Thermal conductivity

As can be seen in figure 4.26a the thermal conductivity of the graphite anode has dropped significantly from the measurements done on a fresh electrode to the ones done on the aged electrode. At the lowest pressure step, the conductivity is down to only 25% of the original value. The LCO cathode materials thermal conductivity in figure 4.26b which has kept over 90% of its original thermal conductivity.

With the substantial difference in the active material conductivity loss for the Anode and cathode, it can look like the anode ageing has a greater impact on the overall thermal performance than the ageing of the cathode. Since we also have seen in section 4.6.1 that it is the Anode that stood for most of the thickness increase in the cell, the effect of a lower thermal conductivity in the Anode affects the thermal resistance in the cell more since the conductivity is measured per unit thickness of the layer.

It must be noted that the measurements are done on dry electrodes without electrolyte added in. We know from Trandem [29], Richter et al. [60] that adding in electrolyte contributes substantially to the thermal conductivity of the active electrode material. Since the aged Anode is less dense than the fresh one, it is taught that it is also more porous. How this will be affected when the electrolyte is added is unknown. Both Trandem [29], Richter et al. [60] reported at least a doubling of the thermal conductivity when electrolyte solvent was added to the samples. If the same is seen or a stronger effect on the aged Anode is uncertain and should be investigated further. Measurements with electrolyte were not prioritized in this work, since the electrolyte also decompose and the ageing of electrolyte itself could add differences to the results [87], this would not have been seen if the method with adding new electrolyte solvent to the samples before measuring thermal conductivity were to be used.

As mentioned in section 2.5.2 Richter [87] did not see the significant change in anode thermal conductivity with ageing as observed here. However, they used a hard-carbon anode cell, while here, a cell with graphite anode was investigated. In section 2.4.2 it was mentioned the difference in expansion and contraction between the hard-carbon and graphite-based anodes. The fact that the hard carbon anodes expands and contracts less in each cycle than the graphite might contribute to less cracking and is possible a contributor to the difference in measured conductivity.

Taking a brief look at the cells effective thru plane thermal conductivity it can be seen from equation 2.17 that for a fresh cell with dry electrodes and separator is  $k_{eff\ Fresh} = 0.3246 \frac{W}{mK}$  and for aged electrodes  $k_{eff\ Aged} = 0.1732 \frac{W}{mK}$ . Values from table 4.3 and 4.5 at 2.7bar is used as to calculate the thermal conductivities. The thickness and thermal conductivity of the separator, current collectors and pouch is from Trandem [29] and is unaltered between  $k_{eff\ Aged}$  and  $k_{eff\ Fresh}$ . As seen, the effective thermal conductivity of a dry aged cell is almost down to half of what the cell was as new, and this is mainly due to the changes in the Anode. Taking the swelling of the cell into account, as well as the change in conductivity, the thermal properties will be even less favourable for the aged cell.

**Table 4.5:** Thermal conductivity. The thermal conductivity for the electrode materials is for the active material only, the current collector thickness is removed. All measurements were done on dry electrodes. Values for fresh electrodes for comparison is from Trandem [29] and is done in the same rig under the same conditions

Material	Fresh 2.7bar [29]	Aged 2.7bar	Fresh 11.6bar [29]	Aged 11.6bar
Graphite Anode	$0.53 \pm 0.21$	$0.131 \pm 0.004$	$0.9 \pm 0.4$	$0.21 \pm 0.03$
LCO Cathode	$0.37 \pm 0.14$	$0.34 \pm 0.07$	$0.441 \pm 0.13$	$0.38 \pm 0.6$

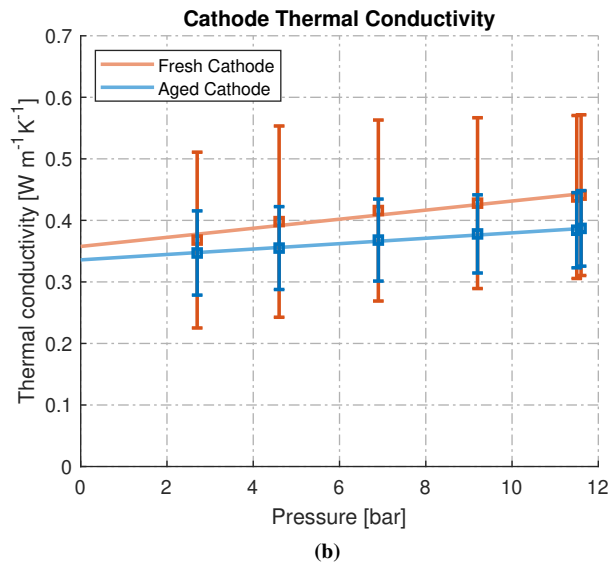
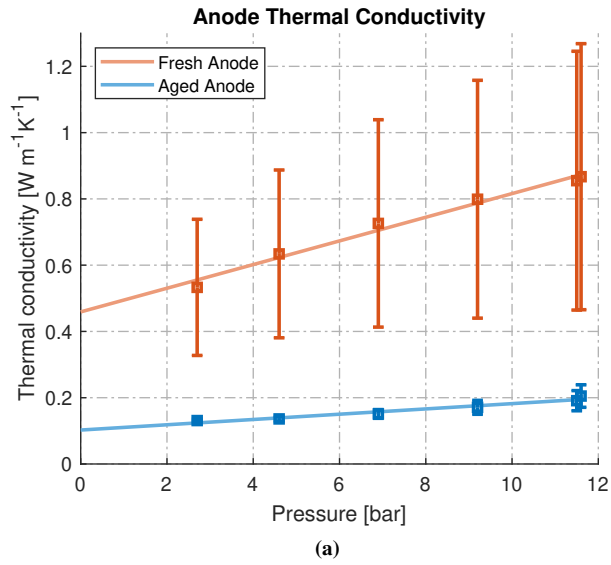
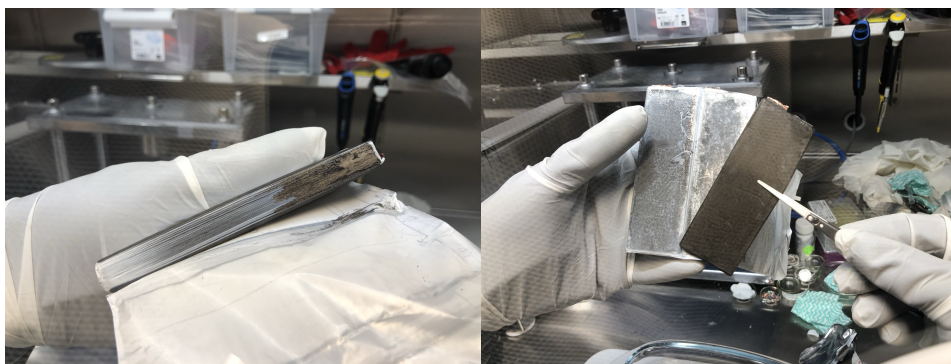


**Figure 4.26:** Thermal conductivity as function of compaction pressure of the electrodes from a fresh and an aged cell. Data from the fresh cell is from Trandem [29]

#### 4.6.4 Visual inspection of electrodes

When visually inspecting the cell upon opening, it was seen that the anode was crumbling and seemed to be in bad condition. Graphite dust was showing outside of the separator on the side where the Z-fold exposed the anode this can be seen in figure 4.27(a), dust from the anode were stuck to the separator when unwinding it, figure 4.27(b) and some parts of the active material had cracked off and were fastened to the separator as seen in figure 4.28.

In figure 4.29 fresh and aged electrodes can be seen. From the pictures and inspection, it looks like the Cathode seems unaffected by the cycling, while the anode seemed to have changed. The active material seemed to be less attached to the current collector, and some white particles were seen on the top of the anode.



(a) The Anode side of the electrode stack

(b) Anode taken out, the graphite can still be seen on the separator

**Figure 4.27:** Anode of aged cell



(a) Cracking of the electrode, also note the graphite dust (b) Delaminated electrode with graphite rests on the separator around the cell

**Figure 4.28:** Signs of mechanical damage on anode.



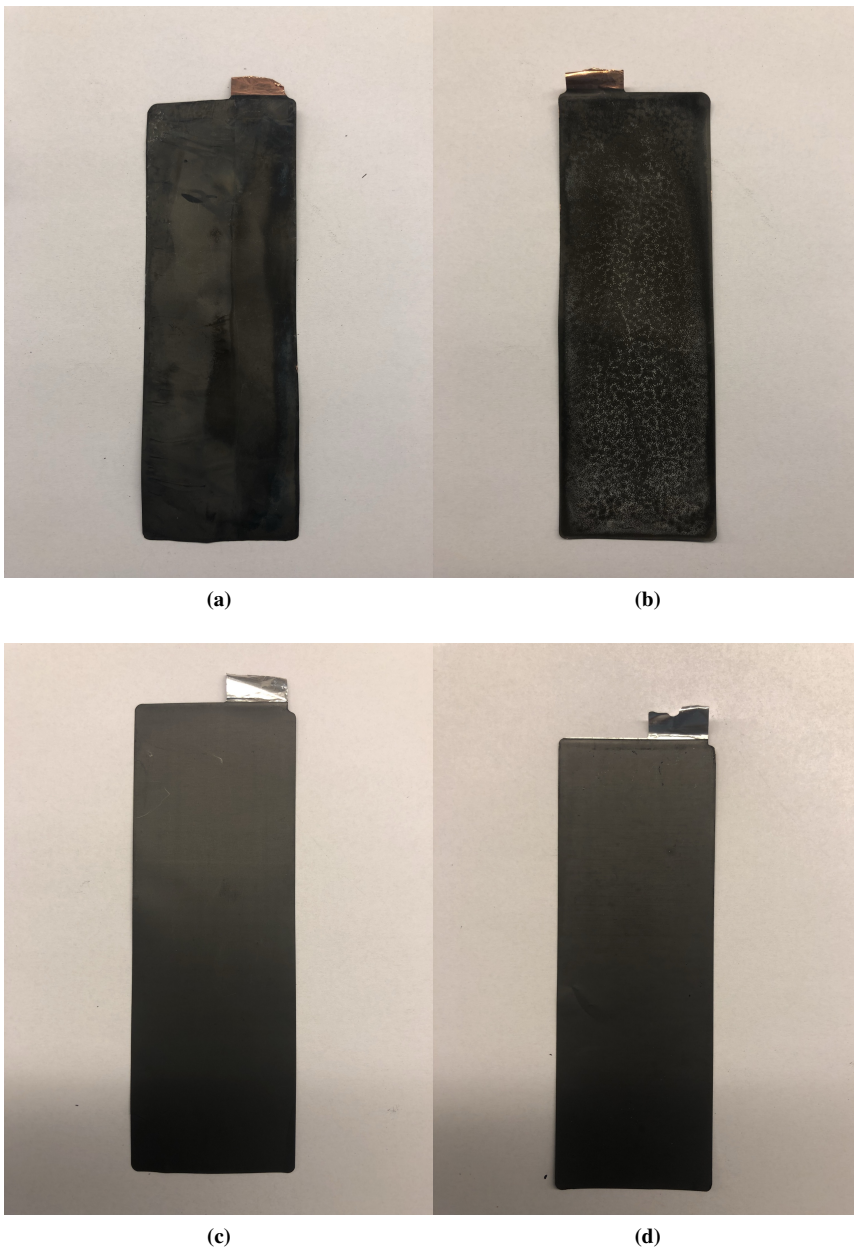


**Figure 4.29:** Pictures of aged and fresh anode and cathode taken out from their cells. The aged electrodes to the right and the fresh to the left.

### 4.6.5 Scanning electron microscope (SEM) Images

The SEM images presented in this section is taken by Silje Nornes Bryntesen at NTNU. The samples from the aged cell are taken from the middle of the stack. The samples pictured were taken from the top of the electrode in the area under the tabs. The aged electrodes comes from cell 26-5 and the fresh electrodes from a previously opened cell from the same batch.

In the images seen in figure 4.30 it can be seen that particles have formed on the surface, these particles can also be seen without enhancing and in figure 4.29b. Note that these particles were only visible after the evaporation of the solvent and only on the aged anode. From observations of the electrodes, it is thought that the particles seen are salt or bi-products from SEI growth from the electrolyte that has dried out after washing and formed the structure seen on the surface.

In figure 4.31 it can be seen that visually the cathode electrode is nearly unchanged before and after the ageing. Some difference can be seen in picture 4.31g and 4.31h, but mainly the cathode seem unaltered.

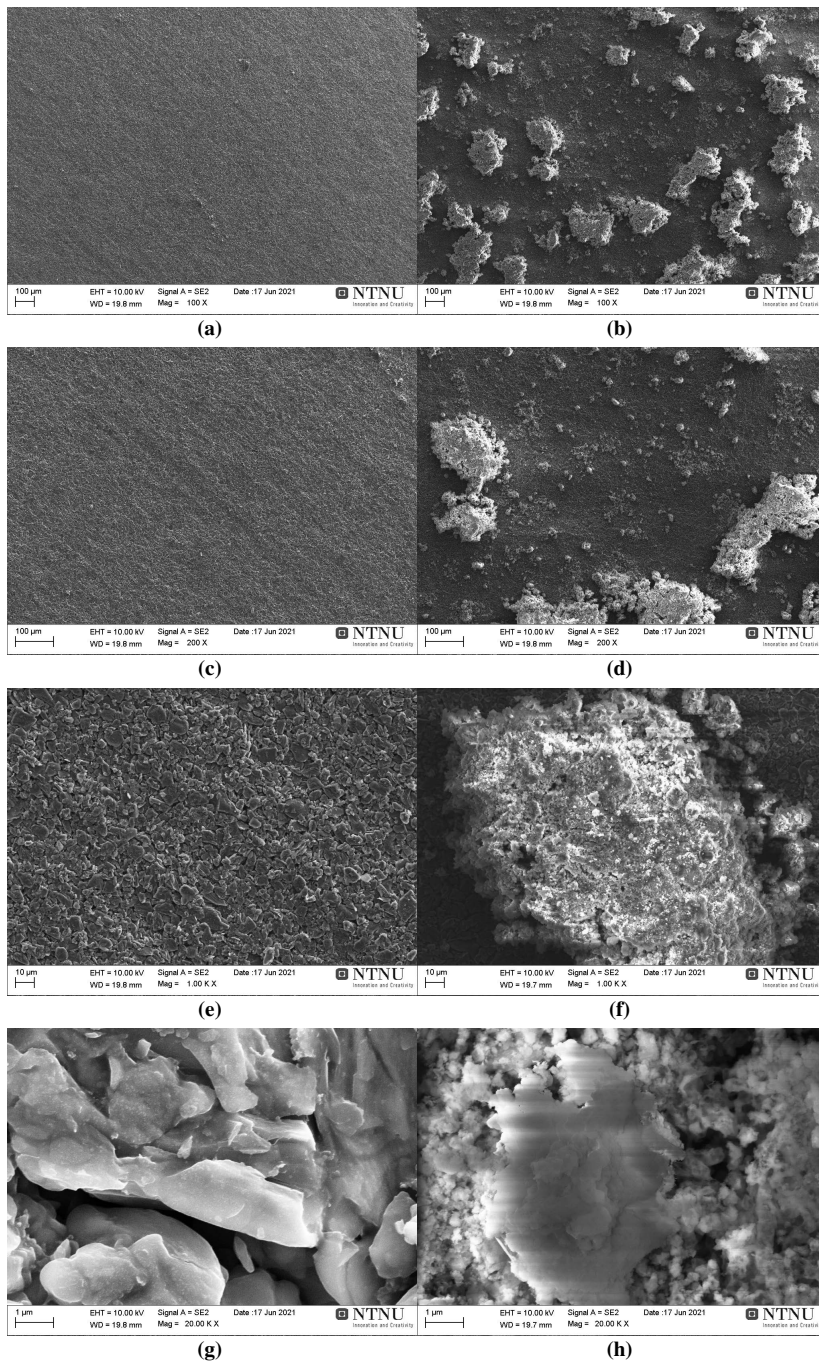


**Figure 4.30:** SEM images of Anode, one fresh cell and one aged. Equal magnification is placed side by side with the aged cell 26-5 to the right and the fresh cell to the left

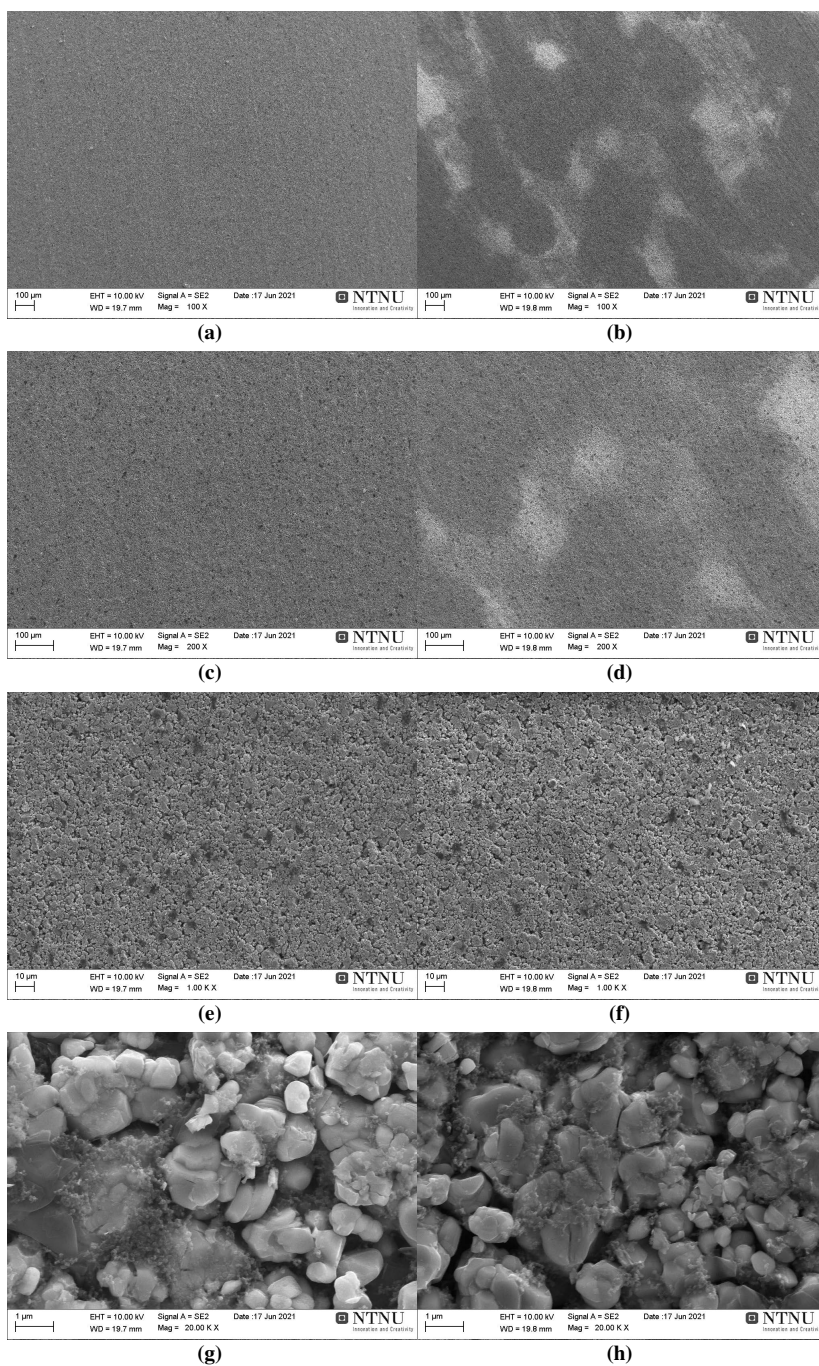


**Figure 4.31:** SEM images of Cathode, one fresh cell and one aged. Equal magnification is placed side by side with the aged cell 26-5 to the right and the fresh cell to the left

### 4.6.6 Summary of visual, mechanical and thermal properties

As seen thru all measurements done on the cell thru the cycling process, there were totally on the cell changes noticed in both density, thickness, CCC and electrical properties. When examining the two electrodes out of an aged cell, the visible changes both observable and from the SEM images the Anode is clearly more different from the pristine condition than the cathode. The same is seen during the mechanical inspection, where the Anode contributes most to the increased thickness of the cell, and the Anode density has changed more than the cathode. When measuring the thermal conductivity of the two electrodes, the Anodes conductivity has changed drastically while the Cathodes seems unaltered.

## 4.7 Degradation mode and mechanisms

This section will discuss the degradation mode and mechanisms which the different tests have indicated.

### 4.7.1 Capacity fade

Even though Cell 27-4 and 27-10 degraded at different rates, there was little evidence that the two cells had different degradation mode and mechanisms. The only difference seen, was a small offset in impedance. This could indicate 27-4 had higher growth of SEI, and is likely due to its higher operating temperature.

The ICA showed that approximately two-thirds of the capacity loss at 0.1C could be attributed to LAM while a third to LLI. The impact of impedance can be studied by the difference in by calculating the increase of capacity loss at 3 C compared to 0.1 C at 80% SOH versus 100%:

$$\% \text{ of loss due to impedance} = \frac{\frac{Cap(0.1C,80SoH)}{Cap(0.1C,100SoH)} - \frac{Cap(3C,80SoH)}{Cap(3C,100SoH)}}{1 - \frac{Cap(0.1C,80SoH)}{Cap(0.1C,100SoH)}} \quad (4.1)$$

where  $Cap(0.1C, 80SoH)$  is the capacity at 0.1C at 80% SOH, where SOH is defined by the 3C ageing cycles.

4.1 showed that 18.5% of the capacity loss at 3C for 27-4 was due to impedance increase. While the number for 27-10 was 12.9%. This is in coherence with the increased impedance measured for 27-4..

The dominating degradation mode, therefore, is believed to be LAM causing approximately 50% of the capacity fade while LLI and impedance increase contribute with approximately 30% and 20%.

LAM is believed to be related to the cyclic volume change of the anode. Both signs of cracking and delamination was found. The increased thickness indicates cracking, and the loss of anode particles as well as delamination from the current collector indicates both cracking as well as decomposition of the binder. The degradation could be explained by both the high C-rates, especially during charging, as well as the use of natural graphite in the anode. Natural graphite has a higher expansion rate than artificial graphite and is therefore, more prone to expansion related degradation mechanisms. [109] There was found little evidence that the cathode had been highly effected by cycling.

The SEM pictures of the anode show what is believed to be salts or agglomerated bi-products from the growth of SEI. The amount of bi-products indicates that a significant amount of electrolyte has reacted. This would both cause a LLI due to Lithium ions being consumed, as well as an impedance increase due to electrolyte consumption.

### 4.7.2 Decrease of CCC

The drastic change in CCC for the pouched cooled cell 27-10 fit the hypothesis; that swelling and decomposing of the electrolyte would decrease the through-plane conductivity. In addition a substansal decrease in thermal conductivity of the anode was measured. This could however be contributed by the swelling and the following increase of porosity. Though it is certian that the anode with electrolyte had an decrease of thermal conductivity, it is not as certian on how much. This is due to the uncertainty to the fraction of the anode filled with the electrolyte, aswell as porosity and tortuosity changes.

Comparing the change in thermal conductance of the pristine and aged cell with the change in CCC can give some insight in the behavior of the cells :

$$C_{eff} = \frac{k_{eff}}{t_{cell}} \quad (4.2)$$

Where  $C_{eff}$  is the thermal conductance of the cell,  $k_{eff}$  is the average thermal conductivity of the cell calculated by equation 2.17 and given in table section 4.6.3 and  $t_{cell}$  is the cells thickness from table 4.3. Using the previously derived values we get:

$$\frac{C_{eff\ Aged}}{C_{eff\ Pristine}} = \frac{12}{31} = 0.53$$
$$\frac{CCC_{Aged}}{CCC_{Pristine}} = \frac{0.58}{1.25} = 0.464$$

Without knowing anything about the effect the electrolyte has on the thermal conductivity of the aged cell, compared to a new, it looks like the CCC measurement follows the change of the thermal conductance to some extent.

It was hypothesised that the tab cooled cell, 27-4, would have a lower change in CCC when cycled. This due to a higher percentage of the thermal resistivity was in the tab and

tab-current collector weld [90, 110]; two parts that are not heavily impacted by cycling. Though the tab cooled cell had a lower absolute reduction of its CCC compared to 27-10, percentage reduction was approximately the same; a little over 50% for cell 27-4. Cell 25-2 did not show the same behaviour, and no conclusion has been drawn about the results of the change in the tab cooled CCC. The following paragraphs will make an assumption that the measurements for 27-4 were correct, and will discuss any underlying mechanisms which could decrease the CCC for a tab cooled cell.

The same degradation mechanisms that impact pouch CCC also impact tab CCC. If an assumption is made that pouch CCC is majorly dependent on the conductivity of separator, electrolyte and electrode, it can be concluded that degradation to other parts also contributes to the lowering of tab CCC. This conclusion can be drawn since pouch and tab CCC both dropped by approximately 50%, but since tab CCC is less dependent on the separator, electrolyte and electrode, other factors must also be at play.

One other possible explanation was that the origin of the heat moved away from the tabs. CCC is not a pure measurement of thermal conductivity; it is also impacted by where the heat is generated. If all the heat is generated in close proximity to the tabs, a higher CCC will be measured than if the heat is produced further away from the cell. If the origin of the heat moved away from the tabs, an increase in CCC could occur. However, Zhao et al. [97] showed the current collectors were not the bottleneck of removing heat through the tabs, but rather the tab weld. This would mean that the origin of the heat generation should not have a big impact on CCC as long as it has to travel through the tab weld.

With the conflicting results in CCC for 27-4 and 25-2 and no good explanation for a drop in CCC, it is suspected that the initial measurements for 27-4 or 25-2 were off. No conclusive conclusion could therefore be made.





# Conclusion & Further Work

## 5.1 Conclusion

The TMS impact on the degradation mechanisms of a LIB was investigated. Two cooling systems and two cooling temperatures were compared. Different ageing rates observed, and the temperature the cells ended up at during cycling was seen as a more dominant ageing mechanism than the thermal gradients occurring caused by the cooling system. For the cell in question with the applied cooling systems, the choice of tab or pouch cooling is a choice between one cycle capacity performance and life span mainly because of the temperature the cooling system managed to cool the cell down to, not the cooling method itself.

Entropy, HPPC, ICA, physical inspection, and capacity measurements done on the cells revealed and isolated the contribution of the different ageing modes and mechanisms. LAM due to cracking and delamination was identified as the dominating mode and mechanism. However, the cell also experienced a substantial LLI and impedance increase, likely due to SEI growth. 27-4 experienced a somewhat higher impedance increase, likely due to increased growth of SEI due to higher temperatures. However, there was little evidence that the thermal gradients in the pouch cooled cells gave other underlying degradation mechanisms.

By the use of the CCC, it was possible to monitor the changes in the thermal behaviour of the cells under cycling. It was observed that the CCC for pouch cooled cells were decreasing and ended up at half the original value at the LIBs End of life. This observation correlated with the data gathered from thermal conductivity testing of the electrodes from a fresh cell and one cell at EOL. The effective thermal conductance calculated from the measurements correlated well with the change in CCC for the pouch cell.

The CCC measurements done for the tab cooled cells were less conclusive, and the two cells monitored showed contradicting behaviour. The first tab cooled cell showed the

same tendencies as the pouch cooled in the change of its CCC halving in the course of its life, while the other cell was measured to have a lower initial CCC which went slightly up at the second measurement done when the cell was at 90% SOH. Unfortunately, time did not allow for more measurements, and no conclusion could be taken on the behaviour of the tab cooled cell.

Thru evaluation of the CCC for both tab and pouch cooled cell, it was seen that the cells used in the thesis were not suited for a tab cooling strategy and even at the EOL the surface cooled cell had a higher CCC value than the highest measurement from the tabs. It was seen that the CCC could be a valuable tool for battery pack designers to dimension cooling system. Using this one metric and knowledge of the heat generation, a choice of cooling system could be made.

Thru ageing analysis of the CCC metric and the heat generation of the cell, it is seen that for a battery cooling system to work thru the entire cells life it is not sufficient to dimension for the BOL conditions. With the changes seen in heat generation and CCC, it was shown that it is crucial to not only have a design that cools sufficiently at cells BOL also at the EOL.

## 5.2 Further Work

The thesis showed that the dominating factor of degradation was temperature. However, how much the thermal gradients impacted the performance was not fully understood. Cycling more pouch and tab cooled cells with the same initial average temperature could uncover how much performance is gained by limiting the thermal gradients.

Reduction in the thermal conductivity of the anode was shown to be an essential factor in the reduction of the CCC of the pouched cooled cells. However, the interaction between the aged anode and electrolyte were not investigated. Each component's contribution as a function of swelling, porosity and solvent fractions can be better understood with a 2-d model. A 2-d thermal model could be used to understand of the measured change in CCC and heat generation is affecting the temperature and temperature gradients inside cells cooled with the different strategies.

No conclusion was made regarding cycles impact on  $CCC_{Tab}$ . Further testing is therefore needed to determine if a tab cooled system dimensioned for BOL is sufficient for the cells whole lifespan.

A lot of the work done in the experimental part were spent on rebuilding the CCC characterization jigs before each measurement. In future studies using the same method, the experiments should be designed so that the cells could be cycled without needing to be move them between characterization and cycle runs. Optimally the cells should be cycled in the CCC jigs so measurements of the CCC can be performed more regularly without a huge effort. A future design of a CCC jig should be designed with temperature sensors permanently mounted to eliminate the possible error from measuring out their placements every time.



# Bibliography

- [1] Laura Lander, Evangelos Kallitsis, Alastair Hales, Jacqueline Sophie Edge, Anna Korre, and Gregory Offer. Cost and carbon footprint reduction of electric vehicle lithium-ion batteries through efficient thermal management. *Applied Energy*, 289 (January):116737, 2021. ISSN 03062619. doi: 10.1016/j.apenergy.2021.116737. URL <https://doi.org/10.1016/j.apenergy.2021.116737>.
- [2] EEA. *Electric vehicles from life cycle and circular economy perspectives*. Number 13. 2018. ISBN 9789292139858. URL <https://www.eea.europa.eu/publications/electric-vehicles-from-life-cycle>.
- [3] Transport & Environment. How clean are electric cars? pages 1–33, 2020. URL <https://www.transportenvironment.org/sites/te/files/downloads/T%26E\OT1\textquoterightsEVlifecycleanalysisLCA.pdf>.
- [4] Ian A. Hunt, Yan Zhao, Yatish Patel, and J. Offer. Surface Cooling Causes Accelerated Degradation Compared to Tab Cooling for Lithium-Ion Pouch Cells. *Journal of The Electrochemical Society*, 163(9):A1846–A1852, 2016. ISSN 0013-4651. doi: 10.1149/2.0361609jes.
- [5] Jacqueline Sophie Edge, Simon O’Kane, Ryan Prosser, Niall D. Kirkaldy, Anisha N Patel, Alastair Hales, Abir Ghosh, Weilong Ai, Jingyi Chen, Jason Jiang, Shen Li, Mei-Chin Pang, Laura Bravo Diaz, Anna Tomaszewska, M. Waseem Marzook, Karthik N Radhakrishnan, Huizhi Wang, Yatish Patel, Billy Wu, and Gregory J. Offer. Lithium Ion Battery Degradation: What you need to know. *Physical Chemistry Chemical Physics*, pages 8200–8221, 2021. ISSN 1463-9076. doi: 10.1039/d1cp00359c.
- [6] Christoph R Birkel, Matthew R Roberts, Euan Mcturk, Peter G Bruce, and David A Howey. Degradation diagnostics for lithium ion cells. *Journal of Power Sources*, 341:373–386, 2017. ISSN 0378-7753. doi: 10.1016/j.jpowsour.2016.12.011. URL <http://dx.doi.org/10.1016/j.jpowsour.2016.12.011>.

- 
- [7] Oskar Dondelewski, Teddy Szemberg O'Connor, Yan Zhao, Ian A. Hunt, Alexander Holland, Alastair Hales, Gregory J. Offer, and Yatish Patel. The role of cell geometry when selecting tab or surface cooling to minimise cell degradation. *eTransportation*, 5:100073, 2020. ISSN 25901168. doi: 10.1016/j.etrans.2020.100073. URL <https://doi.org/10.1016/j.etrans.2020.100073>.
- [8] Alastair Hales, Laura Bravo Diaz, Mohamed Waseem Marzook, Yan Zhao, Yatish Patel, and Gregory Offer. The Cell Cooling Coefficient: A Standard to Define Heat Rejection from Lithium-Ion Batteries. *Journal of The Electrochemical Society*, 166(12):A2383–A2395, 2019. ISSN 0013-4651. doi: 10.1149/2.0191912jes.
- [9] Gregory L. Plett. *Battery Management Systems*. 2015. ISBN 9781630810238.
- [10] Orjan Gjengedal. Real Time Impedance identification of Li- Polymer Battery with Kalman Filter. (November), 2017.
- [11] Wolfgang Haserieder, Arno Kwade, Eike Wiegmann, and Sagar VEmla. Fundamentals of the battery cell production - Processes, products and their interactions. *IBPC Seminar*, 2019.
- [12] Lena Spitthoff, Paul R. Shearing, and Odne Stokke Burheim. Temperature, Ageing and Thermal Management of Lithium-Ion Batteries. *Energies*, 14(5):1248, 2021. ISSN 19961073. doi: 10.3390/en14051248.
- [13] Naoki Nitta, Feixiang Wu, Jung Tae Lee, and Gleb Yushin. Li-ion battery materials: Present and future. *Materials Today*, 18(5):252–264, 2015. ISSN 18734103. doi: 10.1016/j.mattod.2014.10.040. URL <http://dx.doi.org/10.1016/j.mattod.2014.10.040>.
- [14] Gert Berckmans, Lysander De Sutter, Mario Marinaro, Jelle Smekens, Joris Jaguemont, Margret Wohlfahrt-Mehrens, Joeri van Mierlo, and Noshin Omar. Analysis of the effect of applying external mechanical pressure on next generation silicon alloy lithium-ion cells. *Electrochimica Acta*, 306:387–395, 2019. ISSN 00134686. doi: 10.1016/j.electacta.2019.03.138. URL <https://doi.org/10.1016/j.electacta.2019.03.138>.
- [15] Xiuxia Zuo, Jin Zhu, Peter Müller-Buschbaum, and Ya Jun Cheng. Silicon based lithium-ion battery anodes: A chronicle perspective review. *Nano Energy*, 31(October 2016):113–143, 2017. ISSN 22112855. doi: 10.1016/j.nanoen.2016.11.013. URL <http://dx.doi.org/10.1016/j.nanoen.2016.11.013>.
- [16] Ghassan Zubi, Rodolfo Dufo-López, Monica Carvalho, and Guzay Pasaoglu. The lithium-ion battery: State of the art and future perspectives. *Renewable and Sustainable Energy Reviews*, 89(April 2017):292–308, 2018. ISSN 18790690. doi: 10.1016/j.rser.2018.03.002.
- [17] Naoki Nitta, Feixiang Wu, Jung Tae Lee, and Gleb Yushin. Li-ion battery materials: Present and future. *Materials Today*, 18(5):252–264, 2015. ISSN 18734103. doi: 10.1016/j.mattod.2014.10.040. URL <http://dx.doi.org/10.1016/j.mattod.2014.10.040>.

- 
- [18] Benjamin K. Sovacool. The precarious political economy of cobalt: Balancing prosperity, poverty, and brutality in artisanal and industrial mining in the Democratic Republic of the Congo. *Extractive Industries and Society*, 6(3):915–939, 2019. ISSN 2214790X. doi: 10.1016/j.exis.2019.05.018. URL <https://doi.org/10.1016/j.exis.2019.05.018>.
- [19] Ines Baccouche, Sabeur Jemmali, Bilal Manai, Noshin Omar, and Najoua Essoukri Ben Amara. Improved OCV model of a Li-ion NMC battery for online SOC estimation using the extended Kalman filter. *Energies*, 10(6):1–22, 2017. ISSN 19961073. doi: 10.3390/en10060764.
- [20] M. Broussely, Ph Biensan, F. Bonhomme, Ph Blanchard, S. Herreyre, K. Nechev, and R. J. Staniewicz. Main aging mechanisms in Li ion batteries. *Journal of Power Sources*, 146(1-2):90–96, 2005. ISSN 03787753. doi: 10.1016/j.jpowsour.2005.03.172.
- [21] Veerapandian Ponnuchamy, Stefano Mossa, and Ioannis Skarmoutsos. Solvent and Salt Effect on Lithium Ion Solvation and Contact Ion Pair Formation in Organic Carbonates: A Quantum Chemical Perspective. *Journal of Physical Chemistry C*, 122(45):25930–25939, 2018. ISSN 19327455. doi: 10.1021/acs.jpcc.8b09892.
- [22] Pengcheng Zhu, Dominika Gastol, Jean Marshall, Roberto Sommerville, Vanessa Goodship, and Emma Kendrick. A review of current collectors for lithium-ion batteries. *Journal of Power Sources*, 485(December 2020):229321, 2021. ISSN 03787753. doi: 10.1016/j.jpowsour.2020.229321. URL <https://doi.org/10.1016/j.jpowsour.2020.229321>.
- [23] Stephen E. Trask, Yan Li, Joseph J. Kubal, Martin Bettge, Bryant J. Polzin, Ye Zhu, Andrew N. Jansen, and Daniel P. Abraham. From coin cells to 400 mAh pouch cells: Enhancing performance of high-capacity lithium-ion cells via modifications in electrode constitution and fabrication. *Journal of Power Sources*, 259:233–244, 2014. ISSN 03787753. doi: 10.1016/j.jpowsour.2014.02.077. URL <http://dx.doi.org/10.1016/j.jpowsour.2014.02.077>.
- [24] Madhav Singh, Jörg Kaiser, and Horst Hahn. Thick Electrodes for High Energy Lithium Ion Batteries. *Journal of The Electrochemical Society*, 162(7):A1196–A1201, 2015. ISSN 0013-4651. doi: 10.1149/2.0401507jes.
- [25] K.A. Murashko. *Thermal modelling of commercial lithium-ion batteries*. Number January. 2016. ISBN 9789522659071. doi: 10.13140/RG.2.1.3930.0723.
- [26] Alexander Rheinfeld, Johannes Sturm, Alexander Frank, Stephan Kosch, Simon V. Erhard, and Andreas Jossen. Impact of Cell Size and Format on External Short Circuit Behavior of Lithium-Ion Cells at Varying Cooling Conditions: Modeling and Simulation. *Journal of The Electrochemical Society*, 167(1):013511, 2020. ISSN 0013-4651. doi: 10.1149/2.0112001jes.
- [27] Ashkan Nazari and Siamak Farhad. Heat generation in lithium-ion batteries with different nominal capacities and chemistries. *Applied Thermal Engineering*, 125:
-

- 
- 1501–1517, 2017. ISSN 1359-4311. doi: 10.1016/j.applthermaleng.2017.07.126. URL <http://dx.doi.org/10.1016/j.applthermaleng.2017.07.126>.
- [28] Ashkan Nazari and Siamak Farhad. Heat generation in lithium-ion batteries with different nominal capacities and chemistries. *Applied Thermal Engineering*, 125: 1501–1517, 2017. ISSN 13594311. doi: 10.1016/j.applthermaleng.2017.07.126. URL <http://dx.doi.org/10.1016/j.applthermaleng.2017.07.126>.
- [29] Christian Trandem. Heat generation and cooling in lithium-ion pouch cells, 2020.
- [30] Kristian Eggereide Roaldsnes. Exploration of Nonlinearities in a Lithium Ion Battery Cell Model and their impact on Particle Filters and Nonlinear Kalman Filters for State of Charge Estimation. (June), 2018.
- [31] Xuebing Han, Mingguo Ouyang, Languang Lu, Jianqiu Li, Yuejiu Zheng, and Zhe Li. A comparative study of commercial lithium ion battery cycle life in electrical vehicle: Aging mechanism identification. *Journal of Power Sources*, 251:38–54, 2014. ISSN 03787753. doi: 10.1016/j.jpowsour.2013.11.029. URL <http://dx.doi.org/10.1016/j.jpowsour.2013.11.029>.
- [32] Andrea Marongiu, Nsombo Nlandi, Yao Rong, and Dirk Uwe Sauer. On-board capacity estimation of lithium iron phosphate batteries by means of half-cell curves. *Journal of Power Sources*, 324:158–169, 2016. ISSN 03787753. doi: 10.1016/j.jpowsour.2016.05.041. URL <http://dx.doi.org/10.1016/j.jpowsour.2016.05.041>.
- [33] Matthieu Dubarry, Cyril Truchot, and Bor Yann Liaw. Synthesize battery degradation modes via a diagnostic and prognostic model. *Journal of Power Sources*, 219:204–216, 2012. ISSN 03787753. doi: 10.1016/j.jpowsour.2012.07.016. URL <http://dx.doi.org/10.1016/j.jpowsour.2012.07.016>.
- [34] Kuo-hsin Tseng, Jin-wei Liang, Wunching Chang, and Shyh-chin Huang. Regression Models Using Fully Discharged Voltage and Internal Resistance for State of Health Estimation of Lithium-ion Batteries. pages 2889–2907, 2015. doi: 10.3390/en8042889.
- [35] Witold Maranda. Capacity degradation of lead-acid batteries under variable-depth cycling operation in photovoltaic system. *Proceedings of the 22nd International Conference Mixed Design of Integrated Circuits and Systems, MIXDES 2015*, (June):552–555, 2015. doi: 10.1109/MIXDES.2015.7208584.
- [36] Feng Leng, Cher Ming Tan, and Michael Pecht. Effect of Temperature on the Aging rate of Li Ion Battery Operating above Room Temperature. *Scientific Reports*, 5: 1–12, 2015. ISSN 20452322. doi: 10.1038/srep12967.
- [37] J. Vetter, P. Novák, M. R. Wagner, C. Veit, K. C. Möller, J. O. Besenhard, M. Winter, M. Wohlfahrt-Mehrens, C. Vogler, and A. Hammouche. Ageing mechanisms in
-



- 
- lithium-ion batteries. *Journal of Power Sources*, 147(1-2):269–281, 2005. ISSN 03787753. doi: 10.1016/j.jpowsour.2005.01.006.
- [38] Keith. J. Laidler. Reaction rate, 2020.
- [39] Chelsea Snyder. The effects of charge/discharge rate on capacity fade of lithium ion batteries. *Ph.D. Thesis*, 2016. URL <https://ui.adsabs.harvard.edu/abs/2016PhDT.....260S>.
- [40] Saurabh Saxena, Yinjiao Xing, Daeil Kwon, and Michael Pecht. Accelerated degradation model for C-rate loading of lithium-ion batteries. *International Journal of Electrical Power and Energy Systems*, 107(September 2018):438–445, 2019. ISSN 01420615. doi: 10.1016/j.ijepes.2018.12.016. URL <https://doi.org/10.1016/j.ijepes.2018.12.016>.
- [41] Chelsea Snyder. The rate dependency of Li-ion Battery Degradation Mechanisms. 2016.
- [42] Yuliya Preger, Heather M. Barkholtz, Armando Fresquez, Daniel L. Campbell, Benjamin W. Juba, Jessica Romàn-Kustas, Summer R. Ferreira, and Babu Chalamala. Degradation of Commercial Lithium-Ion Cells as a Function of Chemistry and Cycling Conditions. *Journal of The Electrochemical Society*, 167(12):120532, 2020. ISSN 0013-4651. doi: 10.1149/1945-7111/abae37.
- [43] Radu Gogoana, Matthew B. Pinson, Martin Z. Bazant, and Sanjay E. Sarma. Internal resistance matching for parallel-connected lithium-ion cells and impacts on battery pack cycle life. *Journal of Power Sources*, 252:8–13, 2014. ISSN 03787753. doi: 10.1016/j.jpowsour.2013.11.101. URL <http://dx.doi.org/10.1016/j.jpowsour.2013.11.101>.
- [44] Evelina Wikner. Lithium ion Battery Aging: Battery Lifetime Testing and Physics-based Modeling for Electric Vehicle Applications. page 76, 2017.
- [45] Yang Gao, Jiuchun Jiang, Caiping Zhang, Weige Zhang, Zeyu Ma, and Yan Jiang. Lithium-ion battery aging mechanisms and life model under different charging stresses. *Journal of Power Sources*, 356:103–114, 2017. ISSN 03787753. doi: 10.1016/j.jpowsour.2017.04.084. URL <http://dx.doi.org/10.1016/j.jpowsour.2017.04.084>.
- [46] Yu Merla, Billy Wu, Vladimir Yufit, Nigel P. Brandon, Ricardo F. Martinez-Botas, and Gregory J. Offer. Novel application of differential thermal voltammetry as an in-depth state-of-health diagnosis method for lithium-ion batteries. *Journal of Power Sources*, 307:308–319, 2016. ISSN 03787753. doi: 10.1016/j.jpowsour.2015.12.122.
- [47] Rong Xu, Yang Yang, Fei Yin, Pengfei Liu, Peter Cloetens, Yijin Liu, Feng Lin, and Kejie Zhao. Heterogeneous damage in Li-ion batteries: Experimental analysis and theoretical modeling. *Journal of the Mechanics and Physics of Solids*, 129(2019):160–183, 2019. ISSN 00225096. doi: 10.1016/j.jmps.2019.05.003. URL <https://doi.org/10.1016/j.jmps.2019.05.003>.
-

- 
- [48] Pengfei Yan, Jianming Zheng, Meng Gu, Jie Xiao, Ji Guang Zhang, and Chong Min Wang. Intragranular cracking as a critical barrier for high-voltage usage of layer-structured cathode for lithium-ion batteries. *Nature Communications*, 8:1–9, 2017. ISSN 20411723. doi: 10.1038/ncomms14101.
- [49] Yoshio Nishi. Carbonaceous materials for lithium ion secondary battery anodes. *Molecular Crystals and Liquid Crystals Science and Technology Section A: Molecular Crystals and Liquid Crystals*, 340:419–424, 2000. ISSN 1058725X. doi: 10.1080/10587250008025503.
- [50] Li Guobao, Xue Rongjian, and Liqian Chen. The influence of polytetrafluorethylene reduction on the capacity loss of the carbon anode for lithium ion batteries. *Solid State Ionics*, 90(1-4):221–225, 1996. ISSN 01672738. doi: 10.1016/s0167-2738(96)00367-0.
- [51] E Peter Roth and Ganesan Nagasubramanian. Thermal Stability of Electrodes in Lithium-Ion Cells. *Journal of the Electrochemical Society*, 2000.
- [52] R. Spotnitz and J. Franklin. Abuse behavior of high-power, lithium-ion cells. *Journal of Power Sources*, 113(1):81–100, 2003. ISSN 03787753. doi: 10.1016/S0378-7753(02)00488-3.
- [53] Yao Wu, Peter Keil, Simon F Schuster, and Andreas Jossen. Impact of temperature and discharge rate on the aging of a Impact of Temperature and Discharge Rate on the Aging of a LiCoO<sub>2</sub> / LiNi<sub>0.8</sub>Co<sub>0.15</sub>Al<sub>0.05</sub>O<sub>2</sub> Lithium-Ion Pouch Cell. (January), 2017. doi: 10.1149/2.0401707jes.
- [54] Jacob J. Lamb and Bruno G. Pollet. *Micro-optics and energy: Sensors for energy devices*. 2020. ISBN 9783030436766. doi: 10.1007/978-3-030-43676-6.
- [55] Thomas Waldmann, Marcel Wilka, Michael Kasper, Meike Fleischhammer, and Margret Wohlfahrt-Mehrens. Temperature dependent ageing mechanisms in Lithium-ion batteries - A Post-Mortem study. *Journal of Power Sources*, 262: 129–135, 2014. ISSN 03787753. doi: 10.1016/j.jpowsour.2014.03.112. URL <http://dx.doi.org/10.1016/j.jpowsour.2014.03.112>.
- [56] E. Sarasketa-Zabala, I. Gandiaga, E. Martinez-Laserna, L. M. Rodriguez-Martinez, and I. Villarreal. Corrigendum to "cycle ageing analysis of a LiFePO<sub>4</sub>/graphite cell with dynamic model validations: Towards realistic lifetime predictions" [J. Power Sources 275 (2015) 573-587]. *Journal of Power Sources*, 294:602, 2015. ISSN 03787753. doi: 10.1016/j.jpowsour.2015.06.109. URL <http://dx.doi.org/10.1016/j.jpowsour.2015.06.109>.
- [57] Pengjian Guan, Lin Liu, and Yang Gao. Phase-Field Modeling of Solid Electrolyte Interphase (SEI) Cracking in Lithium Batteries. *ECS Transactions*, 85(13):1041–1051, 2018. ISSN 1938-6737. doi: 10.1149/08513.1041ecst.

- 
- [58] Piotr Jankowski, Władysław Wieczorek, and Patrik Johansson. SEI-forming electrolyte additives for lithium-ion batteries: development and benchmarking of computational approaches. *Journal of Molecular Modeling*, 23(1), 2017. ISSN 09485023. doi: 10.1007/s00894-016-3180-0.
- [59] Roman Imhof and Petr Novák. In Situ Investigation of the Electrochemical Reduction of Carbonate Electrolyte Solutions at Graphite Electrodes. *Journal of The Electrochemical Society*, 145(4):1081–1087, 1998. ISSN 0013-4651. doi: 10.1149/1.1838420.
- [60] Frank Richter, Signe Kjelstrup, Preben J.S. Vie, and Odne S. Burheim. Thermal conductivity and internal temperature profiles of Li-ion secondary batteries. *Journal of Power Sources*, 359:592–600, 2017. ISSN 03787753. doi: 10.1016/j.jpowsour.2017.05.045. URL <http://dx.doi.org/10.1016/j.jpowsour.2017.05.045>.
- [61] Frank Richter, Preben J.S. Vie, Signe Kjelstrup, and Odne Stokke Burheim. Measurements of ageing and thermal conductivity in a secondary NMC-hard carbon Li-ion battery and the impact on internal temperature profiles. *Electrochimica Acta*, 250:228–237, 2017. ISSN 00134686. doi: 10.1016/j.electacta.2017.07.173. URL <http://dx.doi.org/10.1016/j.electacta.2017.07.173>.
- [62] K. Jagannadham. Thermal Conductivity Changes Due to Degradation of Cathode Film Subjected to Charge–Discharge Cycles in a Li Ion Battery. *Metallurgical and Materials Transactions A: Physical Metallurgy and Materials Science*, 49(8):3738–3752, 2018. ISSN 10735623. doi: 10.1007/s11661-018-4665-5. URL <https://doi.org/10.1007/s11661-018-4665-5>.
- [63] F. Bonhomme, Ph. Biensan, C. Jordy, D. Germond, J.M. Lалуque, M. Broussely, C. Delmas, L. Croguennec, M. Menetrier, and C. Vaysse. Proceedings of the IBA Meeting. In *IBA*, 2004.
- [64] MSE Supplies. Source of Detrimental Dendrite Growth in Lithium Batteries Discovered, 2019. URL <https://www.msesupplies.com/blogs/news/source-of-detrimental-dendrite-growth-in-lithium-batteries-discovered>
- [65] Cyril A. Truchot. Study of State-Of-Charge and Degradation in Lithium Ion Battery Pack, 2012.
- [66] G. G. Amatucci, J. M. Tarascon, and L. C. Klein. Cobalt dissolution in LiCoO<sub>2</sub>-based non-aqueous rechargeable batteries. *Solid State Ionics*, 83(1-2):167–173, 1996. ISSN 01672738. doi: 10.1016/0167-2738(95)00231-6.
- [67] Kazuma Kumai, Hajime Miyashiro, Yo Kobayashi, Katsuhito Takei, and Rikio Ishikawa. Gas generation mechanism due to electrolyte decomposition in commercial lithium-ion cell. *Journal of Power Sources*, 81-82:715–719, 1999. ISSN 03787753. doi: 10.1016/S0378-7753(98)00234-1.
-

- 
- [68] Roman Imhof and Petr Novák. Oxidative Electrolyte Solvent Degradation in Lithium-Ion Batteries: An In Situ Differential Electrochemical Mass Spectrometry Investigation. *Journal of The Electrochemical Society*, 146(5):1702–1706, 1999. ISSN 0013-4651. doi: 10.1149/1.1391829.
- [69] Doron Aurbach, Boris Markovsky, Gregory Salitra, Elena Markevich, Yossi Talyossef, Maxim Koltypin, Linda Nazar, Brian Ellis, and Daniella Kovacheva. Review on electrode-electrolyte solution interactions, related to cathode materials for Li-ion batteries. *Journal of Power Sources*, 165(2):491–499, 2007. ISSN 03787753. doi: 10.1016/j.jpowsour.2006.10.025.
- [70] Wei Wu, Xinran Xiao, and Xiaosong Huang. ES2011-54. pages 1–10, 2011.
- [71] Dawn Bernardi, Ellen Pawlikowski, and John Newman. General Energy Balance for Battery Systems. *Electrochemical Society Extended Abstracts*, 84-2:164–165, 1984. ISSN 01604619. doi: 10.1149/1.2113792.
- [72] Xiao-feng Zhang, Yan Zhao, Yatish Patel, Teng Zhang, Wei-ming Liu, Mu Chen, Gregory J Offer, and Yue Yan. Potentiometric Measurement of Entropy Change for Lithium Batteries for lithium batteries †. *Physical Chemistry Chemical Physics*, (March 2018), 2017. ISSN 1463-9076. doi: 10.1039/C6CP08505A. URL <http://dx.doi.org/10.1039/C6CP08505A>.
- [73] V. J. Ovejas and A. Cuadras. State of charge dependency of the overvoltage generated in commercial Li-ion cells. *Journal of Power Sources*, 418(July 2018): 176–185, 2019. ISSN 03787753. doi: 10.1016/j.jpowsour.2019.02.046. URL <https://doi.org/10.1016/j.jpowsour.2019.02.046>.
- [74] Christian Fleischer, Wladislaw Waag, Hans-martin Heyn, and Dirk Uwe. On-line adaptive battery impedance parameter and state estimation considering physical principles in reduced order equivalent circuit battery models Part 1 . Requirements , critical review of methods and modeling. *Journal of Power Sources*, 260: 276–291, 2014. ISSN 0378-7753. doi: 10.1016/j.jpowsour.2014.01.129. URL <http://dx.doi.org/10.1016/j.jpowsour.2014.01.129>.
- [75] Stephen J. Bazinski and Xia Wang. Experimental study on the influence of temperature and state-of-charge on the thermophysical properties of an LFP pouch cell. *Journal of Power Sources*, 293:283–291, 2015. ISSN 03787753. doi: 10.1016/j.jpowsour.2015.05.084.
- [76] Anup Barai, Kotub Uddin, W. D. Widanage, Andrew McGordon, and Paul Jennings. A study of the influence of measurement timescale on internal resistance characterisation methodologies for lithium-ion cells. *Scientific Reports*, 8(1):1–13, 2018. ISSN 20452322. doi: 10.1038/s41598-017-18424-5. URL <http://dx.doi.org/10.1038/s41598-017-18424-5>.
- [77] Wladislaw Waag, Stefan Käbitz, and Dirk Uwe Sauer. Experimental investigation of the lithium-ion battery impedance characteristic at various conditions and aging states and its influence on the application. *Applied Energy*, 102:885–897, 2013.

---

ISSN 03062619. doi: 10.1016/j.apenergy.2012.09.030. URL <http://dx.doi.org/10.1016/j.apenergy.2012.09.030>.

- [78] Kotub Uddin, Alessandro Picarelli, Christopher Lyness, Nigel Taylor, and James Marco. An acausal Li-ion battery pack model for automotive applications. *Energies*, 7(9):5675–5700, 2014. ISSN 19961073. doi: 10.3390/en7095675.
- [79] Manoj Mathew, Stefan Janhunen, Mahir Rashid, Frank Long, and Michael Fowler. Comparative analysis of lithium-ion battery resistance estimation techniques for battery management systems. *Energies*, 11(6):121693718, 2018. ISSN 19961073. doi: 10.3390/en11061490.
- [80] Daniel J. Noelle, Meng Wang, Anh V. Le, Yang Shi, and Yu Qiao. Internal resistance and polarization dynamics of lithium-ion batteries upon internal shorting. *Applied Energy*, 212(June 2017):796–808, 2018. ISSN 03062619. doi: 10.1016/j.apenergy.2017.12.086. URL <https://doi.org/10.1016/j.apenergy.2017.12.086>.
- [81] Patrick J. Osswald, Manuel Del Rosario, Jürgen Garche, Andreas Jossen, and Harry E. Hoster. Fast and Accurate Measurement of Entropy Profiles of Commercial Lithium-Ion Cells. *Electrochimica Acta*, 177:270–276, 2015. ISSN 00134686. doi: 10.1016/j.electacta.2015.01.191. URL <http://dx.doi.org/10.1016/j.electacta.2015.01.191>.
- [82] Y. Reynier, R. Yazami, and B. Fultz. The entropy and enthalpy of lithium intercalation into graphite. *Journal of Power Sources*, 119-121:850–855, 2003. ISSN 03787753. doi: 10.1016/S0378-7753(03)00285-4.
- [83] Colin Ringdalen MacDonald. Investigating heat development in a Lithium-ion cell. Technical report, 2020.
- [84] Vilayanur V. Viswanathan, Daiwon Choi, Donghai Wang, Wu Xu, Silas Towne, Ralph E. Williford, Ji Guang Zhang, Jun Liu, and Zhenguo Yang. Effect of entropy change of lithium intercalation in cathodes and anodes on Li-ion battery thermal management. *Journal of Power Sources*, 195(11):3720–3729, 2010. ISSN 03787753. doi: 10.1016/j.jpowsour.2009.11.103. URL <http://dx.doi.org/10.1016/j.jpowsour.2009.11.103>.
- [85] Shin Jang Sung, Wei Jen Lai, Mohammed Yusuf Ali, Jwo Pan, and Saeed Barbat. Compressive Behavior of Representative Volume Element Specimens of Lithium-Ion Battery Cells under Different Constrained Conditions. *SAE International Journal of Materials and Manufacturing*, 7(2):480–487, 2014. ISSN 19463979. doi: 10.4271/2014-01-1987.
- [86] Frank P. Incropera, Theodore L. Bergman, Addriene S. Lavine, and David P. Dewit. *Fundamentals of Heat and Mass Transfer*. JOHN WILEY & SONS, Hoboken, NJ, seventh edition, 2011. ISBN 9780470501979.

- 
- [87] Frank Richter. *Lifetime of Li-ion secondary batteries and measurement of key parameters for internal temperature profile assessment*. PhD thesis, Norwegian University of Science and Technology, Faculty of Natural Sciences, Trondheim, 2019.
- [88] Jiung Cho, Mark D. Losego, Hui Gang Zhang, Honggyu Kim, Jianmin Zuo, Ivan Petrov, David G. Cahill, and Paul V. Braun. Electrochemically tunable thermal conductivity of lithium cobalt oxide. *Nature Communications*, 5(May):2–7, 2014. ISSN 20411723. doi: 10.1038/ncomms5035.
- [89] Guangsheng Zhang, Christian E. Shaffer, Chao-Yang Wang, and Christopher D. Rahn. Effects of Non-Uniform Current Distribution on Energy Density of Li-Ion Cells. *Journal of The Electrochemical Society*, 160(11):A2299–A2305, 2013. ISSN 0013-4651. doi: 10.1149/2.061311jes.
- [90] Yan Zhao, Yatish Patel, Teng Zhang, and Gregory J. Offer. Modeling the Effects of Thermal Gradients Induced by Tab and Surface Cooling on Lithium Ion Cell Performance. *Journal of The Electrochemical Society*, 165(13):A3169–A3178, 2018. ISSN 0013-4651. doi: 10.1149/2.0901813jes.
- [91] Gabriel M. Cavalheiro, Takuto Iriyama, George J. Nelson, Shan Huang, and Guangsheng Zhang. Effects of Nonuniform Temperature Distribution on Degradation of Lithium-Ion Batteries. *Journal of Electrochemical Energy Conversion and Storage*, 17(2):1–8, 2020. ISSN 23816910. doi: 10.1115/1.4045205.
- [92] Gregory Gachot, Sylvie Grugeon, Michel Armand, Serge Pilard, Pierre Guenot, Jean Marie Tarascon, and Stephane Laruelle. Deciphering the multi-step degradation mechanisms of carbonate-based electrolyte in Li batteries. *Journal of Power Sources*, 178(1):409–421, 2008. ISSN 03787753. doi: 10.1016/j.jpowsour.2007.11.110.
- [93] Alastair Hales, Mohamed Waseem Marzook, Laura Bravo Diaz, Yatish Patel, and Gregory Offer. The Surface Cell Cooling Coefficient: A Standard to Define Heat Rejection from Lithium Ion Battery Pouch Cells. *Journal of The Electrochemical Society*, 167(2):020524, 2020. ISSN 0013-4651. doi: 10.1149/1945-7111/ab6985.
- [94] Dafen Chen, Jiuchun Jiang, Gi Heon Kim, Chuanbo Yang, and Ahmad Pesarani. Comparison of different cooling methods for lithium ion battery cells. *Applied Thermal Engineering*, 94:846–854, 2016. ISSN 13594311. doi: 10.1016/j.applthermaleng.2015.10.015. URL <http://dx.doi.org/10.1016/j.applthermaleng.2015.10.015>.
- [95] Ziyue Ling, Zhengguo Zhang, Guoquan Shi, Xiaoming Fang, Lei Wang, Xuenong Gao, Yutang Fang, Tao Xu, Shuangfeng Wang, and Xiaohong Liu. Review on thermal management systems using phase change materials for electronic components, Li-ion batteries and photovoltaic modules. *Renewable and Sustainable Energy Reviews*, 31:427–438, 2014. ISSN 13640321. doi: 10.1016/j.rser.2013.12.017. URL <http://dx.doi.org/10.1016/j.rser.2013.12.017>.
-

- 
- [96] Huaqiang Liu, Zhongbao Wei, Weidong He, and Jiyun Zhao. Thermal issues about Li-ion batteries and recent progress in battery thermal management systems: A review. *Energy Conversion and Management*, 150(August):304–330, 2017. ISSN 01968904. doi: 10.1016/j.enconman.2017.08.016. URL <http://dx.doi.org/10.1016/j.enconman.2017.08.016>.
- [97] Yan Zhao, Laura Bravo Diaz, Yatish Patel, Teng Zhang, and Gregory J. Offer. How to Cool Lithium Ion Batteries: Optimising Cell Design using a Thermally Coupled Model. *Journal of The Electrochemical Society*, 166(13):A2849–A2859, 2019. ISSN 0013-4651. doi: 10.1149/2.0501913jes.
- [98] Shenzhen Melasta Battery Co. Melasta Product specification. Technical Report 1, 2019.
- [99] Xiao Hua, Claas Heckel, Nils Modrow, Cheng Zhang, Alastair Hales, Justin Holloway, Anmol Jnawali, Shen Li, Yifei Yu, Melanie Loveridge, Paul Shearing, Yatish Patel, Monica Marinescu, Liang Tao, and Gregory Offer. The prismatic surface cell cooling coefficient: A novel cell design optimisation tool & thermal parameterization method for a 3D discretised electro-thermal equivalent-circuit model. *eTransportation*, 7:100099, 2021. ISSN 25901168. doi: 10.1016/j.etrans.2020.100099. URL <https://doi.org/10.1016/j.etrans.2020.100099>.
- [100] M. BRAUN Inertgas-Systeme GmbH. UNIlabpro INERT GAS GLOVE-BOX WORKSTATION. 2017. URL <https://www.mbraun.com/us/products/glovebox-workstations.html>.
- [101] M Broussely, Ph Biensan, F Bonhomme, and Ph Blanchard. Main aging mechanisms in Li ion batteries. 146:90–96, 2005. doi: 10.1016/j.jpowsour.2005.03.172.
- [102] O. Burheim, P. J.S. Vie, J. G. Pharoah, and S. Kjelstrup. Ex situ measurements of through-plane thermal conductivities in a polymer electrolyte fuel cell. *Journal of Power Sources*, 195(1):249–256, 2010. ISSN 03787753. doi: 10.1016/j.jpowsour.2009.06.077.
- [103] O. S. Burheim, M. A. Onsrud, J. G. Pharoah, F. Vullum-Bruer, and P. J. S. Vie. Thermal Conductivity, Heat Sources and Temperature Profiles of Li-Ion Batteries. *ECS Transactions*, 58(48):145–171, 2014. ISSN 1938-6737. doi: 10.1149/05848.0145ecst.
- [104] Kohei Honkura and Tatsuo Horiba. Study of the deterioration mechanism of Li-CoO<sub>2</sub>/graphite cells in charge/discharge cycles using the discharge curve analysis. *Journal of Power Sources*, 264:140–146, 2014. ISSN 03787753. doi: 10.1016/j.jpowsour.2014.04.036. URL <http://dx.doi.org/10.1016/j.jpowsour.2014.04.036>.
- [105] Elie Riviere, Ali Sari, Pascal Venet, Frédéric Meniere, and Yann Bultel. Innovative incremental capacity analysis implementation for c/lifepo 4 cell state-of-health estimation in electrical vehicles. *Batteries*, 5(2), 2019. ISSN 23130105. doi: 10.3390/batteries5020037.
-

- 
- [106] L. J. Krause, T. Brandt, V. L. Chevrier, and L. D. Jensen. Surface Area Increase of Silicon Alloys in Li-Ion Full Cells Measured by Isothermal Heat Flow Calorimetry. *Journal of The Electrochemical Society*, 164(9):A2277–A2282, 2017. ISSN 0013-4651. doi: 10.1149/2.0501712jes.
- [107] Hui Xia, S. B. Tang, and Li Lu. Thin film microbatteries prepared by pulsed laser deposition. *Journal of the Korean Physical Society*, 51(3):1055–1062, 2007. ISSN 03744884. doi: 10.3938/jkps.51.1055.
- [108] Elie Riviere, Pascal Venet, Ali Sari, Frederic Meniere, and Yann Bultel. LiFePO<sub>4</sub> Battery State of Health Online Estimation Using Electric Vehicle Embedded Incremental Capacity Analysis. *2015 IEEE Vehicle Power and Propulsion Conference, VPPC 2015 - Proceedings*, 2015. doi: 10.1109/VPPC.2015.7352972.
- [109] S. L. Glazier, Jing Li, A. J. Louli, J. P. Allen, and J. R. Dahn. An Analysis of Artificial and Natural Graphite in Lithium Ion Pouch Cells Using Ultra-High Precision Coulometry, Isothermal Microcalorimetry, Gas Evolution, Long Term Cycling and Pressure Measurements. *Journal of The Electrochemical Society*, 164(14):A3545–A3555, 2017. ISSN 0013-4651. doi: 10.1149/2.0421714jes.
- [110] Yan Zhao, Laura Bravo Diaz, Yatish Patel, Teng Zhang, and Gregory J. Offer. How to Cool Lithium Ion Batteries: Optimising Cell Design using a Thermally Coupled Model. *Journal of The Electrochemical Society*, 166(13):A2849–A2859, 2019. ISSN 0013-4651. doi: 10.1149/2.0501913jes.



---

# Appendix

---

Appendix **A**

# Melasta SLPBB042126HN Product specification

# Product Specification

## Polymer Li-Ion Cell

**3.7V 6550mAh 10C**

(Model No.: SLPBB042126HN)



Shenzhen Melasta Battery Co.,Ltd

Tongfuyu Industrial Zone,Dalang,BaoAn District,Shenzhen,518109,China

Tel:+86-755-83693563

Fax:+86-755-28120114

E-mail:sales@melasta.com

Http://www.melasta.com

**MELASTA**

**锂聚合物电池 LIPO BATTERIES**

**Apr 11th,2019**

This information is generally descriptive only and is not intended to make or imply any representation, guarantee or warranty with respect to any cells and batteries. Cell and battery designs/specifications are subject to modification without notice. Contact MELASTA for the latest information.

## Content

### 目录

1. 序言	3
Preface	
2. 型号: SLPBB042126HN	3
Model: SLPBB042126HN	
3. 产品规格	3
Specification	
4. 电芯性能检查及测试	4
Battery Cell Performance Criteria	
5. 贮存及其它事项	5
Storage and Others	
6. 聚合物锂离子充电电芯操作指示及注意事项	5- 8
Handling Precautions and Guideline	
6.1. 充电	5- 6
Charging	
6.2. 放电	6- 7
Discharging	
6.3. 贮存	7
Storage	
6.4. 电芯操作注意事项	7
Handling of Cells	
6.5. 电池外壳设计注意事项	7
Notice for Designing Battery Pack	
6.6. 电池与外壳组装注意事项	7-8
Notice for Assembling Battery Pack	
7. 其它事项	8-9
Others	

## 1. 序言 PREFACE

此规格书适用于深圳市风云电池有限公司的锂聚合物可充电电池产品

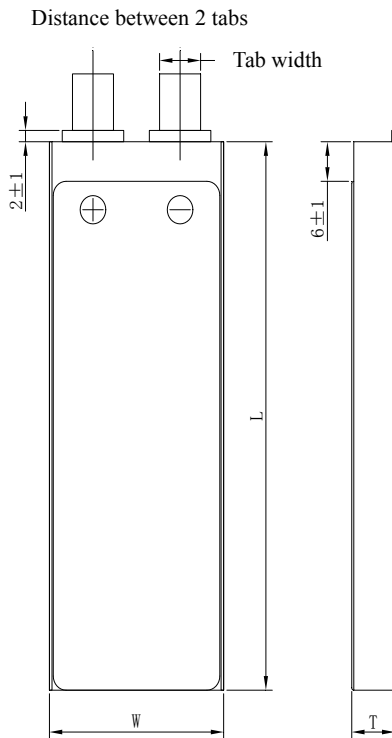
The specification is suitable for the performance of Lithium-Polymer (LIP) rechargeable battery produced by the SHENZHEN MELASTA BATTERY CO., LTD.

## 2. 型号 MODEL

SLPBB042126HN 6550mAh 10C 3.7V

## 3. 产品规格 SPECIFICATION

单颗电池规格 Specifications of single cell



◆ 电芯正极材料 Cell Cathode Material	LiCoO2	
◆ 标称容量 Typical Capacity①	6550mAh	
◆ 标称电压 Nominal Voltage	3.7V	
◆ 充电条件 Charge Condition	最大电流 Max. Continuous charge Current	13.1A
	峰值充电 Peak charge current	64A(≤0.5sec) 54A(≤1sec)
	电压 Voltage	4.2V±0.03V
◆ 放电条件 Discharge Condition	Max Continuous Discharge Current	65.5A
	Peak Discharge Current	98.25A(≤3sec)
	Cut-off Voltage	3.0V
◆ 交流内阻 AC Impedance(mOHM)	<3.0	
◆ 循环寿命【充电:1C,放电:10C】 Cycle Life【CHA:1C,DCH:10C】	>100cycles	
◆ 使用温度 Operating Temp.	充电 Charge	0℃~60℃
	放电 Discharge	-20℃~70℃
◆ 电芯尺寸 Cell Dimensions	厚度 Thickness(T)	10.7±0.3mm
	宽度 Width(W)	42±0.5mm
	长度 Length(L)	127.5±0.5mm
	极耳间距 Distance between 2 tabs	21±1mm
◆ 极耳尺寸 Dimensions of Cell tabs	极耳材料 Tab Material	Nickel-plated Copper
	极耳宽度 Tab Width	12mm
	极耳厚度 Tab Thickness	0.2mm
	极耳长度 Tab Length	30±1.5mm
◆ 重量 Weight(g)	128.5±3.0g	
① 标称容量: 0.2C,4.2V~3.0V@23℃±2℃ Typical Capacity:0.2C,4.2V~3.0V@23℃±2℃		

制造商保留在没有预先通知的情况下改变和修正设计及规格说明书的权力

Melasta reserves the right to alter or amend the design, model and specification without prior notice

#### 4.电芯性能检查及测试 BATTERY CELL PERFORMANCE CRITERIA

在进行下列各项测试前每颗电池应用 0.5C 放至 3.0V。如果没有特别规定，测试应在电池交付 1 个月内按以下各项条件进行：

Before proceed the following tests, the cells should be discharged at 0.5C to 3.0V cut off. Unless otherwise stated, tests should be done within one month of delivery under the following conditions:

环境温度 Ambient temperature: 20°C±5°C

相对湿度 Relative Humidity: 65±20%RH

注意标准充放电为 Note Standard Charge/Discharge Conditions:

充电 Charge: 以 0.5C 电流恒流充电至限制电压 4.2V 时,改为恒压充电,直到截止电流为 0.05C 时停止充电;The battery will be charged to 4.2V with 0.5C from constant current to constant voltage, when the current is 0.05C, stop to charge.;

放电 Discharge: 0.5C to 3.0V/cell

测试项目 Test	单位 Unit	规格 Specification	条件 Condition	备注 Remarks
容量 Capacity	mAh	≥6550	标准充放电 Standard Charge / Discharge	允许循环 3 次 Up to 3 cycles are allowed
开路电压 Open Circuit Voltage (OCV)	V	≥4.15	标准充电后 1 个小时内 Within 1 hr after standard charge	单位颗 Unit cell
内阻 Internal Impedance (IR)	mΩ	≤3.0	充满电后用 1kHz 测试 Upon fully charge at 1kHz	*
高倍率放电 High Rate Discharge (10C)	min	≥5.4	标准充电/休息 5 分钟 用 10C 放电至 3.0V Standard Charge/rest 5min discharge at10C to 3.0V	允许循环 3 次 Up to 3 cycles are allowed
低温放电 Low Temperature Discharge	min	≥210	标准充电后贮藏在-20±2°C 环境中 2 小时 然后用 0.2C 放电 Standard Charge, Storage:2hrs at-2 0±2°C 0.2C discharge at 0±2°C	3.0V/cell Cut-off
自放电 Charge Reserve	min	≥90% (初始容量 First Capacity)	标准充满电后 20 度贮藏 30 天, 标准 0.5C 放电 Standard charge Storage at 20 degree: 30days Standard discharge (0.5C)	3.0V/cell Cut-off
寿命测试 Cycle Life Test	Cycle times	≥100	充电: 0.5C 充电至 4.2V, 放电, 10C 放电至 3.0V, 当放电容量降至初始容量的 80% 时, 所完成的 循环次数定义为该电芯的循环寿命 Charge:0.5C to 4.2V ,Discharge: 10C to 3.0V, 80% or more of 1 <sup>st</sup> cycle capacity at 10C discharge of Operation	Retention capacity 容量保持 ≥80% of initial capacity

短路测试 External Short Circuit	N/A	不着火不爆炸 No Fire and No Explosion	标准充电后, 在 20°C±5 环境中用超过 0.75mm <sup>2</sup> 金属丝将单颗电池短路至电池恢复到常温。 After standard charge, short-circuit the cell at 20°C±5°C until the cell temperature returns to ambient temperature.(cross section of the wire or connector should be more than 0.75mm <sup>2</sup> )	*
自由跌落测试 Free Falling(drop)	N/A	不着火不爆炸 No Fire and No Explosion	跌标准充电后, 搁置 2 小时。从 1.2M 高任意方向自由跌落 30MM 厚木板 3 次 Standard Charge, and then leave for 2hrs, check battery before / after drop Height: 1.2m Thickness of wooden board: 30mm Direction is not specified Test for 3 times	*

5. 贮存及其它事项 STORAGE AND OTHERS

5.1 环境温度 Ambient temperature: 20°C±5°C

相对湿度 Relative Humidity: 65±20%RH

5.2 请每隔 3 个月按下面方法激活电池一次:

Please activate the battery once every 3 months according to the following method:

0.2C 充电至 4.2V, 休息 5 分钟, 然后用 0.2C 放电至每颗电池 3.0V, 休息 5 分钟, 0.2C 充电 3.9V。

Charge at 0.2C to 4.2V, rest 5 min, then discharge with 0.2C to 3.0V/cell, rest 5 min, then charge at 0.2C to 3.9V.

6. 聚合物锂离子充电电芯操作指示及注意事项 HANDLING PRECAUTIONS AND GUIDELINE

声明一:

客户若需要将电芯用于超出文件规定以外的设备, 或在文件规定以外的使用条件下使用电芯, 应事先联系风云公司, 因为需要进行特定的实验测试以核实电芯在该使用条件下的性能及安全性。

Note(1):

The customer is requested to contact MELASTA in advance, if and when the customer needs other applications or operating conditions than those described in this document. Additional experimentation may be required to verify performance and safety under such conditions.

声明二:

对于在超出文件规定以外的条件下使用电芯而造成的任何意外事故, 风云公司概不负责

Note (2):

MELASTA will take no responsibility for any accident when the cell is used under other conditions than those described in this Document.

声明三:

如有必要, 风云公司会以书面形式告之客户有关正确操作使用电芯的改进措施。

MELASTA will inform, in a written form, the customer of improvement(s) regarding proper use and handing of the cell, if it is deemed necessary.

6.1. 充电 Charging

6.1.1 充电电流 Charging current:

充电电流不得超过本标准书中规定的最大充电电流。使用高于推荐值电流充电将可能引起电芯的充放电性能、机械性能和安全性能的问题, 并可能会导致发热或泄漏。

Charging current should be less than maximum charge current specified in the Product Specification.

Charging with higher current than recommended value may cause damage to cell electrical, mechanical and safety performance and could lead to heat generation or leakage.



#### 6.1.2. 充电电压 Charging voltage:

充电电压不得超过本标准书中规定的额定电压 (4.2V/电芯)。4.25V 为充电电压最高极限, 充电器的设计应满足此条件; 电芯电压高于额定电压值时, 将可能引起电芯的充放电性能、机械性能和安全性能的问题, 可能会导致发热或泄漏。

Charging shall be done by voltage less than that specified in the Product Specification (4.2V/cell).

Charging beyond 4.25V, which is the absolute maximum voltage, must be strictly prohibited. The charger shall be designed to comply with this condition. It is very dangerous that charging with higher voltage than maximum voltage may cause damage to the cell electrical, mechanical safety performance and could lead to heat generation or leakage.

#### 6.1.3. 充电温度 Charging temperature:

电芯必须在 0℃~60℃的环境温度范围内进行充电

The cell shall be charged within 0℃~60℃ range in the Product Specification.

#### 6.1.4. 禁止反向充电 Prohibition of reverse charging:

正确连接电池的正负极, 严禁反向充电。若电池正负极接反, 将无法对电芯进行充电。同时, 反向充电会降低电芯的充放电性能、安全性, 并会导致发热、泄漏。

Reverse charging is prohibited. The cell shall be connected correctly. The polarity has to be confirmed before wiring, In case of the cell is connected improperly, the cell cannot be charged. Simultaneously, the reverse charging may cause damaging to the cell which may lead to degradation of cell performance and damage the cell safety, and could cause heat generation or leakage.

### 6.2. 放电 Discharging

#### 6.2.1. 放电电流 Discharging current

放电电流不得超过本标准书规定的最大放电电流, 大电流放电会导致电芯容量剧减并导致过热。

The cell shall be discharged at less than the maximum discharge current specified in the Product Specification. High discharging current may reduce the discharging capacity significantly or cause over-heat.

#### 6.2.2. 放电温度 Discharging temperature

电芯必须在-20℃~70℃的环境温度范围内进行放电。

The cell shall be discharged within -20℃~70℃ range specified in the Product Specification.

#### 6.2.3. 过放电 Over-discharging:

需要注意的是, 在电芯长期未使用期间, 它可能会用其它自放电特性而处于某种过放电状态。为防止放电的发生, 电芯应定期充电, 将其电压维持在 3.6V 至 3.9V 之间。

过放电会导致电芯性能、电池功能的丧失。

充电器应有装置来防止电池放电至低于本标准书规定的截止电压。此外, 充电器还应有装置以防止重复充电, 步骤如下:

电池在快速充电之前, 应先以一小电流 (0.01C) 预充电 15~30 分钟, 以使 (每个) 电芯的电压达到 3V 以上, 再进行快速充电。可用一计时器来实现该预充电步骤。如果在预充电规定时间内, (个别) 电芯的电压仍未升到 3.0V 以上, 充电器应能够停止下一步快速充电, 并显示该电芯/电池正处于非正常状态。

It should be noted that the cell would be at over-discharged state by its self-discharge characteristics in case the cell is not used for long time. In order to prevent over-discharging, the cell shall be charged periodically to maintain between 3.6V and 3.9V.

Over-discharging may causes loss of cell performance, characteristics, or battery functions.

The charger shall be equipped with a device to prevent further discharging exceeding a cut-off voyage specified in the Product Specification. Also the charger shall be equipped with a device to control the recharging procedures as follows:

The cell battery pack shall start with a low current (0.01C) for 15-30 minutes, i.e.-charging, before rapid charging starts. The rapid charging shall be started after the (individual) cell voltage has been reached above 3V within 15-30 minutes that can be determined with the use of an appropriate timer for pre-charging. In case the (individual) cell voltage does not rise to 3V within the pre-charging time, then the charger shall have functions to stop further charging and display the cell/pack is at abnormal state.

### 6.3. 贮存 Storage:

电芯储存温度必须在 0℃~45℃ 的范围内,长期存储电池 (超过 3 个月) 须置于温度为 23±5℃、湿度为 65±20%RH 的环境中,贮存电压为 3.6V~3.9V

The cell shall be storied within 0℃~45℃ range environmental condition, If the cell has to be storied for a long time (Over 3 months),the environmental condition should be; Temperature: 23±5℃ Humidity: 65±20%RH, The voltage for a long time storage shall be 3.6V~3.9V range.

### 6.4. 电芯操作注意事项 Handling of Cells:

由于电芯属于软包装, 为保证电芯的性能不受损害, 必须小心对电芯进行操作。

Since the battery is packed in soft package, to ensure its better performance, it's very important to carefully handle the battery;

#### 6.4.1. 铝箔包装材料易被尖锐部件损伤, 诸如镍片, 尖针。

The soft aluminum packing foil is very easily damaged by sharp edge parts such as Ni-tabs, pins and needles.

·禁止用尖锐部件碰撞电池;

Don't strike battery with any sharp edge parts;

·取放电芯时, 请修短指甲或戴上手套;

Trim your nail or wear glove before taking battery;

·应清洁工作环境, 避免有尖锐物体存在;

Clean work table to make sure no any sharp particle;

#### 6.4.2. 禁止弯折顶封边;

Don't bend or fold sealing edge;

#### 6.4.3. 禁止打开或破坏折边;

Don't open or deform folding edge;

#### 6.4.4. 禁止弯折极片;

Don't bend tab ;

#### 6.4.5. 禁止坠落、冲击、弯折电芯;

Don't Fall, hit, bend battery body;

#### 6.4.6. 任何时候禁止短路电芯, 它会导致电芯严重损坏;

Short circuit terminals of battery is strictly prohibited, it may damage battery;

### 6.5. 电池外壳设计 Notice Designing Battery Pack;

·电池外壳应有足够的机械强度以保证其内部电芯免受机械撞击;

Battery pack should have sufficient strength and battery should be protected from mechanical shock;

制造商保留在没有预先通知的情况下改变和修正设计及规格说明书的权力

Melasta reserves the right to alter or amend the design, model and specification without prior notice

·外壳内安装电芯的部位不应有锋利的边角;

No Sharp edge components should be inside the pack containing the battery;

## 6.6. 电芯与外壳组装注意事项 Notice for Assembling Battery Pack

### 6.6.1. 电芯的连接 Tab connection

建议使用超声波焊接或点焊技术来连接电芯与保护电路模块或其它部分。如使用手工锡焊, 须注意以下事项, 以保证电芯的功能:

Ultrasonic welding or spot welding is recommended to connect battery with PCM or other parts. If apply manual solder method to connect tab with PCM, below notice is very important to ensure battery performance.

#### a) 烙铁的温度可控能防静电;

The solder iron should be temperature controlled and ESD safe

#### b) 烙铁温度不能超过 350℃

Soldering temperature should not exceed 350℃

#### c) 锡焊时间不能超过 3 秒;

Soldering time should not be longer than 3s

#### d) 锡焊次数不能超过 5 次;

Soldering time should not exceed 5 times Keep battery tab cold down before next time soldering

#### e) 必须在极片冷却后再进行二次焊接; 禁止直接加热电芯, 高于 100℃会导致电芯损坏。

Directly heat cell body is strictly prohibited, Battery may be damaged by heat above approx. 100℃

### 6.6.2. 电芯的安装 Cell fixing

·应将电芯的宽面安装在外壳内;

The battery should be fixed to the battery pack by its large surface area

·电芯不得在壳内活动。

No cell movement in the battery pack should be allowed

## 7. 其它事项 OTHERS

### 7.1. 防止电池内短路 Prevention of short circuit within a battery pack

使用足够的绝缘材料对线路进行保护

Enough insulation layers between wiring and the cells shall be used to maintain extra safety protection.

### 7.2. 严禁拆卸电芯 Prohibition of disassembly

#### 7.2.1. 拆卸电芯可能会导致内部短路, 进而引起鼓气、着火及其它问题

The disassembling may generate internal short circuit in the cell, which may cause gassing, firing, or other problems.

#### 7.2.2. 聚合物锂电池理论上不存在流动的电解液, 但万一有电解液泄漏而接触到皮肤、眼睛或身体其它部位, 应立即用清水冲洗电解液并就医

LIP battery should not have liquid from electrolyte flowing, but in case the electrolyte come into contact with the skin, or eyes, physicians shall flush the electrolyte immediately with fresh water and medical advice is to be sought.

#### 7.3. 在任何情况下, 不得燃烧电芯或将电芯投入火中, 否则会引起电芯燃烧, 这是非常危险的, 应绝对禁止

Never incinerate nor dispose the cells in fire. These may cause firing of the cells, which is very dangerous and is prohibited.

7.4 不得将电芯浸泡液体，如淡水、海水、饮料(果汁、咖啡)等

The cells shall never be soaked with liquids such as water, seawater drinks such as soft drinks, juices coffee or others.

7.5 更换电芯应由电芯供应商或设备供应商完成，用户不得自行更换

The battery replacement shall be done only by either cells supplier or device supplier and never be done by the user.

7.6 禁止使用已损坏的电芯 Prohibition of use of damaged cells

电芯在运输过程中可能因撞击等原因而损坏，若发现电芯有任何异常特征，如电芯塑料封边损坏，外壳破损，闻到电解液气体，电解液泄漏等，该电芯不得使用。

有电解液泄漏或散发电解液气味的电池应远离火源以避免着火。

The cells might be damaged during shipping by shock. If any abnormal features of the cells are found such as damages in a plastic envelop of the cell, deformation of the cell package, smelling of electrolyte, electrolyte leakage and others, the cells shall never be used any more.

The cells with a smell of the electrolyte or a leakage shall be placed away from fire to avoid firing.

Edition (版本)	Description (记述)	Prepared by (编制)	Checked (审核)	Date (日期)
A0	First Publish (首次编写)	WXB	JianFu Huang	2019-04-11

